國 立 交 通 大 學

交通運輸研究所

博士論文

No.063

以先進細胞自動機模式探索高速公路時空交通特性

Exploration of Freeway Spatiotemporal Traffic Features with Advanced Cellular Automaton Modeling

指導教授： 藍武王博士

邱裕鈞博士

研 究 生： 許志誠

中 華 民 國 九 十 九 年 六 月

以先進細胞自動機模式探索高速公路時空交通特性

Exploration of Freeway Spatiotemporal Traffic Features with Advanced Cellular Automaton Modeling

研 究 生： 許志誠　　Student: Chih-Cheng Hsu

指導教授： 藍武王 博士　　Advisors: Dr. Lawrence W. Lan

邱裕鈞 博士　　Dr. Yu-Chiun Chiou

國 立 交 通 大 學

交 通 運 輸 研 究 所

博 士 論 文

A Dissertation

Submitted to Institute of Traffic and Transportation

College of Management

National Chiao Tung University

in Partial Fulfillment of the Requirements

for the Degree of Doctor of Philosophy

in

Management

June 2010

Taipei, Taiwan, Republic of China

中 華 民 國 九 十 九 年 六 月

以先進細胞自動機模式探索高速公路時空交通特性

學　　生：許志誠　　指導教授：藍武王　博士
邱裕鈞　博士

國立交通大學交通運輸研究所

摘要

1992 年物理學家 Nagel 及 Schreckenberg 兩人首度將細胞自動機(Cellular Automaton，CA)應用於公路車流行為研究，透過幾個簡單的加減速規則，利用電腦快速運算，讓車輛進行彼此交互作用與規則疊代，呈現出與實測相當之巨觀車流特性，又能描述微觀車流特性。迄今已有相當數量之改良 CA 模式，惟多針對小客車為研究對象，且對細胞單元之定義均相當粗糙，亦未探討異質(指同類型車種可具不同之速率、加減速、變換車道行為)混合(指同一道路空間可同時運行不同類型車種，如機車、小型車、大型車)車流課題。為更符合實際車流現象，本研究發展精緻型 CA 模式，並改良傳統 CA 模式加減速過大之不合理現象，用以探索異質混合車流之時空交通特性。

本研究首先提出一個基礎的異質混合車流細胞自動機模式，該模式比以往細胞自動機模式研究更為精細的「細胞」及「網格」概念，定義「基本單元」(CU)作為衡量車輛及道路空間之共通單位。並進一步以時空網格被車輛細胞移動軌跡所佔用之比例代表佔有率，以車輛細胞每個時階移動的格位數代表速率，每個時階通過的細胞數代表流量，定義一般化佔有率、速率與流量，以精確描述異質混合車流車輛的總體行為。經發展 CA 基本模式，模擬不同車流密度情況下純車流之時空交通特性，再構建總體交通流量、速率與佔有率的基本關係。惟模擬結果顯示車輛運行過程車速會驟降停止之情形，模式規則待改進。

接著本研究針對前述規則之缺點提出一個修正 CA 模式，該模式進一步整合駕駛跟車空間預期效應、採取速度相依之隨機項、啟動延遲規則、變換車道與大小車互動規則等。模擬環境設定在二車道的高速公路中進行，模擬情境為在車流中加入慢速車(如同慢速移動瓶頸)與停止車(如同固定地點瓶頸)，探討混合車流之時空交通特性，並進一步探討車流軌跡、流量密度關係與時空車流型態。模擬結果顯示修正 CA 模式能夠呈現出真實交通環境重要的車流特性與型態。

研究最後針對模擬過程中以往 CA 模式均未處理之缺點，即車輛在接近前方為停止車輛或固定物時所出現不合理急煞車之情形，提出一個更精緻的 CA 模式來改善。模式在規則中引入 Forbes 的跟車概念，利用多段線性速率修正傳統 CA 模式加減速過大之不合理現象。經高速公路之驗證與測試發現，確能改正車輛速率驟降之缺失，並能顯示 Kerner 所提出的三相交通現象及其相變。本研究進一步利用此修正 CA 模式應用在施工區，探討不同速率控制策略對行車效率及安全之影響。

關鍵字：異質車流、混合車流、細胞自動機、時空交通特性、高速公路

Exploration of Freeway Spatiotemporal Traffic Features with Advanced Cellular Automaton Modeling

Student: Chih-Cheng Hsu

Advisors: Dr. Lawrence W. Lan
Dr. Yu-Chiun Chiou

Institute of Traffic and Transportation
National Chiao Tung University

Abstract

Cellular automata (CA) model was first proposed by Nagel and Schreckenberg in 1992 to simulate the highway traffic. The core logic was to introduce several simple update rules for vehicle movement in computer programs to efficiently simulate the complicated interactive traffic behaviors. A considerable number of revised or extended CA models have been developed to date, most of which only focused on pure traffic with coarse cell units in the simulations. Very little has devoted to the heterogeneous traffic situations and/or mixed traffic contexts, which comprise different types of vehicle. This research aims to develop advanced CA models to simulate the spatiotemporal behaviors under heterogeneous mixed traffic contexts on freeway.

Firstly, a basic CA model is developed to explore the fundamental traffic features. Generalized definitions of traffic variables, in spatiotemporal sense, and a new concept of common unit (CU) for gauging non-identical vehicle sizes and various lane widths are presented. Pure light vehicle and pure heavy vehicle experiments are tested on a two-lane freeway context. Vehicular trajectories, flow-occupancy diagrams, and spatiotemporal traffic patterns under deterministic and stochastic conditions are displayed. The results show that abrupt speed drops occasionally emerge during the simulations.

To resolve this shortcoming, this study continues to propose a revised CA model, which considers the anticipation effect, velocity-dependent randomization, slow-to-start, lane change, and interaction among vehicles. The effects of both stationary and slow-moving bottlenecks on global traffic are examined using this revised CA model. Vehicular trajectories, flow-occupancy, and spatiotemporal traffic patterns are displayed. The results reveal noticeable traffic patterns with free flow, wide moving jam and synchronized flow phases, suggesting that the revised CA model is capable of capturing the essential features of traffic flows.

Finally, this study further proposes a refined CA model using the rationale of Forbes' car-following concept with a piecewise-linear movement mechanism, which aims to rectify the common defect of abrupt deceleration existent in most conventional CA models. The proposed CA model is validated in a two-lane freeway mainline context. It shows that this refined CA model can fix the unrealistic deceleration behaviors, thus can reflect the genuine driver behaviors in real world. The model is also capable of revealing Kerner's three-phase traffic patterns and phase transitions among them. Furthermore, the refined CA model is applied to simulate a highway work zone wherein traffic efficiency (maximum flow rates) and safety (speed deviations) impacted by various control schemes are investigated.

Keywords: Heterogeneous Traffic, Mixed Traffic, Cellular Automata, Spatiotemporal Traffic Features, Freeway.

誌謝

回顧這段帶職攻讀博士的歷程，真的就像一場長跑！鳴槍起跑充滿動力的衝出去，很快的完成修課、通過資格考，並同時進行著研究，原以爲順利然而事實上挑戰才開始。研究過程不斷發現問題與找尋解決方法，加上繁重的工作負荷，經常在 5 天忙碌的工作後，週六日接著到學校研究室做研究，那就像是跑步停下來還沒喘完，又要接著再跑的感覺。終於堅持跑完全程得以畢業，接受太多的幫助，要感謝的人實在太多。

首先感謝我的指導教授　藍武王老師及邱裕鈞老師。感謝您們悉心、耐心的指導，師恩浩瀚，無盡感恩。跟隨老師研究的過程，老師追求卓越的研究精神，以及嚴謹務實的態度，是我需要持續提升與學習的地方。藍老師總是用最清楚的觀念傳授知識，用以身作則嚴以律己的態度教育治學，得以投入師門學習我受益甚深。邱老師在研究過程不斷在知識、課題、方法、資料與遭遇問題等給予細心的指導與幫助，使論文得以順利完成，敬表由衷謝忱。感謝藍老師及邱老師的包容與體諒，容忍我緩慢的研究與期刊投稿進度，並帶領我走過這一段歷程。感謝口試委員陳惠國教授、胡大瀛教授、曾平毅教授、汪進財教授與許鉅秉教授，因爲您們的指導與斧正，讓我的論文更臻嚴謹完善。感謝所上的各位師長許鉅秉所長、汪進財教授、黃台生教授、黃承傳教授、徐淵靜教授、馮正民教授與陳穆臻教授，求學過程渥蒙您們的諄諄教誨與指導，讓我在學習與研究的過程，擁有更多專業知識與啓發。

感謝林局長重昌的提攜，並且讓我在最後關頭得以全心投入完成學業。感謝好友、學長姐與學弟妹許多協助。感謝滈善(Gary)全力投入協助開發模擬程式，沒有您的幫忙論文無法完成。感謝戰友日新學長，研究成果得以被國際期刊快速接受，歸功於您，研究室共同奮鬥的日子，將是我難忘的回憶。感謝瓊文師母的指導讓我很快能進入 CA 的研究領域，感謝仁傑學弟的加入，發展出新的研究方向與成果。感謝杰炤、益三、豐裕學長修業期間的照顧，特別感謝易詩總是給我最及時的幫助。感謝孟佑、世昌、彥蘅、承憲、沛儒、國洲、昭弘、永祥、群明、文斌、魏瑜、士軒、姿慧與彥斐等修業期間的研討與協助。

感謝摯愛的家人，他們是背後支持我完成學業最大的力量。最要感謝是愛妻嘉瑜，公務之餘還承擔所有家務及女兒的教養工作，看著女兒平安快樂成長，我滿心感激，也讓我在修業期間得以無後顧之憂的完成學業。感謝女兒馨云總在我感覺壓力繁重之際，給我貼心的擁抱，心裡總會湧起一股暖流。感謝爸媽養我育我，還有岳父母、大哥、大嫂、二哥一直以來對我的支持與鼓勵，我要將這篇論文獻給摯愛的您。

志誠 謹誌 2010.8

TABLE OF CONTENTS

LIST OF FIGURES

Chapter 1 INTRODUCTION

1.1 Background

Cellular automaton (CA), a newly developed microscopic traffic stream modeling approach, is a powerful tool to describe the phenomena of real traffic flows characterized with complex dynamic behaviors. Different CA models have been developed to describe the basic phenomena of real traffic flows characterized with complex dynamic behaviors over the past two decade. Nagel and Schreckenberg (1992) proposed a minimal model (hereafter NaSch model) of vehicular traffic on idealized single-lane highways to reproduce the basic features of real traffic. In NaSch model, the road is divided into cells of length 7.5 meters. Each cell can either be empty or occupied by at most one car. The space, speed, acceleration and even the time are treated as discrete variables. The state of the road at any time-step can be obtained from that at any one time-step ahead by applying acceleration, braking, randomization, and driving rules for all cars at the same time (parallel dynamics). Obviously, such a description is an extreme simplification of the real world conditions. Therefore, a considerable number of modified NaSch CA models have been extended.

For instance, Rickert *et al*. (1996) examined a simple two-lane CA model and pointed out important parameters defining the shape of the fundamental diagram (flow-density). Chowdhury *et al*. (1997) generalized the NaSch model by introducing a particle hopping model for two-lane traffic with two different vehicle speeds (fast and slow). Barlović *et al*. (1998) introduced a velocity-dependent randomization (VDR) parameter, in contrast to the constant randomization in the NaSch model. The VDR model is a simple generalization of the NaSch model leading to a completely different jam dynamics, i.e., the existence of wide phase separated jams and metastable free-flow states. Wang *et al*. (2000) introduced Fukui-Ishibashi (FI) model to investigate the asymptotic self-organization phenomena of one-dimensional traffic flow. From the point of view of practical applications, modeling vehicular traffic on multi-lane highways are more relevant than that on idealized single-lane highways, which are, nevertheless, interesting from the point of fundamental understanding of true non-equilibrium phenomena in driven-diffusive lattice gases (Chowdhury *et al*., 2000). Rickert et al. (1996) examined a simple two-lane CA model and pointed out important parameters defining the shape of the traffic fundamental diagram. Chowdhury *et al*. (1997) generalized the NaSch model by introducing a particle hopping model for two-lane traffic with two speed types (fast and slow) of vehicles. Nagel (1996, 1998) employed the concept of stochastic traffic cellular automata (STCA) and treated each particle with randomized integer speed between zero and maximum speed. Nagel *et al*.

(1998) proposed a simple lane-change model — if vehicles are fulfilled both incentive criterion and safety criteria, they will change the positions to the available adjacent lane(s).

Using CA simulations to explore the formation of traffic patterns, including the vehicular trajectories, flow-occupancy fundamental diagrams, spatiotemporal traffic features associated with stationary and moving bottlenecks, among others, is a challenging task. But it can provide with more insightful information to help understand the formation of traffic phenomena so as to evaluate the effectiveness of any promising control or management tactics. Many scientists have been searching for the fundamental principles governing the dynamics of traffic flow. Treiterer (1975) used a series of aerial photography to analysis phantom jams, which may be induced due to spontaneous velocity fluctuations or lane changes. Hermann and Kerner (1998) applied CA technique and self-organization process to explore the formation of traffic congestion. Knospe *et al*. (1999) dealt with the effect of slow cars in two-lane systems and found that even few slow cars can initiate the formation of platoons at low densities. Wolf (1999) employed a modified NaSch model to address the metastable states at the jamming transition in detail. Research to improve the behavior of CA models by finer discretization of cells was carried out by Knospe *et al*. (2000). Pottmeier *et al*. (2002) studied the impact of localized defect in a CA model for traffic flow exhibiting metastable states and phase separation. Kerner (2002; 2002; 2004) introduced a three-phase traffic theory which consists of free flow, synchronized flow and wide moving jam phases. The later two phases exist in congested states where downstream front of the synchronized flow phase is often fixed at a bottleneck but the wide moving jam will propagate through the spatial locations of the bottleneck. To explore the emergence of such traffic patterns, Kerner and partners have shown complex spatiotemporal behaviors based on empirical freeway traffic analysis. (e.g., Kerner *et al*., 1996, 1998, 2002, 2004). Bham and Benekohal (2004) developed a high fidelity traffic simulation model based on CA and car-following concepts, which had been satisfactorily validated at the macroscopic and microscopic levels using two sets of field data.

Most of the aforementioned conventional traffic flow models are based on the assumption of the homogeneity of traffic flow. In addition, recent CA models are mainly developed assuming identical vehicle parameters. These models can be used to simulate the interactions of individual vehicles in traffic vehicular system; however, they cannot demonstrate the real vehicle traffic conditions due to the lack of consideration of the driver heterogeneity in individual characteristics and driving behaviors. Except for Lan and

Chang's works (2003, 2005), few have devoted to mixed traffic flows, composed of different vehicle types. In reality, mixed traffic is prevailing around the world either in developed or under developing countries. For instance, bicycles, motorcycles, rickshaws or tricycles, cars, vans, mini-buses, regular buses and even articulated buses are ubiquitous in urban streets. Cars, coaches, trucks, trailers and even twin-trucks are very popular in freeways. Some of such different-dimensioned vehicles, with different in length and width, may share the same lane while moving (e.g., a motorcycle and a car can move together in one single lane that is used by a bus). Moreover, these vehicles also move with different parameters (e.g., different acceleration/deceleration rate, desired speed and different safe driver speeds). There are heterogeneous behaviors across drivers (e.g., aggressive or timid driver) with very different characteristics. For the purpose of planning, design and operational control, it is always important to capture the traffic flow features so that more realistic traffic flow models can be developed to better represent the prevailing traffic situations.

To accommodate different vehicle types moving on the surface streets, Lan and Chang (2005) first developed inhomogeneous CA models to elucidate the interacting movements of cars and motorcycles in mixed traffic contexts. The car and motorcycle are represented by non-identical particle sizes that respectively occupy 2×6 and 1×2 cell units; each cell is of 1.25×1.25 meters. To accommodate different vehicle types moving on the freeways, Lan and Hsu (2005, 2006 and 2007) first introduced generalized definitions of spatiotemporal occupancy, flow and speed to precisely capture the collective behavior of traffic features. They further introduced a common unit (CU) of 1.25×1 meters to represent a "fine cell" and a "fine site" that can satisfactorily gauge the non-identical vehicle sizes and the non-identical lane widths, respectively. The concept of CU has major advantages for CA simulations in describing the different vehicle sizes moving on non-identical lane widths existent in different roadways.

1.2 Motivation

The core logic of CA modeling was to introduce several simple update rules for vehicle movement in computer programs to efficiently simulate the complicated interactive traffic behaviors. A considerable number of CA models have been developed to date; most of them, however, only focused on pure traffic (single type of vehicle) with coarse cell units in the simulations. Very little has devoted to the heterogeneous traffic situations (vehicles of the

same type moving in different speeds, accelerations, and decelerations) and/or mixed traffic contexts, which comprise different types of vehicle (e.g., light and heavy vehicles). This study, therefore, will develop CA models to look into the spatiotemporal behaviors for heterogeneous mixed traffic on freeway.

In the well-known NaSch (1992) CA model and the subsequent modified NaSch models, the road is divided into squared cells of length 7.5 meters. Obviously, such a coarse description of cells is an extreme simplification of the real world conditions. Therefore, this study motivates to refine the cells so as to capture the sizes of different vehicle types in a more realistic manner.

The slow down rule of NaSch's model will lead to abrupt speed drops occasionally emerged during the simulations. The acceleration rule proposed by Knospe *et al*. (2000) and Jiang and Wu (2003) still exhibited the deficit of abrupt change in speed at the upstream front of traffic jam. This study therefore motivates to rectify the abrupt speed drops by introducing limited deceleration capabilities when vehicles are confronted with stationary obstacles, traffic jams or signalized intersections.

The refined model is developed to explore pure-homogeneous, mixed-homogeneous, pure-heterogeneous, and mixed-heterogeneous traffic. The empirical traffic flow features, such as the traffic hysteresis and capacity drop can also be reproduced by mixed traffic, even no randomization is considered.

1.3 Research Objectives

This study proposes CA models for heterogeneous traffic flow with consideration of the heterogeneity of drivers' characteristics and driving behaviors. There are some objectives in this research:

1. Introduce a concept of "common unit (CU)" to represent a "fine cell" and a "fine site" that can satisfactorily gauge the non-identical vehicle sizes and the non-identical lane widths, respectively. The concept of CU has major advantages for CA simulations in describing the different vehicle sizes moving on non-identical lane widths existent in different roadways.

2. Redefine the traffic variables in the spatiotemporal (3-D) domain so as to precisely capture the collective traffic behavior and to reveal the traffic features.

3. Propose basic CA rules to explore the fundamental traffic features.

4. Propose revised CA rules, including anticipation effect, slow-to-start, lane change, and interaction among vehicles to explore the fundamental traffic features.

5. Propose refined CA rules using Forbes' car-following concept associated with a piecewise-linear movement to rectify the abrupt deceleration existent in conventional CA models.

6. Exploring the discrepancy among the different fundamental diagrams that derived from various traffic scenarios (pure-homogeneous, mixed-homogeneous, pure-heterogeneous, and mixed-heterogeneous), especially those profiles in the congested traffic flow phases.

All of the proposed CA models in this study will be limited in the freeway contexts.

1.4 Chapters Organization

Given the objectives, the research framework was illustrated in Figure 1-1. The research is organized as follows. Chapter one introduces the background of the research. Chapter two discusses literature review. Chapter three defines the "common unit" used in this study, the global traffic variables including occupancy, speed and flow, and the local traffic variables are defined. Chapter four develops a basic CA model with applications on the fundamental diagrams and the speed distributions at specific instantaneous time-steps and at two specific locations in pure traffic contexts. Chapter five develops a revised CA model with applications on moving and fixed bottlenecks in heterogeneous mixed traffic contexts. Chapter six proposes a refined CA model to rectify the abrupt speed drop existent in most previous CA models. Chapter seven concludes this research with some future research recommended.

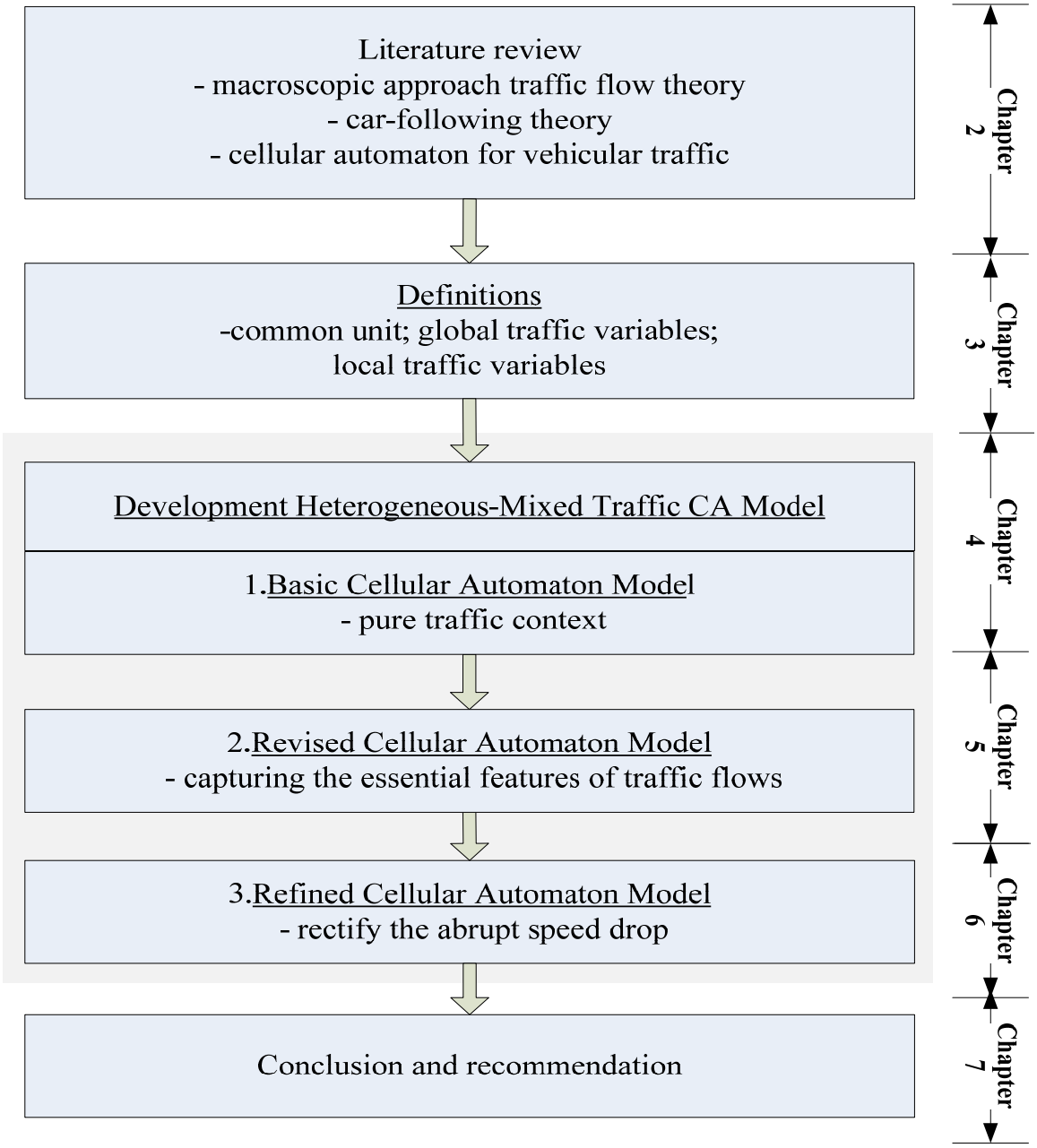

FIGURE 1-1 Research framework.

Chapter 2 LITERATURE REVIEW

The conventional traffic flow models have three different conceptual frameworks. The macroscopic traffic stream models, the traffic is view as a compressible fluid, are mostly devoted to elucidating the relations between speed, density and flow in various traffic conditions (e.g., free flow, capacity flow, jammed flow) and roadway environments (e.g., tunnel, freeway, urban arterial) (May, 1990). The fluid-dynamical description models analogize vehicular flows to fluids by assuming the aggregate homogeneous behavior of drivers. The microscopic traffic flow models, in contrast, describe the interrelationship of individual vehicle movements with other vehicles. In the microscopic theories vehicular traffic is treated as a system of interacting particles driven far from equilibrium (Chowdhury, Santen, and Schadschneider, 2000). A third approach of traffic stream models is mesoscopic models that fill the gap between the macroscopic traffic stream models and the microscopic ones (Daganzo, 1994, 1995, and 1999). Recently, various cellular automata (CA) models, comprehensive based on the aforementioned conventional traffic flow theory, have been developed to describe the phenomena of real traffic flows characterized with complex dynamic behaviors.

The chapter consists of three sections. Section 2.1 addresses the macroscopic models of the conventional traffic flow theory. Section 2.2 discusses the microscopic models-car-following theory. Section 2.3 addresses the related vehicular traffic of cellular automata models.

2.1 Macroscopic approaches

Lighthill and Whitham (1955) and Richard (1956) treated the flow (vehicles per hour) as function of only the local density (vehicles per miles) and developed the most well-known one-order fluid-dynamical (LWR) models. The shock wave theory used by LWR model was to explain many traffic phenomena such as congested traffic upstream of a freeway bottleneck. Other researchers such as Payne (1971), Liu *et al*. (1998) and Zhang (1998) derived high-order similar models. Wong and Wong (2002) formulated a multi-class traffic flow model as an extension of LWR model with heterogeneous drivers. The main concepts are described as follow:

2.1.1 Conservation law equation

When viewing from an aircraft at a freeway, one can imagine the vehicular traffic flow is regarded as a stream. Due to this analogy, traffic is explained in relationship of flow,

density, and speed. For a road section with an upstream and downstream observing station (as shown in Figure 2-1), the conservation law can be simply formulated as the equations (2-1~2-3) (Kühne, 1998):

$$\Delta q = \frac{N_2 - N_1}{\Delta t} \tag{2-1}$$

$$\Delta k = \frac{-(N_2 - N_1)}{\Delta x} \tag{2-2}$$

$$\frac{\Delta q}{\Delta x} + \frac{\Delta k}{\Delta t} = 0 \tag{2-3}$$

where N_1 represents the incoming vehicles amount passing station 1 for a period of time, Δt. N_2 is the outgoing vehicles amount passing station 2. Δx is the distance between these two stations. q represents the flow and k, the density.

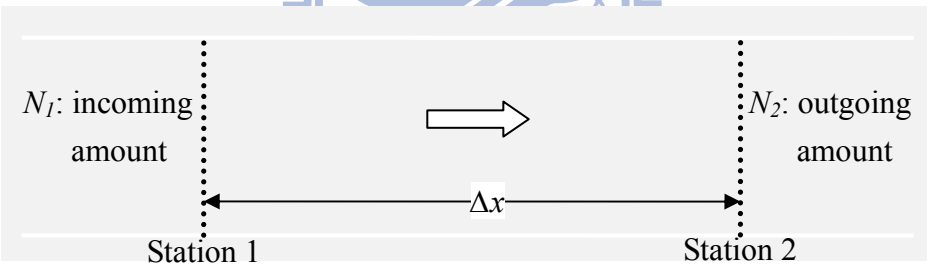

FIGURE 2-1 An illustration for the road section with two observing stations.

For a freeway with entering or exiting traffic, the continuity of the traffic flow can be formulated as the equation (2-4). The *k(x, t)* represents the density and *q(x, t)* is the flow at location *x* at instant of time *t*. (Chowdhury *et al.*, 2000):

$$\frac{\partial k(x,t)}{\partial t} + \frac{\partial q(x,t)}{\partial x} = \sum_{i=1}^{q_{in}} \alpha_i (x - x_i, t) - \sum_{j=1}^{q_{out}} \beta_j (x - x_j, t) \tag{2-4}$$

where the first term on the right hand side, $\sum_{i=1}^{q_{in}} \alpha_i(x - x_i, t)$ represents entering sources at the q_{in} on-ramps located at x_i ($i=1,2,\ldots,q_{in}$). The next term on the right hand side, $\sum_{j=1}^{q_{out}} \beta_j(x - x_j, t)$ takes care of exiting sinks, the q_{out} off-ramps located at x_j ($j=1,2,\ldots,q_{out}$).

The above equation (2-4) can be further simplified, if it reflects a highway with no entries or exits ramp. Under such special circumstances the equation (2-4) reduces to the simpler form (Lighthill and Whitham, 1955) as the following equation (2-5).

$$\frac{\partial \rho(x,t)}{\partial t} + \frac{\partial q(x,t)}{\partial x} = 0 \tag{2-5}$$

2.1.2 LWR model (Lighthill-Whitham-Richards model)

Lighthill and Whitham (1955) and Richards (1956) used the hypothesis about the fundamental diagram. The flow rate q is a function of the vehicle density ρ:

$$q = q(\rho) \tag{2-6}$$

Using equation (2-6), the balance equation (2-5) takes the form as equation (2-7):

$$\frac{\partial \rho(x,t)}{\partial t} + \frac{\partial q(\rho(x,t))}{\partial x} = 0 \tag{2-7}$$

Therefore, there is now only one independent variable in the equation (2-7), the vehicles density ρ (Figure 2-2). This makes it possible to solve this equation if initial and boundary conditions are given. Thus, the application of the hypothesis about the fundamental diagram leads to a solvable traffic flow model.

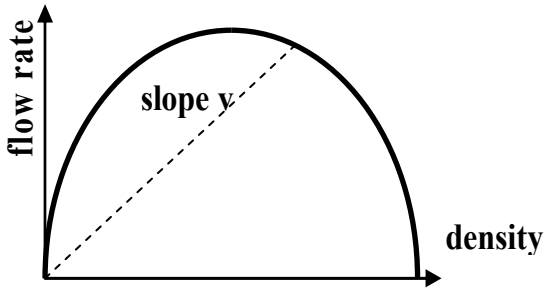

FIGURE 2-2 The theoretical fundamental diagram.

Solutions of the Lighthill-Whitham-Richards (LWR) model, equation (2-6), (2-7) are kinematic waves moving with the velocity.

$$\text{Kinematic Waves (KW)} \quad c = \frac{dq(\rho)}{d\rho} \tag{2-8}$$

The KW velocity is a function of the density as shown in equation (2-8). The KW velocity is positive on the part of the flow-density diagram where the flow rate increases with density, and it is negative on the part of the flow-density diagram where the flow rate decreases with density. Equation (2-8) would leads to turnover of the KW front in some conditions. Then a shock wave is formed (figure 2-3). This shock wave would propagate at the KW velocity (May, 1990).

$$q_1 = v_1\rho_1, \qquad q_2 = v_2\rho_2 \tag{2-9}$$

$$v_s = \frac{q(\rho_2) - q(\rho_1)}{\rho_2 - \rho_1} \tag{2-10}$$

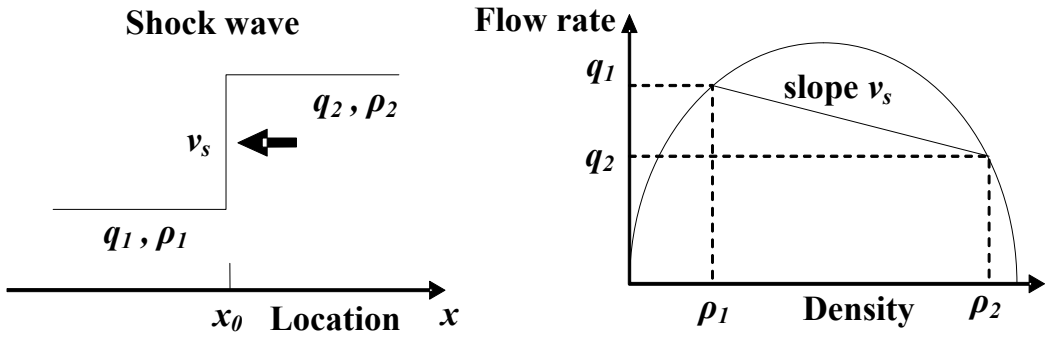

FIGURE 2-3 Representation of a shock wave in space and in the fundamental diagram.

2.2 Microscopic approaches

The microscopic models, on the other hand, describe the interrelationship of individual vehicle movements interacted with other vehicles. These models of vehicular traffic attention are focused on individual vehicle each of which is represented by a "particle". Car-following models are the most pertinent ones to explicate the one-dimensional movements in a longitudinal lane such that the following vehicle adjusts its speed to maintain desirable or safe distance headways with the lead vehicle. Stimulus-response model is perhaps the most prominent type developed in the 1950s and 1960s by the General Motors (GM) research group, which is still being applied or extended (Rothery, 1998; Brackstone, and McDonald, 1999; Chakroborty, and Kikuchi, 1999; Lan, and Yeh, 2001). The main concepts are described as follows:

2.2.1 Stimulus-Response model

The concept of car following on a motorway indicates a driver reacts to the altering headway with his predecessor the behavior of a driver. The main idea is that a driver will through control of the vehicle deceleration and acceleration to maintain a suitable distance and time gap between it and the vehicle that precedes it in the same lane. Many studies have been devoted to find mathematical formulas to descript the following behavior of the individual driver. The starting point of define the equation of motion is usually the analogue of the Newton's equation for each individual vehicle. In Newtonian mechanics, the acceleration of the vehicle may be considered as the vehicle response to stimulus from other vehicle. This approach assumes within a range of distance, a stimulus-response relationship exist. The basic stimulus-response equation can be expressed as follows:

$$[response]_n = \lambda \times [stimulus]_n \tag{2-11}$$

where n represents number of vehicle. λ is a proportionality factor.

The stimulus function can be composed of many factors: the speed of the vehicle, distance headway (spacing), relative speed, etc. Each driver can respond to the surrounding traffic conditions only by accelerating or decelerating the vehicle. Different forms of the equations of motion of the vehicles in the different versions of the car-following models arise from the differences in their postulates regarding the nature of the stimulus. The equation can be expressed as follow:

$$[response]_n(t) = a_n(t) = \ddot{x}_n(t) \tag{2-12}$$

where $x_n(t)$ is the location of the n^{th} vehicle at time t. The stimulus-response relationship can be further expressed as follow equation (2-13):

$$\ddot{x}_n = f_{sti}(v_n, \Delta x_n, \Delta v_n) \tag{2-13}$$

where the function f_{sti} represents the stimulus by the n^{th} vehicle. v_n is the speed, Δx_n represents the distance headway (spacing), Δv_n represents relative speed of the n^{th} vehicle, accordingly.

2.2.2 Follow-the-leader model

Chandler *et al*. (1958) proposed the first follow-the-leader model, the different in the velocities of the following n^{th} and the leading $n+1^{th}$ vehicles was supposed to be the stimulus for the n^{th} vehicle as shown in equation (2-14). It was assumed that every driver be likely to keep with the synchronized velocity as that of the front vehicle. Joining the equation (2-12) into equation (2-14), the stimulus-response relationship becomes equation (2-15):

$$[stimulus]_n(t+T) = v_{n+1}(t) - v_n(t) \tag{2-14}$$

$$\ddot{x}_n(t+T) = \lambda[\dot{x}_{n+1}(t) - \dot{x}_n(t)] \tag{2-15}$$

where T is a response time.

2.2.3 Pipes car-following model

Pipes (1953) car-following theory is a linear model that depicts vehicular traffic behavior. The equation is derived by differentiating from equation (2-15) with respect to time. The first term of equation (2-16) in right hand side means that with the purpose of avoid crash with the leading vehicle, each driver must keep a safe distance ($(\Delta x)_{safe}$) from the leading vehicle. The second term of equation (2-16) in right hand side represents that: if the velocity of the n^{th} vehicle is higher, the spacing to its leading vehicle needs to keep larger. It can be further explain that drivers obey the driving laws recommended in the California Motor Vehicle Code, leave one car length in front for every 10 miles per hour of speed increase. The equation can be expressed as the form:

$$\Delta x_n(t) = x_{n+1}(t) - x_n(t) = (\Delta x)_{safe} + \tau\, \dot{x}_n(t) \tag{2-16}$$

where τ sets the time scale.

Forbes *et al*. (1958, 1963) proposed that the reaction time, τ, is larger when the distance headway increases and vice versa. The main concepts of Forbes's car-following model can be expressed as equation (2-17).

$$\ddot{x}_n(t) = \frac{1}{\tau}(\dot{x}_{n+1}(t) - \dot{x}_n(t)) \tag{2-17}$$

2.2.4 GM Models

A series of models have been developed in the 1950s and 1960s by Herman and his colleagues at the General Motors Research Laboratories (Chandler, Herman, and Montroll, 1958; Gazis, Herman, and Potts, 1959; Gazis, Herman, and Rothery, 1961) to address microscopic approaches that focused on describing the driver car-following behaviors. Five generations of the GM car-following models are recognized and they provided an essential contribution to realize the traffic flow. Nowadays they are still applied in various aspects, including traffic stability and safety studies, level of service and capacity analysis, driver's reaction times, etc.

$$\ddot{x}_{n+1}(t+T) = \alpha\,[\dot{x}_n(t) - \dot{x}_{n+1}(t)] \qquad (m=0, l=1) \tag{2-18}$$

where α is the sensitivity coefficient, a experimental constant independent of n, and α varies from 0.17~0.74.

$$\ddot{x}_{n+1}(t+T) = \alpha_i\,[\dot{x}_n(t) - \dot{x}_{n+1}(t)] \qquad (m=0, l=1) \tag{2-19}$$

where α_1 is the coefficient for driving in platoon; α_2 is the coefficient for driving not in platoon.

$$\ddot{x}_{n+1}(t+T) = \left[\frac{\alpha_0}{x_n(t) - x_{n+1}(t)}\right][\dot{x}_n(t) - \dot{x}_{n+1}(t)] \qquad (m=0, l=1) \tag{2-20}$$

$$\ddot{x}_{n+1}(t+T) = \left[\frac{\alpha_0 \dot{x}_{n+1}(t+T)}{x_n(t) - x_{n+1}(t)}\right][\dot{x}_n(t) - \dot{x}_{n+1}(t)] \qquad (m=1, l=1) \tag{2-21}$$

$$\ddot{x}_{n+1}(t+T) = \left[\frac{\alpha_{lm}(\dot{x}_{n+1}(t+T))^m}{(x_n(t) - x_{n+1}(t))^l}\right][\dot{x}_n(t) - \dot{x}_{n+1}(t)] \tag{2-22}$$

2.2.5 Car-following theory for multiphase

Zhang and Kim (2005) hypothesize that drivers drive differently in different traffic situations and present a new car-follow theory that can reproduce both the capacity drop and traffic hysteresis, two prominent features of multiphase vehicular traffic flow. Conventional car-following models treat both drivers and roads as homogeneous entities—that is, they are modeling identical drivers who travel on homogeneous roads (Figure 2-4 (a)). The traffic that produces capacity drops and hysteresis loops, on the other hand, comprises diverse groups of drivers who travel on inhomogeneous roads and may behave differently under different driving conditions. A plausible car-following theory that explains these nonlinear phenomena must consider these inhomogeneities (Figure 2-4 (b)).

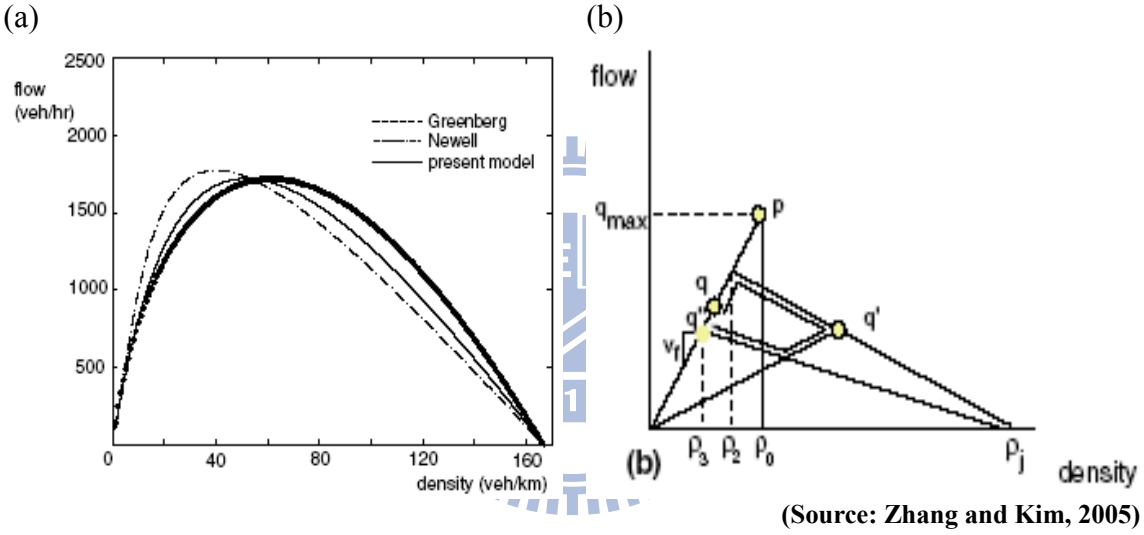

(Source: Zhang and Kim, 2005)

FIGURE 2-4 Comparison the homogeneous and inhomogeneous car-following models with fundamental diagrams.

2.2.6 Optimal velocity (OV) models

The main concept of the optimal velocity models is depicted the driving strategy of the driver when following the leading vehicle. The formulas can be expressed as equation (2-23):

$$\ddot{x}_n(t) = \frac{1}{\tau}[V_n^{desired}(t) - v_n(t)] \tag{2-23}$$

where $V_n^{desired}$ is the desired speed of the n^{th} vehicle at time t. In the equation (2-15) of follow-the-leader model, driver tends to keep the same speed of the leading vehicle, $V_n^{desired}(t) = \dot{x}_{n=1}(t)$. The optimal velocity models assume that $V_n^{desired}$ depends on spacing, Δx_n of the n^{th} vehicle as shown in equation (2-24). A more realistic model that driver can keep optimal velocity based on corresponding spacing are shown in equation (2-25). (Bando *et al*., 1994; Bando *et al*., 1995; Nakanishi *et al*., 1997; Sugiyama and Yamada, 1997; Chowdhury *et al*., 2000)

$$\ddot{x}_n(t) = \frac{1}{\tau}[V_n^{opt}(\Delta x_n(t)) - v_n(t)] \tag{2-24}$$

$$V^{opt}(\Delta x) = \begin{cases} 0 & \text{for} \quad \Delta x < \Delta x_A \\ f\ \Delta x & \text{for} \quad \Delta x_A \le \Delta x \le \Delta x_B \\ v_{\max} & \text{for} \quad \Delta x_B < \Delta x \end{cases} \tag{2-25}$$

The presentation of OV model depends intensively on the proper decision of the optimal velocity function. Through introduction of appropriate optimal velocity, some important macroscopic characteristics, such as traffic jam and hysteresis effects can be observed.

2.2.7 Traffic hysteresis models

Newell (1965) supposed that drivers react to a stimulus in a different way in their acceleration and deceleration behaviors (Figure 2-5(a)) and developed the hysteresis loop. Treiterer and Myers (1974) first propose the apparent experiment proof of the traffic hysteresis effect. In real traffic environment, the traffic metastable phases have been confirmed to exist, and to be the derivation of the traffic hysteresis. Since the traffic metastable phases, the relationship of traffic flow and density will not be one-to-one association. Koshi *et al*. (1983) analyzed empirical traffic data and proposed the well known flow–density diagrams (Figure 2-5(b)).

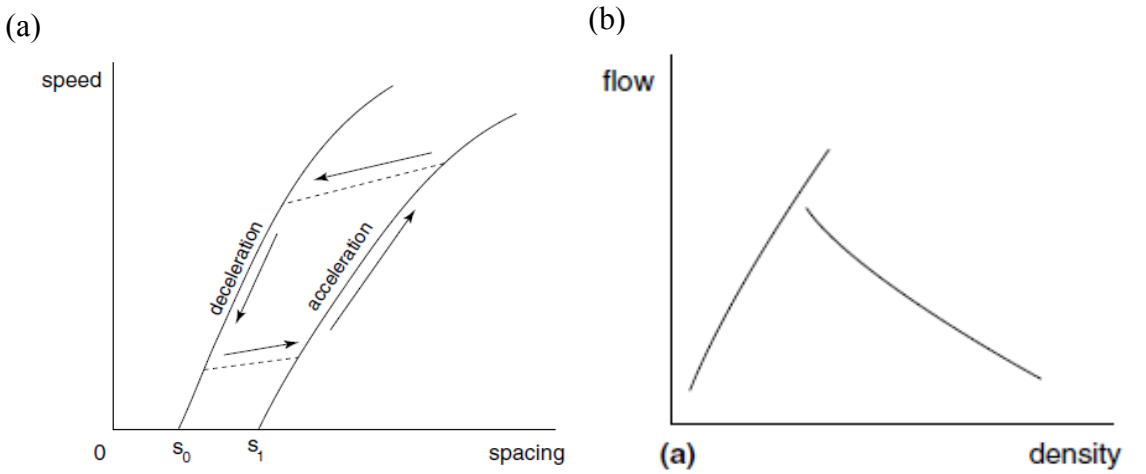

(Source: Zhang and Kim, 2005)

FIGURE 2-5 The relationship of drivers react to a stimulus.

2.2.8 Gap acceptance models

Gap acceptance models have shown success to capture drivers' decision to carry out various maneuvers (e.g. Mahmassani and Sheffi (1981), Hamed *et al*., (1997), Polus *et al*., (2003)). These models suppose the existence of a latent space, which is the value where drivers are unresponsive. More recently, Sheu (2008) proposed to introduce the theorem of quantum mechanics in optical flows to explain the motion-related perceptual phenomena and to model the induced car-following while vehicles approach the incident site in adjacent lanes.

2.3 Related CA approaches

Cellular automaton (CA) is a powerful tool to describe the phenomena of real traffic flows characterized with complex dynamic behaviors. Nagel and Schreckenberg (1992) first proposed the renowned NaSch model to reproduce the basic features of real traffic. In their model, the road is divided into squared-cells of length 7.5 meters. Each cell can either be empty or occupied by at most one car. The space, speed, acceleration and even the time are treated as discrete variables. The state of the road at any time-step is derived from one time-step ahead by applying acceleration, braking, randomization and driving rules for all cars at the same time (i.e., parallel dynamics). Obviously, their coarse description of cells is an extreme simplification of the real world conditions. Therefore, a considerable number of modified NaSch CA rules have been found in the past decade (for instance, Nagel *et al*. (1996, 1998); Rickert *et al*. (1996); Chowdhury *et al*. (1997); Barlović *et al*. (1998)). Other related works that improved NaSch coarse cells with finer cells have also been found (for

instance, Knospe *et al*. (2000); Bham and Benekohal (2004); Lan and Chang (2003, 2005); Lárraga *et al*. (2005)). In addition, Wolf (1999) employed a modified NaSch model to address the metastable states at the jamming transition in detail. Wang *et al*. (2000) introduced NaSch model and Fukui-Ishibashi model to investigate the asymptotic self-organization phenomena of one-dimensional traffic flow. Pottmeier et al. (2002) studied the impact of localized defect in a CA model for traffic flow exhibiting metastable states and phase separation.

2.3.1 NaSch model

NaSch model was proposed by K. Nagel & M. Schreckenber in 1992. Capable of reproduce important entities of real traffic flow, e.g. density-flow relation. Model description, one-lane traffic, divided into cells of length 7.5 m. Each cell can either be empty or occupied by at most one car with discrete velocity: $v=\{0, \ldots, v_{max}\}$ (Figure 2-6).

The state of road at time $t+1$ can be obtained from that at time t by applying the following forward rules:

Step 1 : Acceleration $v_n = \min (v_n + 1, v_{max})$ (2-26)

Step 2 : Braking $v_n = \min (v_n, d_n - 1)$ (2-27)

where d_n is the distance-headway to next vehicle ahead.

Step 3 : Randomization with probability p

$v_n = \max (v_n - 1, 0)$ (2-28)

Step 4 : Driving $x_n = x_n + v_n$ (2-29)

where x_n is the position of n^{th} vehicle.

The NaSch model is a minimal model in the sense that all the four steps are necessary to reproduce the basic features of real traffic; however, additional rules need to be formulated to capture more complex situations.

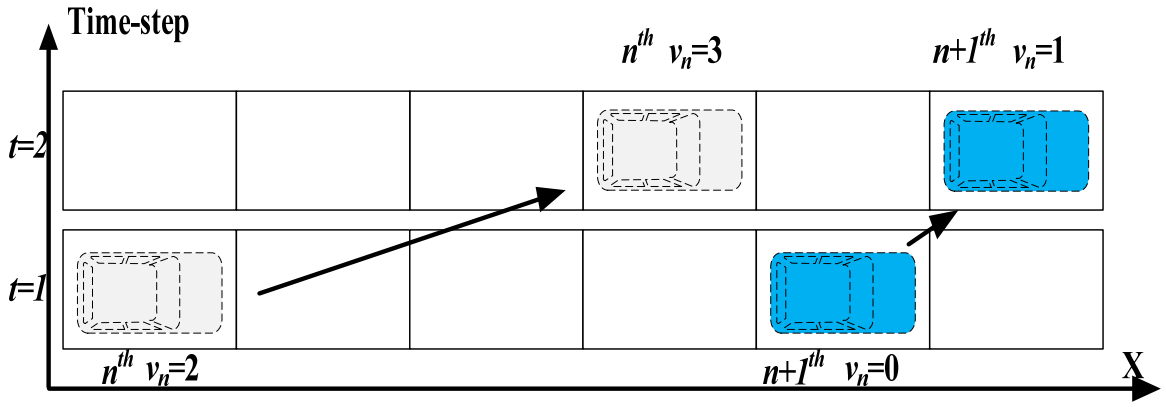

FIGURE 2-6 The action of a single-lane NaSch cellular automaton model.

2.3.2 Velocity-Dependent Randomization (VDR) Model

Barlovic, *et. al*. (1998) based on the original NaSch model, for sake of simulating the phase separation phenomena in real world (Figure 2-7). The randomization parameter is set as:

$$P_n(v_n) = \begin{cases} P_0 & for \quad v = 0, \text{ i.e. outflow from jam} \\ P_n & for \quad v > 0, \text{ i.e. flow in metastable states} \end{cases} \tag{2-30}$$

Usually $P_0 < P_n$, as to reflect the fact that when driving out from the downstream of jams, drivers are more likely to postpone acceleration. This is the so-called slow-to-start case.

The state of road at time $t+1$ can be obtained from that at time t by applying the following rules:

Step 0 : randomization parameter $P_n = P(v_n)$ (2-31)

Step 1 : Acceleration $v_n = \min(v_n+1, v_{max})$ (2-32)

Step 2 : Braking $v_n = \min(v_n , d_n -1)$ (2-33)

Step 3 : Radomization with probability p_n

$$v_n = \begin{cases} \max(v_n - 1, 0) & \text{with probability } P_n \\ v_n & \text{with probability } 1 - P_n \end{cases} \tag{2-34}$$

Step 4 : Movement $x_n = x_n + v_n$ (2-35)

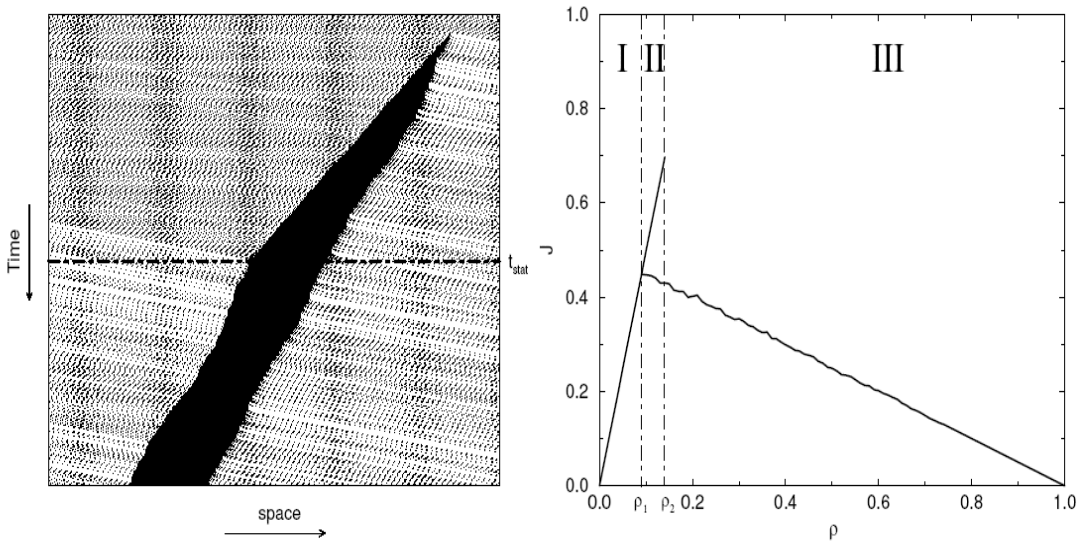

(Source: Barlović, 2003)

FIGURE 2-7 Space-time diagram and fundamental diagram of a spontaneously emerging jam.

2.3.3 Comfortable Driving (CD) Model

Knospe, *et al*. (2000) based on original VDR model and the following driving strategy. At large distances the cars move (apart from fluctuations) with their desired velocity v_{max}. At intermediate distances drivers react to velocity changes of the next vehicle downstream, i.e. to 'brake lights'. At small distances the drivers adjust their velocity such that safe driving is possible. The acceleration is delayed for standing vehicles and directly after braking events.

Randomization parameter P is decided through equation (2-36):

$$P_n(v_n(t), b_{n+1}(t)) = \begin{cases} p_b & \text{if } b_{n+1} = 1 \text{ and } t_h < t_s \\ P_0 & \text{if } v_n = 0 \\ P_d & \text{in all other cases} \end{cases} \quad (2\text{-}36)$$

where P_0, P_d and P_b, depends on the current velocity v_n and b_n is the status of the brake light (on (off)→b_n = 1 (0)). $b_{n+1}(t)$ is the status of the brake light of preceding vehicle n+1th at time t. $d_n = x_{n+1} - x_n - l$ is the gap between consecutive cars (where l is the length of the cars). $t_h = d_n / v_n(t)$ is the temporal headway; $t_s = \min(v_n(t), h)$ is the safety time headway required; h determine the range of interaction with brake light.

Step 0 : Randomization parameter $P_n = P(v_n(t), b_{n+1})$ (2-37)

Step 1 : Acceleration if ($b_{n+1} = 0 \,\&\, b_n = 0$) or $t_h \geq t_s$

then $v_n(t+1) = \min(v_n(t)+1, v_{\max})$ (2-38)

Step 2 : Braking $v_n(t+1) = (v_n(t), d_n^{eff})$

if $v_n(t+1) < v_n(t)$ then $b_n = 1$ (2-39)

where $d_n^{eff} = d_n + \max(v_{anti} - \text{gap}, 0)$; $v_{anti} = \min(v_{n+1}, d_{n+1})$

Step 3 : Randomization if (*rand*()<*P*) then $v_n(t+1) = \max(v_n(t+1) - 1, 0)$

if $P = P_b$,then b_n=1. (2-40)

Step 4 : Movement $x_n(t+1) = x_n(t) + v_n(t+1)$ (2-41)

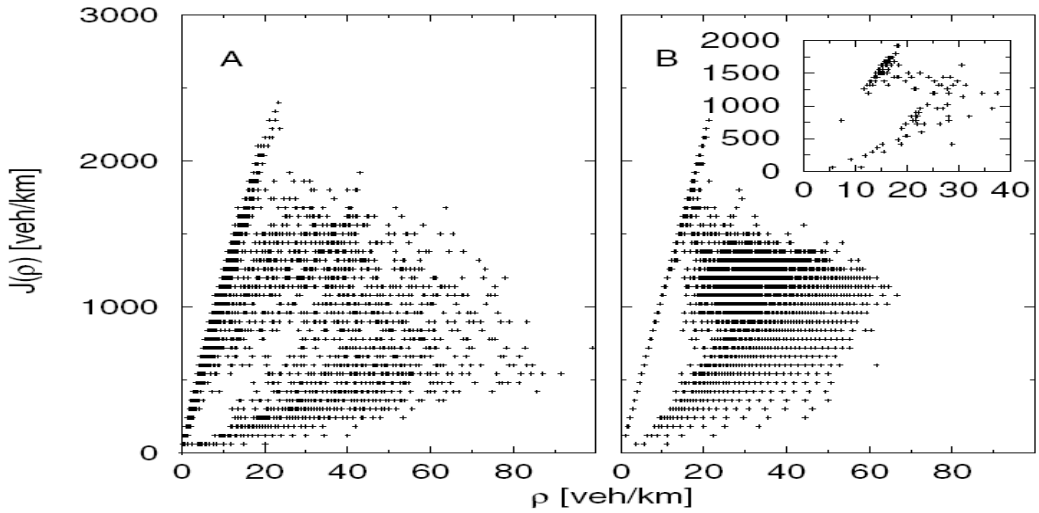

(Source: Knospe, et al., 2000)

FIGURE 2-8 Comparison the CD model simulation result (left) with empirical data (right).

The simulation results of the approach show that the empirical data are reproduced in great detail (Figure 2-8).

2.3.4 Three-Phase traffic Theory

Boris Kerner (2004), a German traffic physician, introduced a three-phase traffic theory which consists of free flow, synchronized flow and wide moving jam phases. The later two phases exist in congested states where downstream front of the synchronized flow phase is often fixed at a bottleneck but the wide moving jam will propagate through the spatial locations of the bottleneck.

To explore the emergence of such traffic patterns, Kerner and partners have shown complex spatiotemporal behaviors based on empirical freeway traffic analysis (Figure 2-9) (see, for example, Kerner and Rehborn (1996); Kerner (1998); Kerner and Klenov (2002); Kerner *et al*. (2002); Kerner and Klenov (2004)). The effect of slow cars in two-lane systems was further studied by Knospe *et al*. (1999) who found that even few slow cars could initiate the formation of platoons at low densities.

Moreover, Kerner (2005) also compared the congested pattern control approach with the free flow control approach at an on-ramp bottleneck with ramp metering. It was found that the congested pattern control approach has higher throughputs on the main road downstream of the bottleneck and considerably lower vehicle waiting times at the light signal on the on-ramp. The upstream propagation of congestion does not occur even if large amplitude perturbations appear in traffic flow.

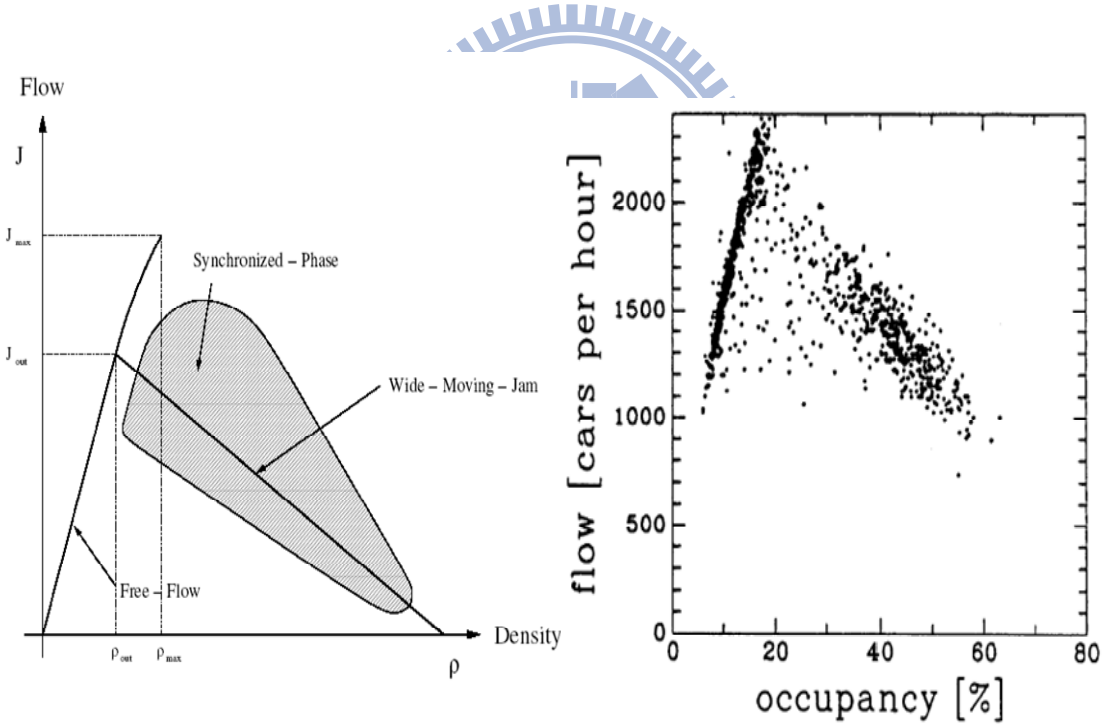

(Source: Barlović, 2003) **(Source: Nagel and Schreckenberg, 1992)**

FIGURE 2-9 Comparison the fundamental diagrams of three-phases interpretation and real traffic.

2.4 Summary

Most of the aforementioned conventional traffic flow models are based on the assumption of the homogeneity of the system. In addition, recent CA models are mainly developed assuming identical vehicle parameters. These models can be used to simulate the interactions of individual vehicles in traffic vehicular system; however, they cannot demonstrate the real vehicle traffic conditions due to the lack of consideration of the driver heterogeneity in individual characteristics and driving behaviors. In reality, mixed traffic is prevailing around the world either in developed or under developing countries. Some of such different-dimensioned vehicles, with different in length and width, may share the same lane while moving. Moreover, these vehicles also move with different parameters (e.g., different acceleration/deceleration rate, different desired speeds and safe driver speeds). There are heterogeneous driving behaviors across drivers with very different characteristics. It is always important to capture the traffic flow features so that more realistic traffic flow models can be developed to better represent the prevailing traffic situations.

Chapter 3 DEFINITIONS

This chapter introduces the definitions applied in this research. Section 3.1 addresses the common unit for cells and sites; the global traffic variables are introduced in Section 3.2; the local traffic variables are introduced in Section 3.3, followed by a summary in Section 3.4.

3.1 Common Unit for Cells and Sites

Lan and Chang (2005) first developed inhomogeneous CA models to elucidate the interacting movements of cars and motorcycles in mixed traffic on surface roads. The car and motorcycle in their study are represented by non-identical particle sizes that occupy 6×2 and 2×1 cell units, respectively. Each cell is a squared grid of 1.25×1.25 meters, which is regarded as a "common unit (CU)" of the non-identical vehicle sizes. The concept of CU has advantages of describing the inhomogeneous vehicle sizes and of accommodating non-identical lane widths in various roadway environments, while CA simulations are performed. This research continues to use the word "cells" to describe the vehicles but will use the concept of CU to gauge the different vehicle types. In line with the physical dimensions and their required clearances for safe movement, for instance, a bicycle or a motorcycle can be defined as a small-sized particle of 2×1 CUs. A car can be defined as a median-sized particle of 6×2 CUs. A single-unit truck or a regular bus can be defined as a large-sized particle of 12×3 CUs. Of course, other types of vehicles, such as rickshaw or tricycle, semi-trailer, trailer, twin-truck, and articulated bus, can also be defined in terms of different common units of cells.

To accommodate different vehicle types moving in various widths of lanes or roadways, this research uses another term, "sites," to represent the two-dimensional roadway space. This research propose the CA traffic simulation models to elucidate the behavior of vehicles moving in a longitudinal (X) direction and transverse (Y) direction of a two-dimensional (2-D) roadway space. The dimensions of sites, cells and the rules of vehicle movements are defined in such a way that they can best conform to the mixed traffic context. The roadway is composed of numerous identical "sites," each of which is also a squared grid of 1.25×1.25 meters, which has exactly the same size as one cell, the basic CU in gauging the vehicles. Thus, each "site" in this study will be exactly occupied or unoccupied by a "cell." A 3.75-meter (12-feet) standard freeway lane is equivalent to a lane width of three sites. Likewise, a 2.5-meter urban narrow street lane can be regarded as a lane width of two sites. The vehicle sizes and roadway spaces defined by a common unit (CU) were depicted in Figure 3-1.

To further reflect the situations for Taiwan freeways where speed limit is 110 kph, this study continues to use the concept of CU proposed by Lan and Hsu (2005, 2006), but will reduce the CU size to a grid of 1.25×1.0 meters. Therefore, the maximum speed of CA simulations can be set equal to 31sites/sec (111.6 *kph*), very close to the speed limit (110 *kph*), and the incremental speed for vehicles is 1 meter per time-step (3.6 *kph*). Since each "site" will also be exactly occupied or unoccupied by a "cell," the dimension of a "site" in this study must be defined as a grid of 1.25×1.0 meters. A 3.75-meter (12-feet) standard freeway lane is equivalent to a lane width of "three sites." Likewise, a 2.5-meter urban narrow street can be regarded as a lane width of only "two sites." Accordingly, a car is defined as a median-sized particle of 2×6 cells whereas a twin-truck is defined as a super large-sized particle of 3×24 cells. Of course, other types of vehicles, such as motorcycle, bus, and single-unit truck can also be defined in terms of different common units of cells.

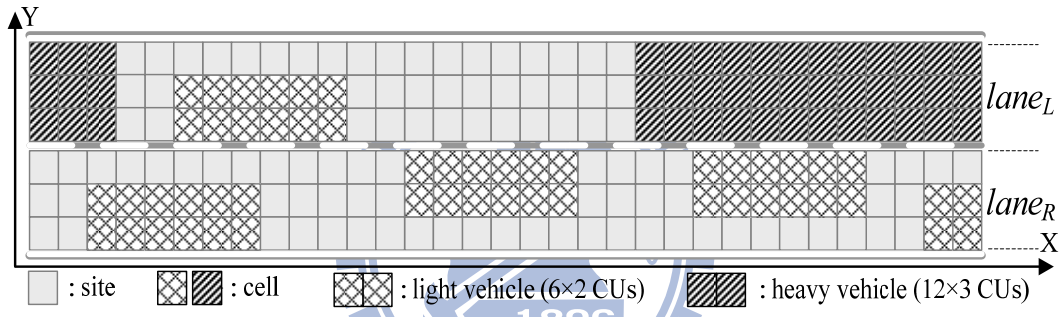

FIGURE 3-1 Heterogeneous vehicle sizes and roadway spaces defined by a common unit (CU) of grid-cell and grid-site.

3.2 Global Traffic Variables

3.2.1 Generalized Traffic Variables

1. Density

The conventional density at a specific time t over a road section of length L is defined as the number of vehicles $n(t)$ observed in a photograph of the section at the given time divided by the length of the section, expressed in first term of eq. (3-1). Multiplying the numerator and denominator of this expression by a small time interval, Δt, the average density over a thin vertical rectangular region $L \times \Delta t$ formed by the dotted lines of Figure 3-2 can be defined as "the ratio of total time spent in time-space region (e.g., veh-hrs.) to the area of that time-space region (e.g., mile-hrs.)," also expressed in eq. (3-1), see, for example, Daganzo (1997).

$$k(t) = \frac{n(t)}{L} = \frac{n(t)\Delta t}{L\Delta t} \tag{3-1}$$

The density over a large rectangular region A, of length L and width T formed by the bold lines of Figure 3-2, $k(A)$, can therefore be defined as:

$$k(A) = \frac{\sum_{\Delta t} n(t)\Delta t}{\sum_{\Delta t} L\Delta t} = \frac{t(A)}{|A|} \tag{3-2}$$

where $t(A)$ is the total time spent in A and $|A|$ denotes the area of A.

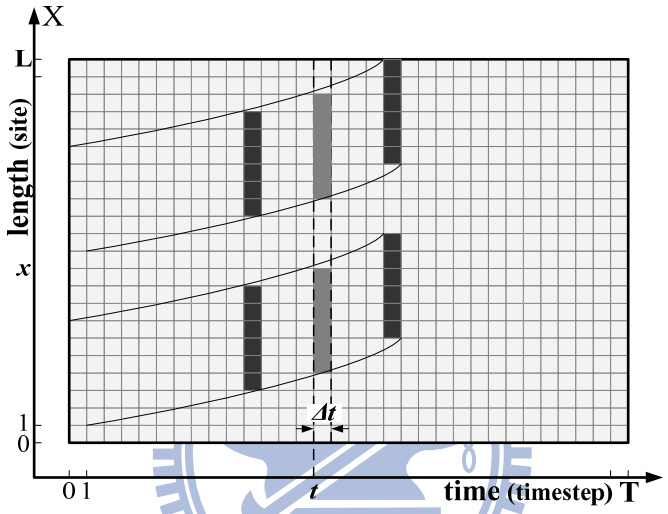

FIGURE 3-2 An illustration of generalized definition of density over a space-time rectangular region.

2. Flow

The conventional flow rate at a specific stationary location x over a period of observed time T is defined as the number of vehicles $m(x)$ passing through that stationary location divided by the period of time, expressed in first term of eq. (3-3). Likewise, multiplying the numerator and denominator of this expression by a small distance interval, Δx , the average flow over the thin horizontal rectangular region $T \times \Delta x$ formed by the dotted lines of Figure 3-3 can be defined as "the ratio of total distance traveled in time-space region (e.g., veh-miles.) to the area of time-space region (e.g., mile-hrs.)," also expressed in second term of equation (3-3).

$$q(x) = \frac{m(x)}{T} = \frac{m(x)\Delta x}{T\Delta x} \tag{3-3}$$

Thus, the flow over the same rectangular region A, of length L and width T formed by the bold lines of Figure 3-3, $q(A)$, can be defined as:

$$q(A) = \frac{\sum_{\Delta x} m(x)\Delta x}{\sum_{\Delta x} T\Delta x} = \frac{d(A)}{|A|} \tag{3-4}$$

where $d(A)$ represents the total distance traveled in A.

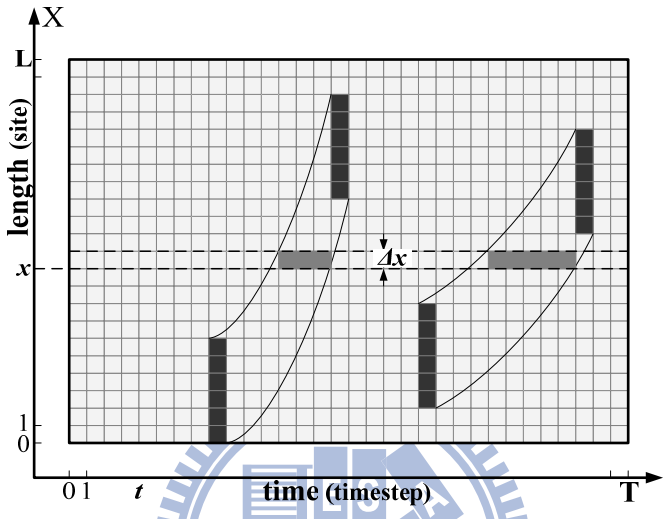

FIGURE 3-3 An illustration of generalized definition of flow over a space-time rectangular region.

3. Space-mean-speed

The ratio of eq. (3-4) to eq. (3-2) becomes the space-mean-speed in A, which can be further reduced to "the ratio of the total distance traveled to the total time spent by all vehicles in A," as expressed in eq. (3-5):

$$v(A) = \frac{q(A)}{k(A)} = \frac{d(A)}{t(A)} \tag{3-5}$$

3.2.2 Spatiotemporal Traffic Variables

The above generalized density, flow and speed are defined on vehicle (or particle) basis over a 2-D time-space region (Daganzo, 1997). Such definitions may not exactly depict the collective behaviors of traffic moving over a 3-D domain, including 2-D for the roadway (longitudinal and transverse) and 1-D for the time. To be precise in the CA simulations, this research need to redefine the traffic variables in a 3-D spatiotemporal domain on site or cell basis, not on vehicle basis. Therefore, the study proposes new

definitions of traffic variables in spatiotemporal sense so as to precisely facilitate the following simulations on various sizes of vehicles sharing the same "lane" in mixed traffic contexts.

To regard a vehicle as several cells and to reflect the realistic traffic movement in a 2-D road, this study defines the instantaneous approach-based occupancy ($\rho(t)$) , a proxy of instantaneous density, as:

$$\rho(t) = \frac{N_o(t)}{N} = \frac{\sum_{\Delta y} N_{0\Delta y}(t)}{N} \tag{3-6}$$

where the denominator N stands for the total number of sites in road and the numerator $N_0(t)$ represents the total number of sites occupied by cells of vehicles at instantaneous time t in road. Hence, N-$N_0(t)$ represents the instantaneous total number of empty (unoccupied) sites in road. $N_{0\Delta y}(t)$ represents the total number of sites occupied by cells in the specific transverse slice Δy at instantaneous time t . Figure 3-4 and figure 3-5 illustrate the instantaneous approach-based occupancy that is summation all the specific transverse slice Δy at instantaneous time t.

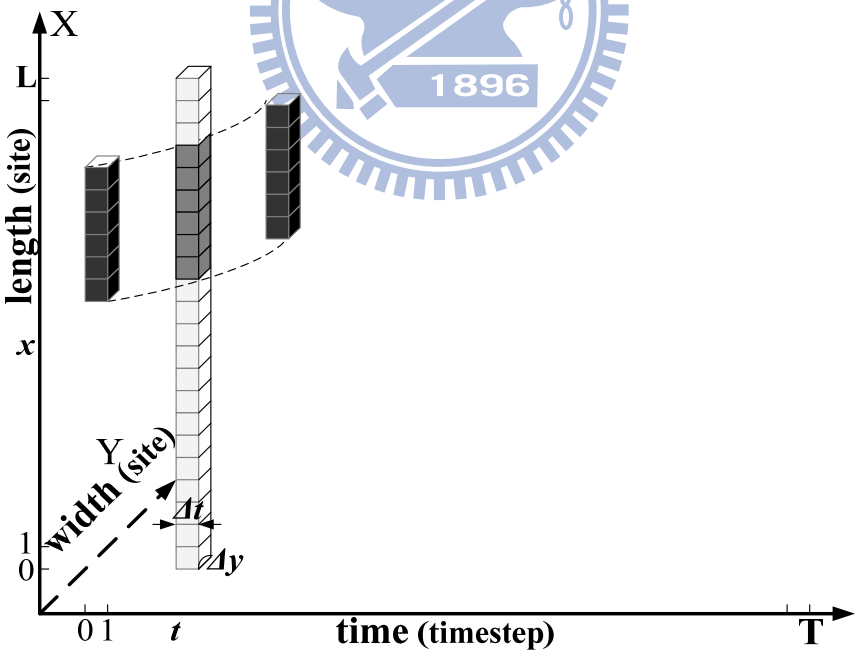

FIGURE 3-4 Vehicular trajectories over a specific transverse slice in a spatiotemporal domain enclosed by $L \times \Delta y \times \Delta t$.

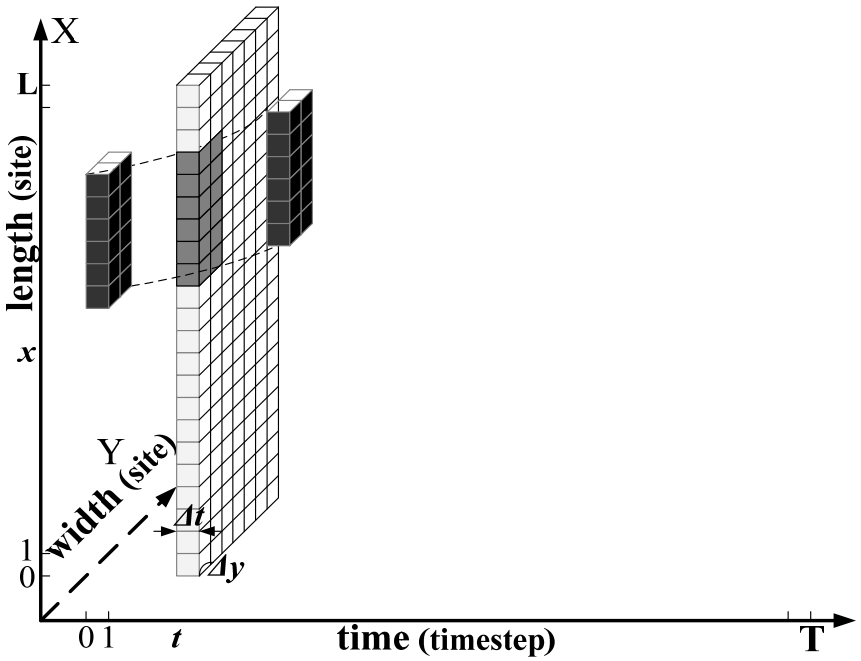

FIGURE 3-5 Vehicular trajectories over a specific transverse slice in a spatiotemporal domain enclosed by *L*×*W*×Δ*t*.

Figure 3-6 illustrates the trajectories of three light vehicles (each represented by 6×2 CUs) in a specific transverse slice (e.g., $\Delta y = 1$) of a spatiotemporal domain S enclosed by $L \times W \times T$, where L denotes the longitudinal length ($\Delta x = 1, 2, 3, ..., L$), W the transverse width ($\Delta y = 1, 2, 3, ..., W$) of a roadway, and T the number of observed time-steps ($\Delta t = 1, 2, 3, ..., T$). In this spatiotemporal domain S enclosed by $L \times W \times T$, if one repeats the same procedure from eq. (3-1) to eq. (3-2), a similar but more generalized definition of occupancy over this spatiotemporal domain S, $\rho(S)$, can be defined as eq. (3-7):

$$\rho(S) = \frac{\sum_{\Delta t} N_0(t)\Delta t}{\sum_{\Delta t} N \Delta t} = \frac{t(S)}{|S|} \tag{3-7}$$

where $t(S)$ is the total time spent by all cells in S; $t(S) = \sum N_0(t)\Delta t$. $|S|$ represents the 'volume' of this spatiotemporal domain S. Likewise, a more generalized definition of flow in the spatiotemporal domain S can be defined as eq. (3-8):

$$q(S) = \frac{\sum_{\Delta x} M_0(x)\Delta x}{\sum_{\Delta x} T \Delta x} = \frac{d(S)}{|S|} \tag{3-8}$$

where $M_0(x)$ is the total number of sites occupied by cells of vehicles at a specific location x in road. $d(S)$ is the total distance traveled by all cells of vehicles in the space S; $d(S) = \sum M_0(x)\Delta x$.

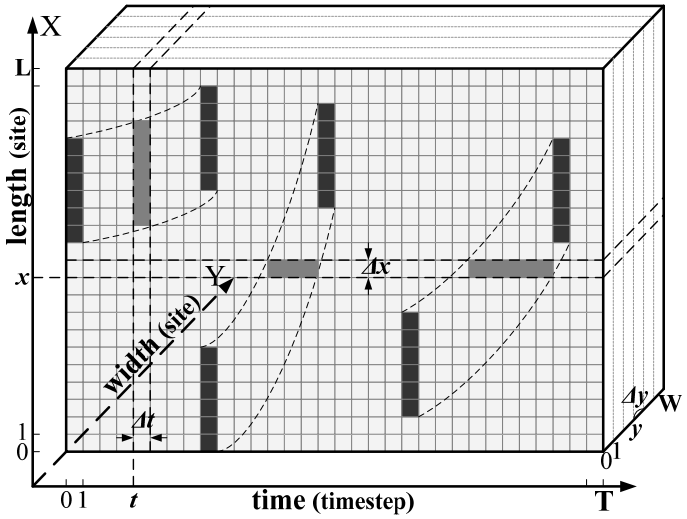

FIGURE 3-6 Vehicular trajectories over a specific transverse slice in a spatiotemporal domain S enclosed by *L*×*W*×*T*.

The ratio of eq. (3-8) to eq. (3-7) defines the generalized space-mean-speed in *S*, which can be further reduced to the ratio of the total distance traveled to the total time spent by all cells in *S*, as expressed in eq. (3-9):

$$v(S) = \frac{q(S)}{\rho(S)} = \frac{d(S)}{t(S)} \tag{3-9}$$

The above generalized definitions of average spatiotemporal occupancy, flow and speed of "cells" moving over 3-D (2-D sites plus 1-D time-step) spatiotemporal domain, as expressed in eqs. (3-7), (3-8) and (3-9), are used in the following CA simulations to describe the collective behaviors of traffic flow patterns.

3.3 Local Traffic Variables

The localized definitions of occupancy, flow and speed of "cells" moving over a virtual detector, as expressed in equations. (3-10), (3-11) and (3-12), are used in the following CA simulations:

1. Occupancy

Flow rate, *q(L)*, is total number of "cells" counted, *N*, in the transverse width *W* ($\Delta y=1, 2, \ldots, W$) in each time-step.

$$q(L) = \frac{N}{W} \tag{3-10}$$

2. Occupancy

Occupancy (proxy of density), $\rho(L)$, is the portion of this time-step that "cells" are over the virtual detector on road.

$$\rho(L) = \frac{N}{W \times v_n} \tag{3-11}$$

3. Speed

Speed, $v(L)$, is average the actual speed of the n-th vehicle.

$$v(L) = \frac{1}{N}\sum v_n \tag{3-12}$$

3.4 Simulation setting

The simulations in the following chapters are performed on a closed track containing 6×1,800 site CUs, which represents a two-lane freeway mainline of width 7.5 meters and length 2,250 meters (length of site 1.25 m) or 1,800 meters (length of site 1 m). We simulate various occupancy scenarios for 600 time-steps. Initially, all the vehicles are set equally spaced or line up from end of road section on the circular track, with speed 0 at time-step 0. To avoid the initial settings biasing the simulated results, the first 30 time-steps are viewed as the warm-up period. Thus, the average occupancy, flow and speed over a spatiotemporal domain are calculated from the 31st time-step to the end at the 630th time-step (Figure 3-7).

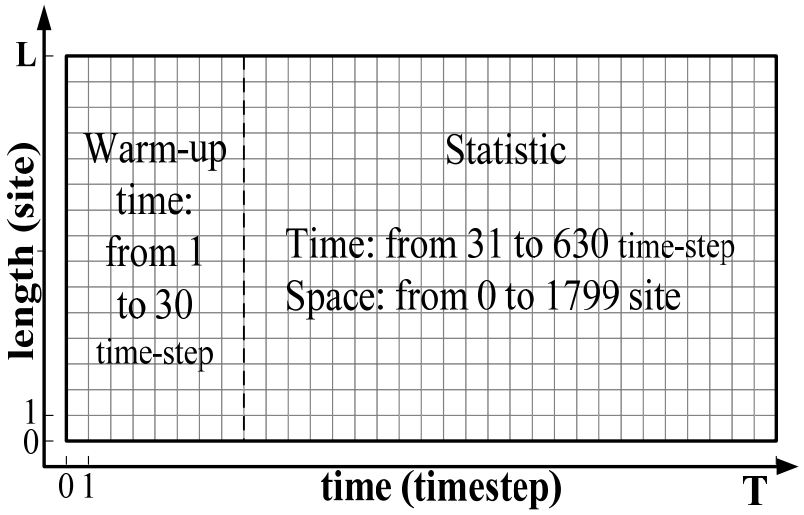

FIGURE 3-7 An illustration of setting the simulation parameters.

3.5 Summary

Most of the previous traffic flow models present the "density" by calculating how many vehicles existent in a specific road. As the distinction of "occupied areas" for different vehicles can be large (e.g., a heavy vehicle can be three times of the occupied area of a light vehicle), using the conventional density concept to elucidate mixed traffic flow will not capture the full traffic features. The generalized spatiotemporal definitions of traffic variables which can better measure the traffic flow features in the contexts of mixed traffic traveling in multi-lane roadways. A concept of "common units" (CUs) is introduced to gauge the non-identical vehicle sizes as well as the various roadway lane widths, in which vehicle are represented by cells and roadways are denoted by sites. Each site or cell is exactly the same size as one CU, a much finer squared grid than most previous CA models (7.5×7.5 meters). As such, a two-cell wide car may move at an arbitrary location of a three-site lane at any arbitrary instant of time. This undertaking will not change the freeway capacity analysis; however it has greatly improved over the previous CA models that fail to explain the real situations that some motorcycles share the same lane with adjacent cars on the surface streets. With our finer-cell definition, study of small-sized vehicles, such as motorcycles, moving alone with other vehicles, such as cars, in urban streets would become much easier and more realistic.

Previous studies measuring traffic features with density, flow and speed are defined on vehicle basis over a 2-D time-space region (Daganzo, 1997). Such definitions may not exactly depict the collective behaviors of traffic moving over a 3-D domain, including 2-D for the roadway (longitudinal and transverse) and 1-D for the time. This research redefines the traffic variables in a 3-D spatiotemporal domain on site or cell basis, not on vehicle basis.

Chapter 4 BASIC CELLULAR AUTOMATON MODEL

This chapter demonstrates the basic cellular automaton rules applied in this research. Section 4.1 addresses the forward rules. The lane-changing rules are introduced in Section 4.2. The framework of the CA rules was introduced in Section 4.3. The pure traffic simulation results are presented in Section 4.4. This chapter ends with a summary in Section 4.5.

In this basic CA model, both deterministic and stochastic CA traffic simulation models are developed to elucidate the behavior of vehicles moving in a longitudinal (X) direction and transverse (Y) direction of a two-dimensional (2-D) roadway space. The dimensions of sites, cells and the rules of vehicle movements are defined in such a way that they can best explain the mixed traffic in multi-lane contexts. Figure 4-1 illustrates a mixed traffic with two types of vehicles (light and heavy) moving in a two-lane freeway. In terms of CUs, it becomes easier to measure the relative distances of any specific vehicle to its nearby vehicles. Corresponding to different vehicle types and different roadway conditions, the CA rules, including moving forward and lane-changing, are respectively established to govern their movements over a 3-D space. The updated rules will renew the velocity (also termed as speed in this research) and position of each vehicle in parallel in every time-step. The vehicles may have "vehicle-following" and "lane-changing" behaviors, determined by a given probability of perturbation in the randomization step. This model sets the time step Δt as one second, thus the positions and speeds for all vehicles are updated in parallel per second. A much finer discretization of cell is defined in this basic model, rather than the coarse cell used in most previous CA literature.

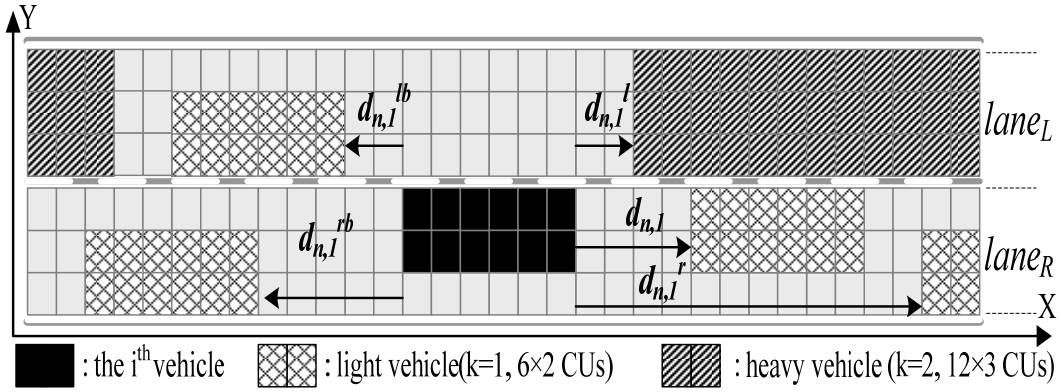

FIGURE 4-1 The relative distances of any specific vehicle to its nearby vehicles.

4.1 Forward Rules

The mixed flow condition leads to the necessity to partition the vehicles into cell units to clearly define the corresponding traffic variables. In the previous 1-D CA models, the forward rules depend on the gap, which is simply defined as the number of sites between the head of a vehicle to the rear of its preceding. The forward rules in this CA model are based on 2-D mixed traffic prerequisites; thus, a gap in this model is defined as the "minimum number of sites" between the head cells of a vehicle and the tail cells of all its preceding vehicles. For instance, if two motorcycles (2×1 CUs) moving in parallel (one is a little behind the other) in front of a car (6×2 CUs), the gap should be measured from the tail of the behind motorcycle to the head of that car. In addition, since all vehicles may move at different speeds, the closest preceding vehicle of a vehicle may vary over time-step. Consequently, the calculation of a gap is a dynamical process in this model. Since only light and heavy vehicles are considered in the present paper, we will check the distances (in terms of number of sites) from each cell head of a vehicle to its preceding occupied sites and choose the minimum one as the gap.

Similar to the NaSch model, the forward rules comprise four successive steps:

1. Step 1: Acceleration: increase vehicle velocity by 1 if the vehicle velocity is lower than the desired velocity.

$$\text{Acceleration}: \text{if } d_{n,k}^{clr}(t+1) > v_{n,k}(t) \text{ then } v_{n,k}(t+1) = \min[v_{n,k}(t)+1, v_{n,k,\max}] \quad (4\text{-}1)$$

2. Step 2: Slow down: decrease vehicle velocity if the minimum distance to the preceding vehicles ahead at the next time-step is not larger than vehicle velocity.

$$\text{Slow down}: \text{if } d_{n,k}^{clr}(t+1) \le v_{n,k}(t) \text{ then } v_{n,k}(t+1) = \min[v_{n,k}(t), d_{n,k}^{clr}(t+1)] \quad (4\text{-}2)$$

3. Step 3: Randomization (perturbation): with probability R the velocity of a vehicle is decreased by 1 at the next time-step.

$$\text{Randomization}: \text{if } rand() < R \text{ then } v_{n,k}(t+1) = \max[v_{n,k}(t+1)-1, 0] \quad (4\text{-}3)$$

4. Step 4: Update position: move a vehicle in accordance with the calculated velocity. Mathematically, these four steps are expressed as follow.

$$\text{Update position}: x_{n,k}(t+1) = x_{n,k}(t) + v_{n,k}(t+1) \quad (4\text{-}4)$$

where n is the number of vehicle. k represents different types of vehicles ($k=1$ for light vehicle, $k=2$ for heavy vehicle). $v_{n,k}(t)$ denotes the vehicle velocity at time-step t and $v_{n,k,max}$

is the maximum velocity. This basic model sets $v_{n,1,max}$ =16 sites/time-step for light vehicles and $v_{n,2,max}$ =14 sites/time-step for heavy vehicles. $d_{n,k}^{clr}(t+1)$ refers to the clear gap of the n^{th} vehicle at time step $t+1$. It is the minimum number of sites between the head of a vehicle and the cell tails of all its preceding vehicles at time step $t+1$. Namely, $d_{n,k}^{clr}(t+1) = d_{n,k}(t) + \max[v_a^f(t) - g_{safe}, 0]$, where $d_{n,k}(t)$ represents the minimum gap of a vehicle, which is to check the number of sites from the cell heads of a vehicle to its preceding occupied sites at time step t. g_{safe} is the safe gap, which is to reflect the drivers' anticipation. $v_a^f(t)$ is the expected velocity of the front vehicles at time step t. It is the minimum of $d_{n,k}^f(t)$ and $v_{n,k}^f(t)$. Namely, $v_a^f(t) = \min[d_{n,k}^f(t), v_{n,k}^f(t)]$.

4.2 Lane-Changing Rules

The basic CA model proposes new lane-change rules to accommodate the mixed traffic contexts. Previous two-lane CA models considered only the coherence of changing lane in the subject lane rather than the transverse width of the lane. The present model simulates the two-lane freeway of lane width 3 CUs, thus a light vehicle (with width 2 CUs) will occupy two-thirds of the transverse width of a lane and a heavy vehicle (with width of 3 CUs) will occupy the entire width of a lane. Figure 4-2 demonstrates the possible lane changes for a light vehicle on a two-lane freeway. With the restriction that vehicles are not allowed to travel above the lane "marking," a light vehicle on the left lane ($lane_L$) may have four lane-change scenarios, including 1→3, 1→4, 2→3, and 2→4, depending on its original and final positions. The fundamental principles of the lane-change rules contain the following four steps.

1. Step 1: Vehicle orientation: for example, if a light vehicle is on the left lane of a two-lane road, the four possible lane-changing scenarios are 1→3, 1→4, 2→3, 2→4 and vice versa.

2. Step 2: Check incentive criterion: estimate the clear gaps on its lane and the other lane at the next time-step. If the clear gap on the other lane is larger than its own lane, it means that the other lane would have higher degree of freedom, thus the vehicle has incentive to change lane.

3. Step 3: Check clear gap ahead: estimate its current speed and the clear gap at the next time-step. If the clear gap is smaller than its current speed, it means someone is in your way.

4. Step 4: Check safety criterion: estimate the gap between the vehicle and its frontal vehicle on the other lane at the next time-step. If the gap on the other lane is larger than its frontal vehicle's velocity, it means that a safe lane change can be performed without

cutting in someone else's way. However, in real situations, not all drivers will make the lane changes. Thus, in the stochastic CA simulations, this paper assumes that with probability *R* the drivers will remain in-lane even if the above lane change rules are met.

Taking light vehicle lane-change 2→3 and 2→4 for examples, the above four-step rules can be further expressed as:

$$
\begin{aligned}
LC^{2\to3}: \text{If } & [d_{n,1}^{clr_{L(1,2)}}(t+1) < v_{n,1}(t)] \\
& \text{and } [d_{n,1}^{clr_{L(1,2)}}(t+1) < d_{n,1}^{clr_{R(2,3)}}(t+1)] \\
& \text{and } [d_{n,1}^{R^U(2,3)}(t) > v_{n,1}^{R^U(2,3)}(t)] \\
& \text{then change lane from } L(1,2) \text{ to } R(2,3)
\end{aligned} \tag{4-5}
$$

$$
\begin{aligned}
LC^{2\to4}: \text{If } & [d_{n,1}^{clr_{L(1,2)}}(t+1) < v_{n,1}(t)] \\
& \text{and } [d_{n,1}^{clr_{L(1,2)}}(t+1) < d_{n,1}^{clr_{R(1,2)}}(t+1)] \\
& \text{and } [d_{n,1}^{R^U(1,3)}(t) > v_{n,1}^{R^U(1,3)}(t)] \\
& \text{then change lane from } L(1,2) \text{ to } R(1,2)
\end{aligned} \tag{4-6}
$$

$$
\begin{aligned}
\text{If } & LC^{2\to3} \text{ and } LC^{2\to4} \text{ is true} \\
& \text{and } [d_{i1}^{clr_{R(2,3)}}(t+1) \geq d_{i1}^{clr_{R(1,2)}}(t+1)] \\
& \text{then change lane from } L(1,2) \text{ to } R(2,3)
\end{aligned} \tag{4-7}
$$

$$
\begin{aligned}
\text{If } & LC^{2\to3} \text{ and } LC^{2\to4} \text{ is true} \\
& \text{and } [d_{n,1}^{clr_{R(2,3)}}(t+1) < d_{n,1}^{clr_{R(1,2)}}(t+1)] \\
& \text{then change lane from } L(1,2) \text{ to } R(1,2)
\end{aligned} \tag{4-8}
$$

$LC^{2\to3}$ denotes the lane change from location 2 to location 3. $L(1,2)$ represents a vehicle occupying site 1 and 2 of $lane_L$. is the clear gap of the vehicle on site 1 and 2 of $lane_L$ at time-step $t+1$. $d_{i1}^{R^U(2,3)}(t)$ is the minimum gap between the vehicle on $lane_L$ and its upstream vehicle on $lane_R$ occupying site 2 and/or 3 at time-step t; $v_{i1}^{R^U(2,3)}(t)$ is the velocity of its upstream vehicle on $lane_R$ occupying site 2 and/or 3 at time-step t. Therefore, the trajectory of the vehicle will move from *L(1,2)* to *R(2,3)* in one time-step if $LC^{2\to3}$ rules are met. Furthermore, whenever any two of the aforementioned rules are met, the vehicle is to choose the one with larger gap because a rational driver is presumed to move with higher degree of freedom.

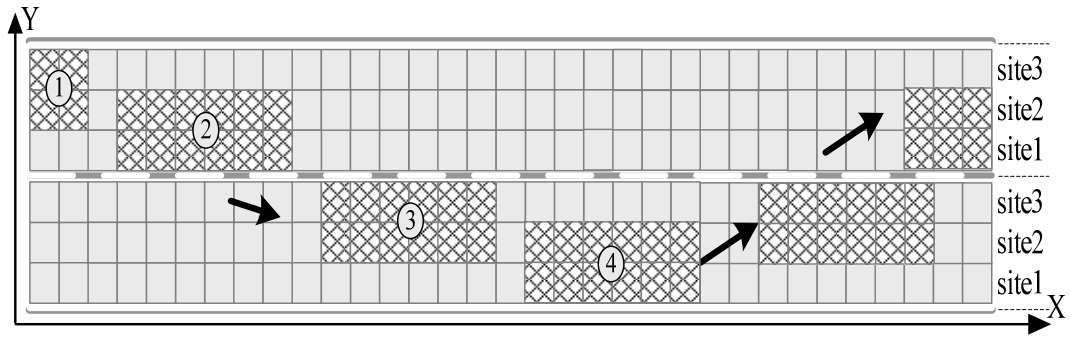

FIGURE 4-2 Lane changes for a light vehicle on a two-lane 7.5-meter width roadway.

The lane-change rules for heavy vehicles are much simpler, as demonstrated in Figure 4-3. Similarly, any heavy vehicle is not allowed to drive above the lane "marking." In the same two-lane freeway context, a heavy vehicle on the left lane ($lane_L$) can only have one lane-change scenario 1→2 from $lane_L$ to $lane_R$. The above-mentioned four-step fundamental principles also apply for heavy vehicles' lane changes. Accordingly, the following conditions can describe the lane change behaviors for a heavy vehicle:

$$LC^{1\to 2}: \text{If } [d_{n,2}^{clr_L}(t+1) < v_{n,2}(t)]$$
$$\text{and } [d_{n,2}^{clr_L}(t+1) < d_{n,2}^{clr_R}(t+1)]$$
$$\text{and } [d_{n,2}^{R^U}(t) > v_{n,2}^{R^U}(t)]$$
$$\text{then change lane from } L \text{ to } R. \tag{4-9}$$

$$LC^{2\to 3}: \text{If } [d_{n,2}^{clr_R}(t+1) < v_{n,2}(t)]$$
$$\text{and } [d_{n,2}^{clr_R}(t+1) < d_{n,2}^{clr_L}(t+1)]$$
$$\text{and } [d_{n,2}^{L^U}(t) > v_{n,2}^{L^U}(t)]$$
$$\text{then change lane from } R \text{ to } L. \tag{4-10}$$

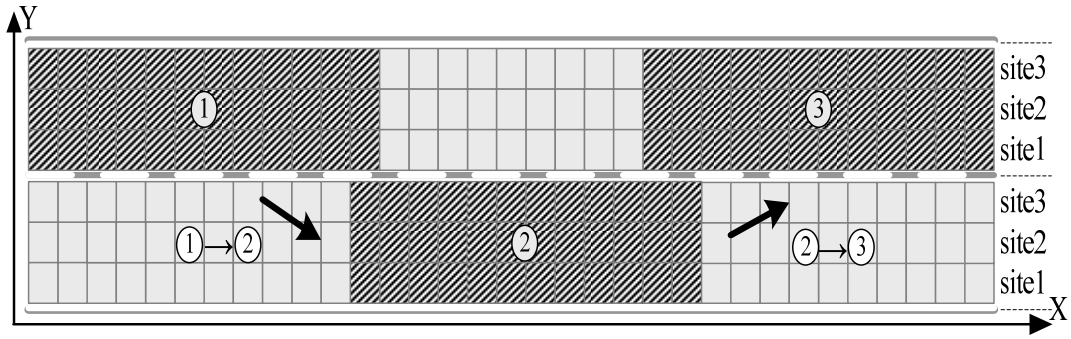

FIGURE 4-3 Lane changes for a heavy vehicle on a two-lane 7.5-meter width roadway.

4.3 Framework

The states of vehicles in the CA model are updated once per each time-step (1 second) according to the above forward and lane-change rules. The framework of the CA rules is depicted in Figure 4-4. The current velocity of each vehicle is checked at each time-step. A vehicle will fulfill the forward rules if its clear gap is larger than its current velocity; otherwise, the vehicle will undertake the lane-change rules. If the state of a vehicle cannot fulfill the lane-change rules, the vehicle will take the slow-down step in the forward rules. In the stochastic CA simulation (with traffic perturbation), the randomization will be applied to both forward rules (with probability *R* the velocity of a vehicle is decreased by 1 at next time step) and lane-change rules (with probability *R* the vehicle will keep in-lane even if the lane-change rules are met) to reflect the heterogeneous drivers.

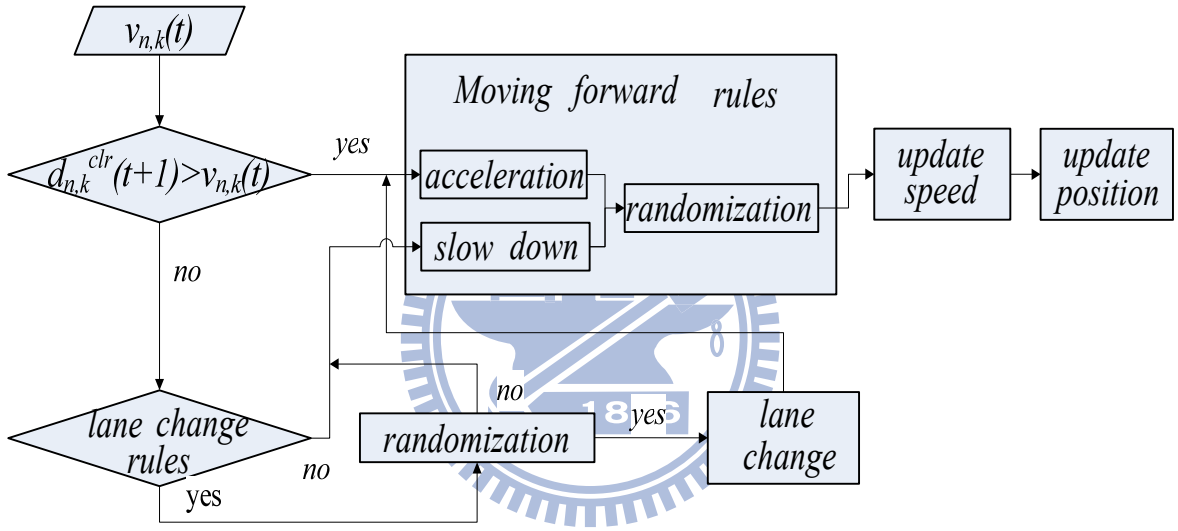

FIGURE 4-4 The framework of this proposed CA model.

4.4 Pure Traffic Simulation Results

4.4.1 Light Vehicles

The initial condition (at time-step 0) for each occupancy scenario is to set all the vehicles equally-spaced over the circular track with velocity 0. Figure 4-5 presents the fundamental (flow-occupancy) diagrams, speed-occupancy diagrams and speed-flow diagrams, with different settings of safe gaps (g_{safe}=0, 4, 8, 16) without perturbation ($R=0$). Different safe gaps represent the driver population with various degrees of aggressiveness or conservativeness. The more aggressive the drivers are the shorter safe gaps they will keep. Note from Figures 4-5(a) to 4-5(c) that as the safe gap gets larger (more conservative drivers), the maximum flow drops off and the "critical occupancy" (i.e., an occupancy corresponding to the maximum flow) also decreases.

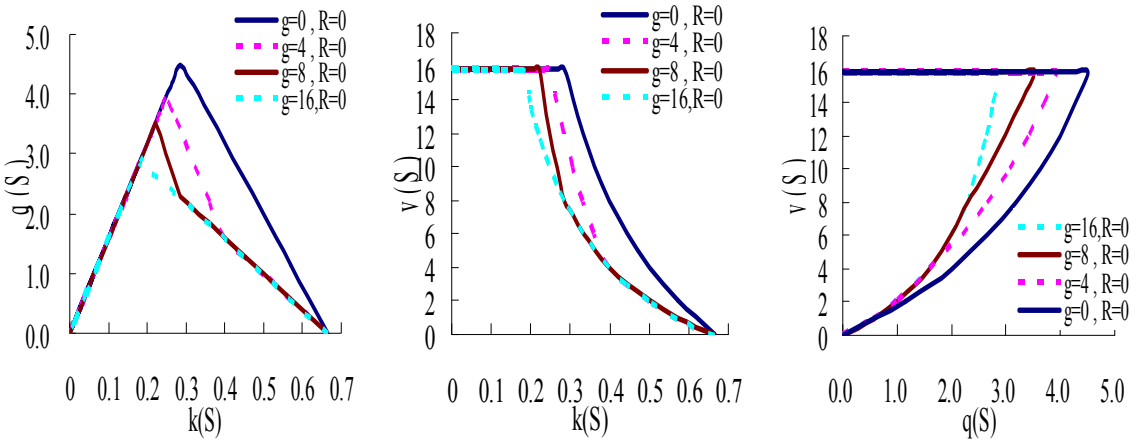

(a) Flow-occupancy curves (b) Speed-occupancy curves (c) Speed-flow curves

FIGURE 4-5 The simulation results for light vehicles without traffic perturbation.

Figure 4-6 compares the simulation results between a deterministic condition (without traffic perturbation, *R=0*) and a stochastic condition (with traffic perturbation *R=0.4*) given that the safe gap is fixed at *g=8*. Obviously, traffic perturbation will reduce the maximum flow and critical occupancy. For instance, The dotted circle in Figure 4-6(c) indicates that the collective behavior of maximum flow is *q(S)*=3.51 cells/time-step under a deterministic condition; whereas the solid circle shows that *q(S)* would drop to 2.96 cells/time-step under that specific stochastic condition. It suggests that the capacity-drop due to traffic perturbation can be significant (a 15.7% drop off in case of perturbation *R=0.4*).

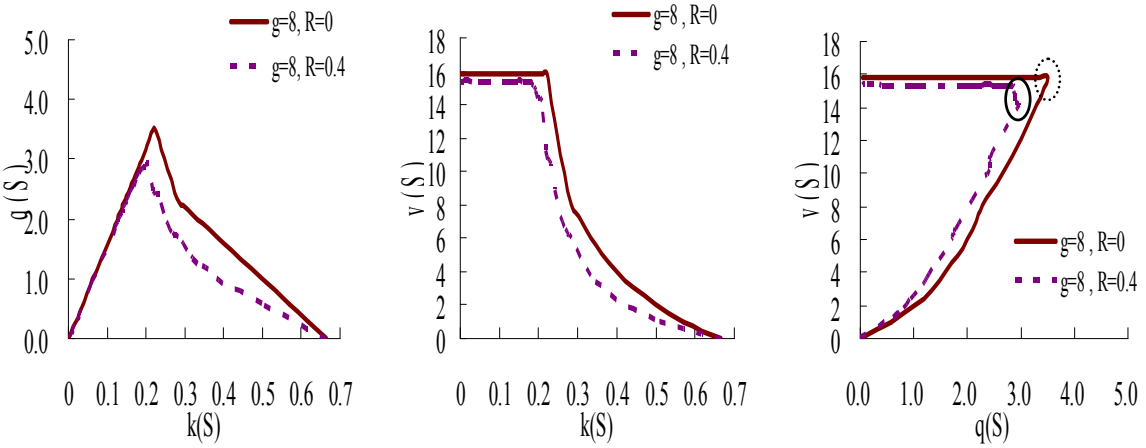

(a) Flow-occupancy curves (b) Speed-occupancy curves (c) Speed-flow curves

FIGURE 4-6 Comparison of simulation results for light vehicles with and without traffic perturbation (safe gap fixed at 8).

Figure 4-7 demonstrates the vehicular trajectories and the formation of traffic flow patterns under deterministic and stochastic conditions. The vertical axis in Figures 4-7(a) and 4-7(b) represents the distance (vehicles moving from bottom to top) and the X axis represents the time (progressing from left to right). As anticipated, without traffic perturbation all vehicular trajectories are parallel in Figure 4-7(a), indicating that all vehicles travel with constant velocity (equal to the slopes of trajectories). This corresponds to a free-flow phase shown in Figures 4-7(c) and 4-7(e). With traffic perturbation, however, the vehicular trajectories in Figure 4-7(b) have revealed quite complex behaviors with noticeable propagation of backward shock waves. These shock waves have formed so-called "wide moving jams," also propagating backward to bottom and continuing from the top, as shown in Figures 4-7(d) and 4-7(f). Note that the right and left lanes have slightly different traffic flow patterns due to the random term. The rise and fall of velocities in Figures 4-7(d) and 4-7(f) show that most vehicles travel at nearly maximum speed in free flow phase but their velocities can significantly drop to nearly zero in wide moving jam phase. In the congested traffic, there exists so-called "synchronized flow phase" where vehicles may travel at various speeds from high speed (stable state) to low-speed (metastable state).

(a) Vehicular trajectories (R=0)　　(b) Vehicular trajectories (R=0.4)

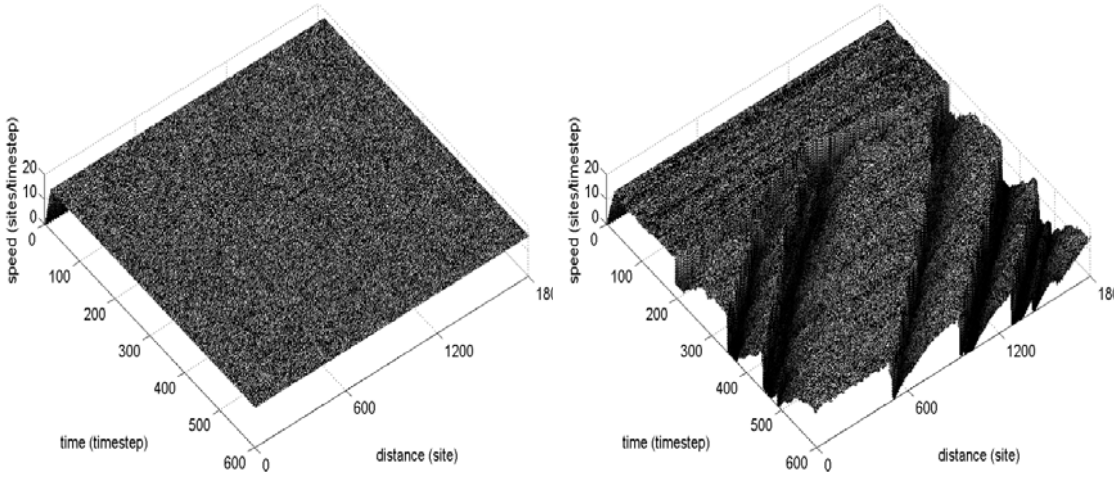

(c) Left lane (R=0)　　(d) Left lane (R=0.4)

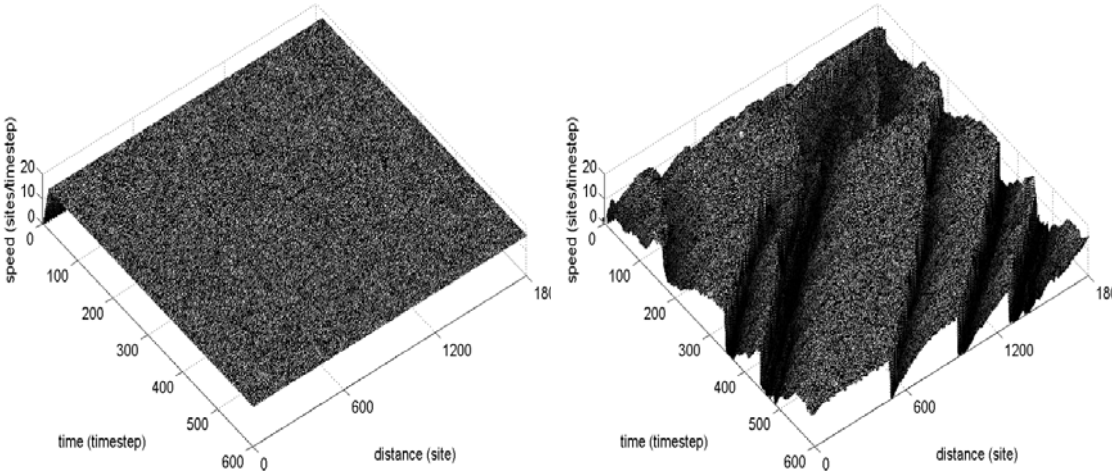

(e) Right lane (R=0) (f) Right lane (R=0.4)

FIGURE 4-7 Vehicular trajectories and traffic patterns for light vehicles with and without traffic perturbation.

To further investigate how vehicles traveling in the above three traffic phases, Figures 4-8 and 4-9 demonstrate the speed distributions at two specific instantaneous (200th and 400th) time-steps and at two specific stationary (600th and 1200th) sites, respectively. In Figure 4-8, the instantaneous-time-step speeds have revealed that vehicles can travel at free-flow (maximum) constant speed without perturbation but they are profoundly influenced by wide moving jams with traffic perturbation. The abrupt speed drop to nearly zero indicates that three wide moving jams have emerged in the simulation.

Similarly, in Figure 4-9, the stationary-site speeds have indicated that wide moving jams propagate backward at the stationary sites with traffic perturbation. The speed distributions over the simulated spatial sites in Figure 4-8 and over the temporal instants in Figure 4-9 clearly signify the existence of synchronized flow phase in congested condition, in which stable and metastable traffic patterns emerge. These traffic patterns can support Kerner's three-phase traffic theory.

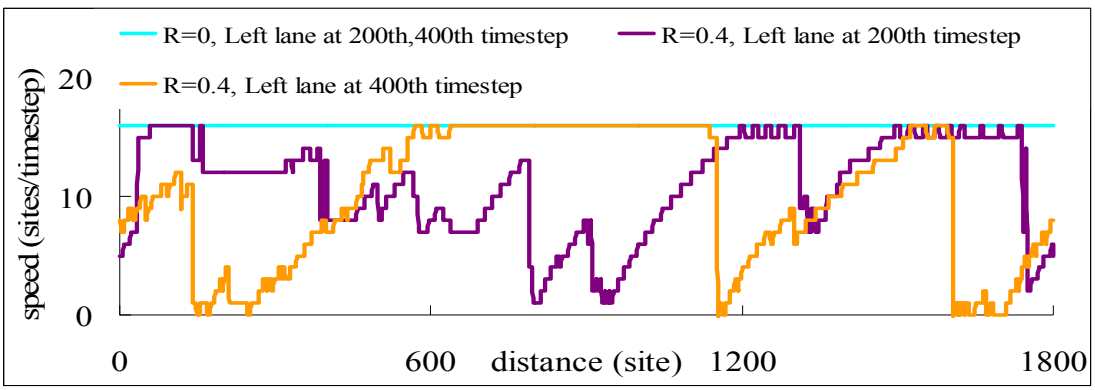

(a) left lane

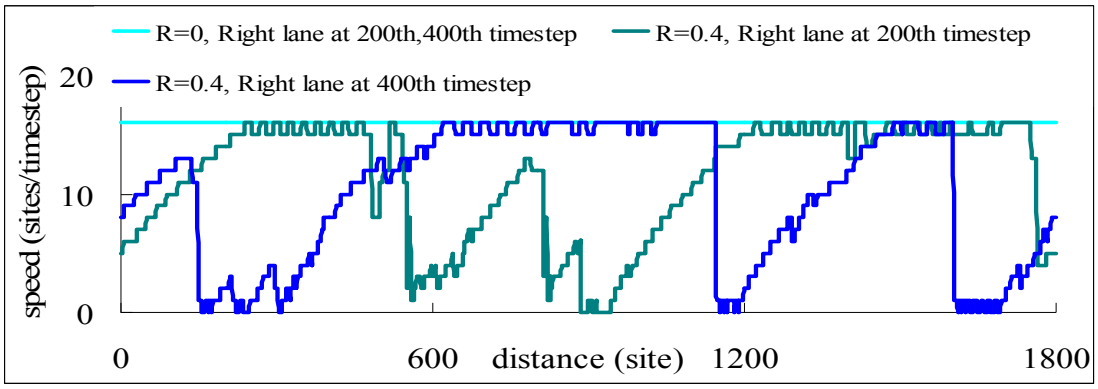

(b) right lane

FIGURE 4-8 Speed distributions for light vehicles at two instantaneous time-steps.

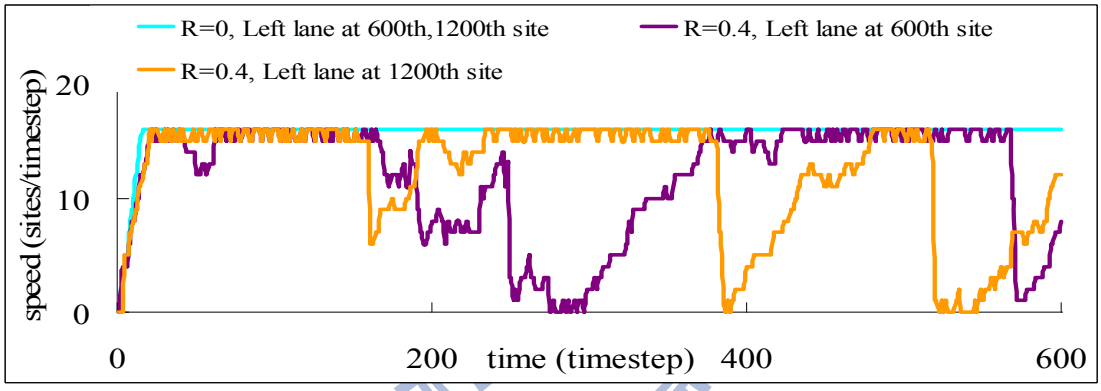

(a) left lane

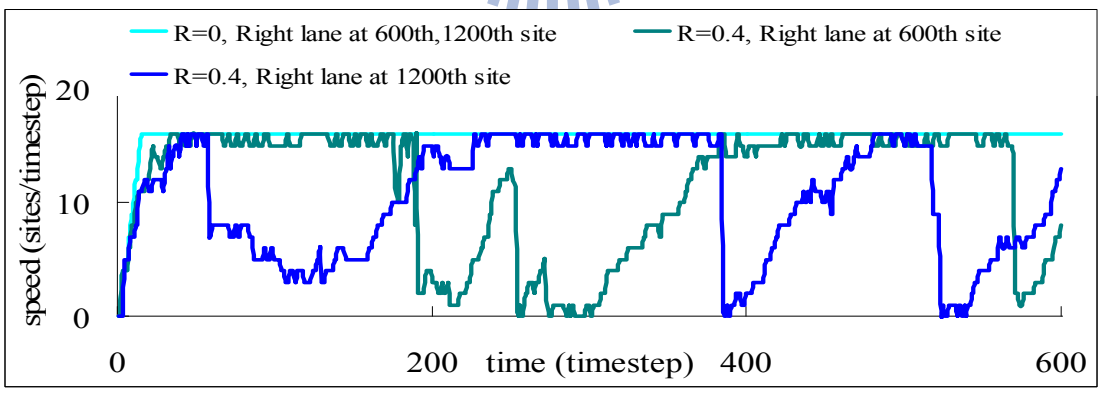

(b) right lane

FIGURE 4-9 Speed distributions for light vehicles at two stationary sites.

3.3.2 Heavy Vehicles

Figure 4-10 displays the flow-occupancy, speed-occupancy and speed-flow curves for heavy vehicles under the conditions of different safe gaps (g_{safe}=0, 4, 8, 12, 14) without perturbation (*R=0*). Similar to the light vehicles, as the safe gap gets larger, the maximum flow drops off and the critical occupancy also decreases. It is interesting to compare the simulation results between these two types of vehicles. As what we anticipated, in the light-vehicle case, the maximum occupancy *ρ(S)* equal to 0.67 represents that all light vehicles have formed two platoons, bumper-to-bumper without gap, on the two-lane track. The simulation results agree to the generalized spatiotemporal definition of occupancy because each light vehicle (2 CUs wide) takes only two-thirds of one lane-width (3 CUs) and all the vehicles obey the lane marking while moving forward. In the heavy-vehicle case, because a heavy vehicle (3 CUs wide) takes away the entire lane width, thus the maximum occupancy *ρ(S)* is equal to 1, which also agrees to the generalized spatiotemporal definition of occupancy.

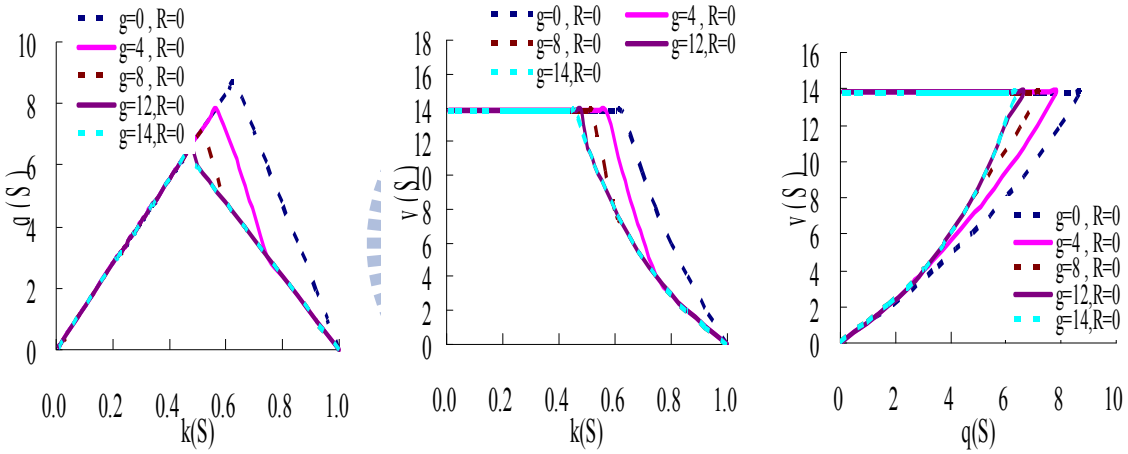

(a) Flow-occupancy curves (b) Speed-occupancy curves (c) Speed-flow curves

FIGURE 4-10 The simulation results for heavy vehicles without perturbation.

Figure 4-11 compares the simulation results for heavy vehicles between a deterministic condition (*R=0*) and a stochastic condition (*R=0.4*) at a fixed safe gap *g=8*. Similar to the light-vehicle case, traffic perturbation can also reduce the maximum flow and critical occupancy. For instance, The dotted circle in Figure 4-11(c) indicates that the collective behavior of maximum flow is *q(S)*=7.21 cells/time-step under a deterministic condition; whereas the solid circle shows that *q(S)* would drop to 6.72 cells/time-step under that specific stochastic condition (a 6.8% drop off). Compared with light vehicles under the same traffic perturbation, the capacity-drop for heavy vehicles due to traffic perturbation is less significant.

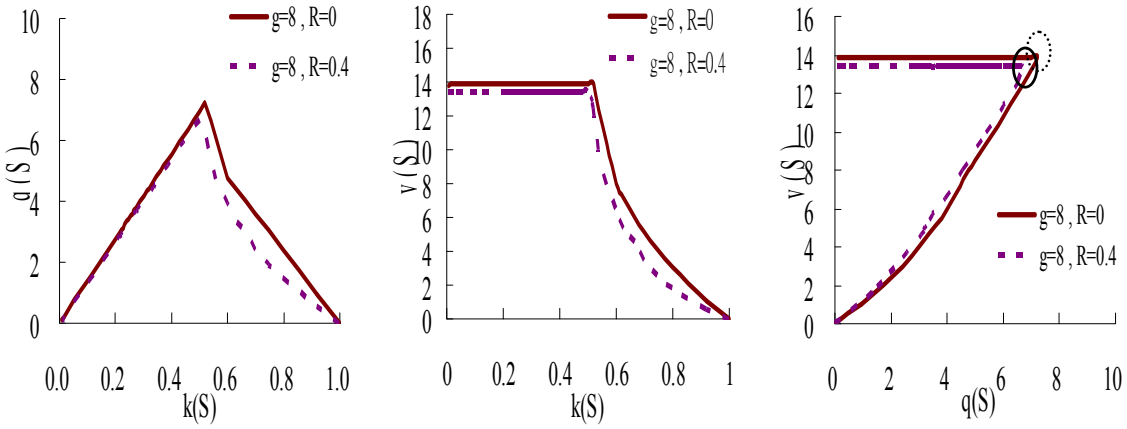

(a) Flow-occupancy curves (b) Speed-occupancy curves (c) Speed-flow curves

FIGURE 4-11 Comparison of simulation results for heavy vehicles with and without traffic perturbation (safe gap fixed at 8).

Figure 4-12 displays the vehicular trajectories and the formation of traffic flow patterns for heavy vehicles under deterministic and stochastic conditions. Like the light-vehicle case, without traffic perturbation all the heavy vehicles move with constant velocity (trajectories are parallel in Figure 4-12(a), corresponding to a free-flow phase shown in Figures 4-12(c) and 4-12(e). With traffic perturbation, however, the vehicular trajectories in Figure 4-12(b) have revealed wide moving jams, also propagating backward to bottom and continuing from the top, as shown in Figures 4-12(d) and 4-12(f). The variation of velocities in Figures 4-12(d) and 4-12(f) show that most heavy vehicles travel at nearly maximum speed in free flow phase but their velocities significantly drop to nearly zero in wide moving jam phase. The synchronized flow phase also exists here.

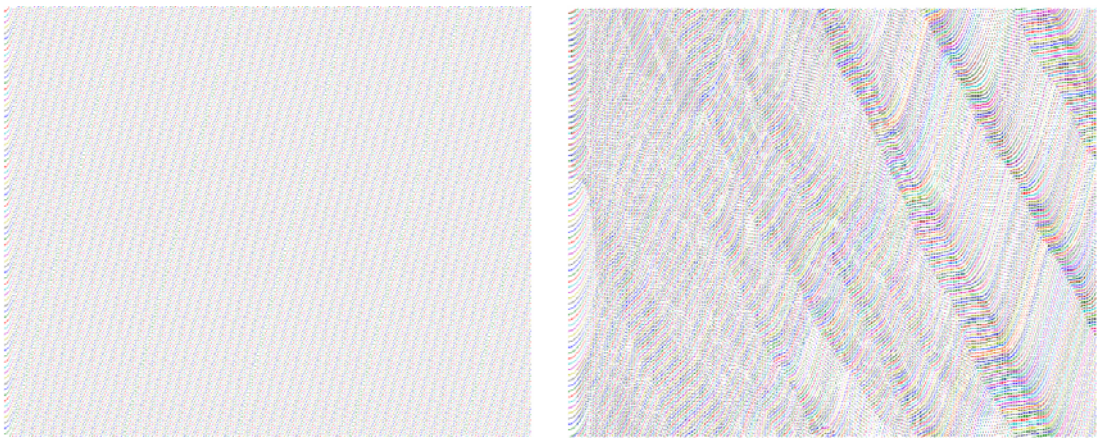

(a) Vehicular trajectories (R=0) (b) Vehicular trajectories (R=0.4)

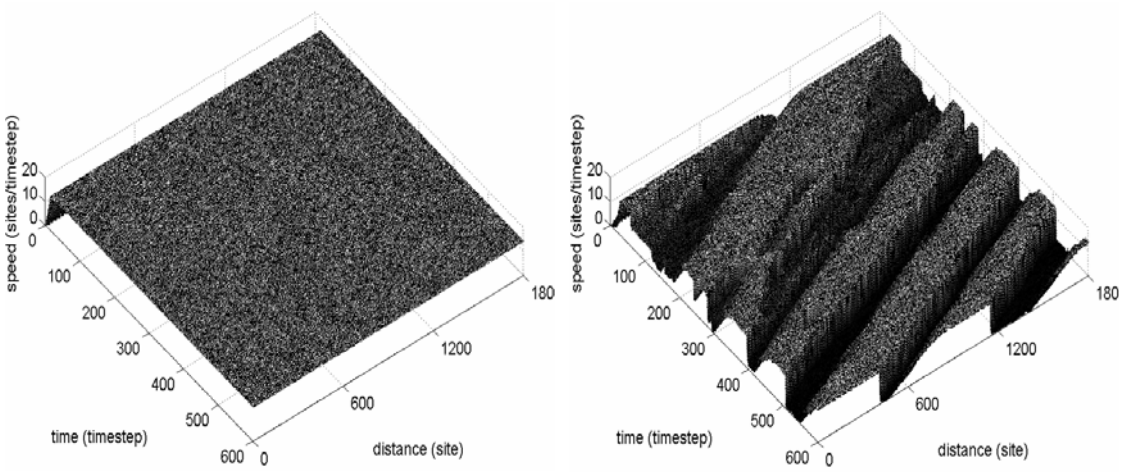

(c) Left lane (R=0)

(d) Left lane (R=0.4)

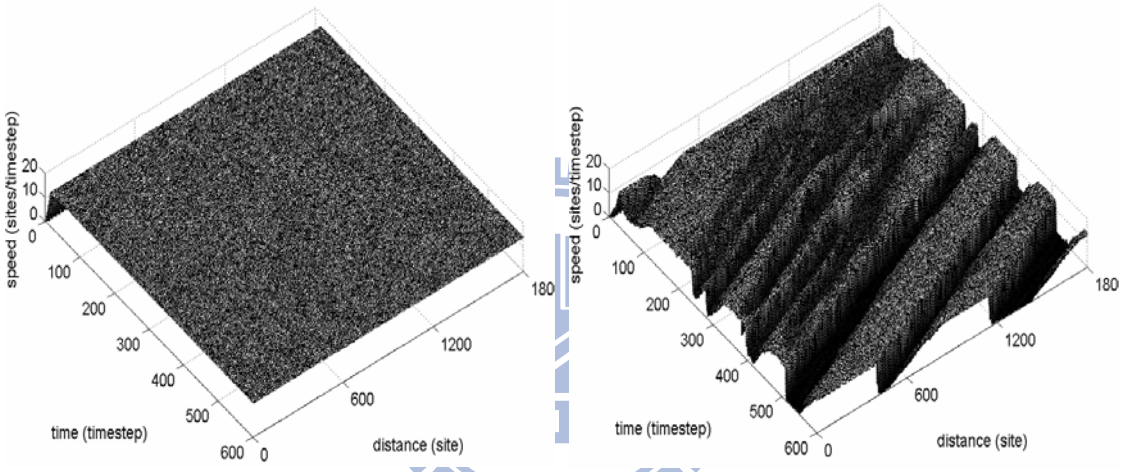

(e) Right lane (R=0)

(f) Right lane (R=0.4)

FIGURE 4-12 Vehicular trajectories and traffic patterns for heavy vehicles with and without traffic perturbation.

Figures 4-13 and 4-14 demonstrate the speed distributions of heavy vehicles at two specific instantaneous (200^{th} and 400^{th}) time-steps and at two specific stationary (600^{th} and 1200^{th}) sites, respectively. The instantaneous-time-step speeds in Figure 4-13 reveal that heavy vehicles can travel at free-flow (maximum) constant speed without perturbation but their speeds are greatly affected by wide moving jams with traffic perturbation. In Figure 4-14, the stationary-site speeds disclose that wide moving jams propagate backward at the stationary sites under traffic perturbation (*R=0.4*). Both Figures 4-13 and 4-14 have indicated the existence of synchronized flow phase in congested condition, which also supports the three-phase traffic theory.

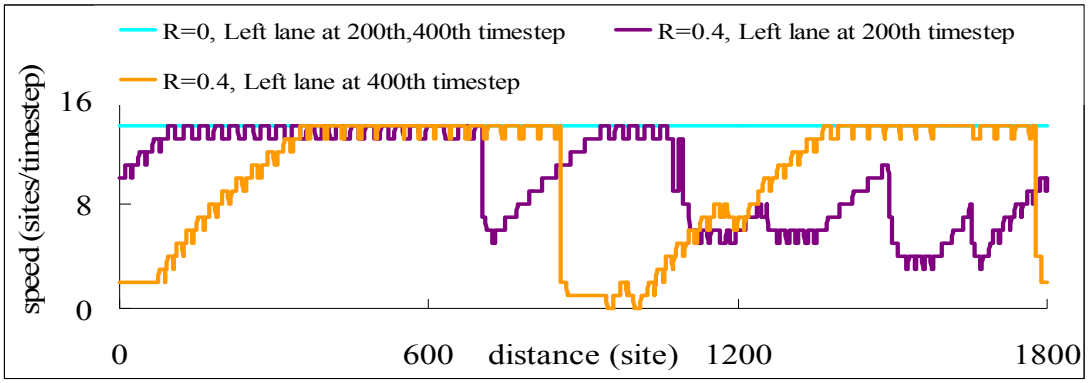

(a) left lane

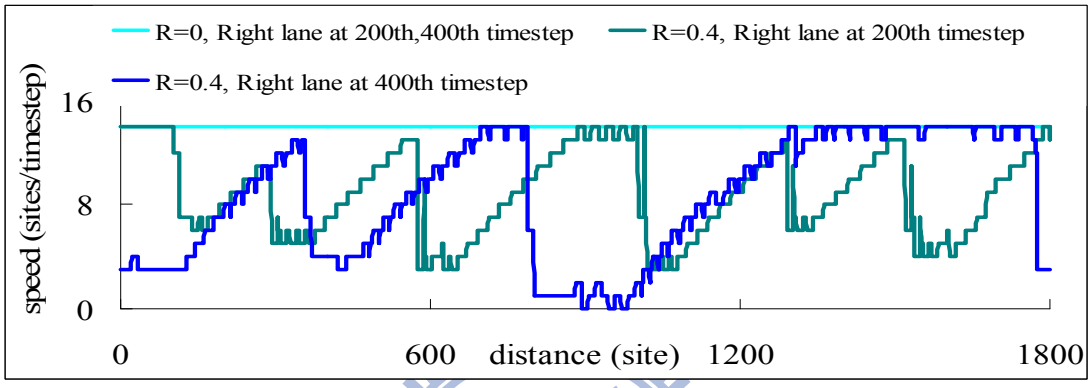

(b) right lane

FIGURE 4-13 Speed distributions for heavy vehicles at two instantaneous time-steps.

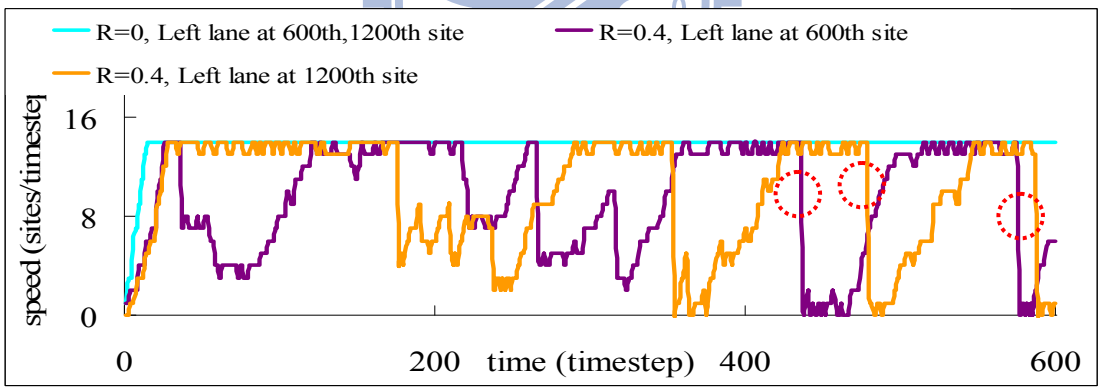

(a) left lane

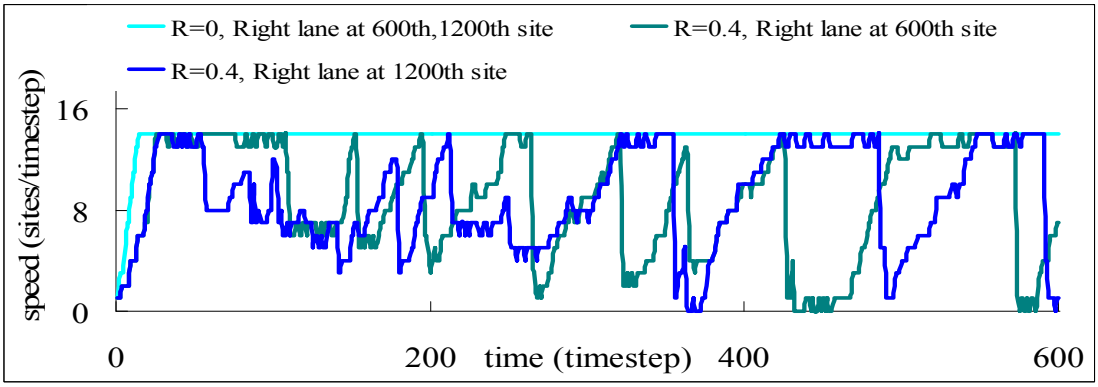

(b) right lane

FIGURE 4-14 Speed distributions for heavy vehicles at two stationary sites.

4.5 Summary

This basic CA model proposes generalized spatiotemporal definitions of traffic variables which can better elucidate the traffic flow features in the contexts of mixed traffic traveling in multi-lane roadways. A concept of "common units" (CUs) is introduced to gauge the non-identical vehicle sizes as well as the various roadway lane widths, in which vehicle are represented by cells and roadways are denoted by sites. Each site or cell is exactly the same size as one CU, a much finer squared grid (1.25×1.25 meters) than most of the previous CA models (7.5×7.5 meters). As such, a two-cell wide car may move at an arbitrary location of a three-site lane at any arbitrary instant of time.

Our basic CA model follows NaSch's slow down rule, thus abrupt speed drops occasionally emerge during the simulations (Figure 4-14 dotted line circles). The shortcoming can be resolved by introducing maximum deceleration rates into the slow down rule. Another shortcoming of this basic CA model is incapable of capturing the essential features of traffic flows. In the next chapter, a revised CA rules will be proposed to improve this shortcoming, and simulations with more vehicle types are also attempted. The effect of stationary bottlenecks (such as work zones) can be examined.

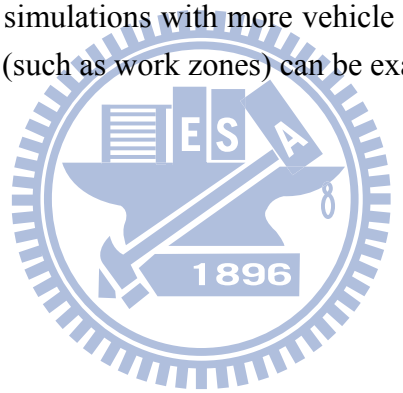

Chapter 5 REVISED CELLULAR AUTOMATON MODEL

This chapter proposes a revised CA model to overcome the shortcomings found in the basic CA model presented in Chapter 4 so as to reflect the real driver behavior. The medications are discussed in Section 5.1. Some validation and comparison with empirical data are discussed in Section 5.2; and the effects of stationary and moving bottlenecks are presented in Section 5.3. This chapter ended in a summary in Section 5.4.

5.1 Modification

5.1.1 Revised common unit size

To further reflect the situations for Taiwan freeways where speed limit is 110 kph, this revised model continues to use the concept of CU, but will reduce the CU size to a grid of 1.25×1.0 meters. Therefore, the maximum speed of CA simulations can be set equal to 31sites/sec (111.6 kph), very close to the speed limit (110kph), and the incremental speed for vehicles is 1 meter per time-step (3.6 kph). Since each "site" will also be exactly occupied or unoccupied by a "cell," the dimension of a "site" is also defined as a grid of 1.25×1.0 meters. Consequently, a 3.75-meter (12-feet) standard freeway lane is equivalent to a lane width of "three sites." Likewise, a 2.5-meter urban narrow street can be regarded as a lane width of only "two sites."

5.1.2 Forward rules

Basically the renowned NaSch model is utilized. However, some modifications are introduced, in accordance with the scheme proposed by Knospe *et al*. (2000) and Jiang et al (2003), into the new CA models to reflect the real driver behavior to the extent as possible. These include the anticipation effect, the velocity-dependent randomization (VDR) concept (Barlovi´c, 1998), and the delay-to-start phenomena, etc. The forward rules used in this study can be described as the following seven steps.

1. Step 1: Determination of the randomization probability. Three possibility values are introduced, P_b-which considers the impact of decelerating vehicle in close front, P_0 - which reflects the delay-to-start behaviors of some vehicles located on downstream front of traffic jam, and P_d -the probability for all the other situations.

$$p(v_n(t),t_h,t_s,S_{n+1}(t)=\begin{cases} p_b: & \text{if } S_{n+1}=1 \quad \text{and} \quad t_h < t_s \\ p_0: & \text{if } v_n=0 \quad \text{and} \quad t_{st} \geq t_{k,c} \\ p_d: & \text{in all other cases} \end{cases} \tag{5-1}$$

where $t_h = d_n / v_n(t)$, $t_s = \min(v_n(t), h_k)$

t_{st} denotes the time the vehicle stops. Only when the car has stopped for a certain time $t_{k,c}$ does the driver become less sensitive. $d_n = x_{n+1} - x_n - l$ is the gap between consecutive cars (where l is the length of the vehicles). $t_h = d_n / v_n(t)$ is the temporal headway; $t_s = \min(v_n(t), h)$ is the safety time headway required; h determine the range of interaction with brake light.

2. Step 2: Acceleration. Determine the speed of vehicles in next time step. Here the status identifier, $S_n(t)$, is also taken into consideration. The value of $S_n(t)$ is determined in Step 5.

$$\text{if } (S_{n+1}(t) = 0 \text{ and } S_n(t) = 0) \text{ or } (t_h \geq t_s) \text{ then } v_n(t+1) = \min(v_n(t) + a_k, v_{k,\max})$$
$$\text{else } v_n(t+1) = v_n(t) \qquad (5\text{-}2)$$

where $v_{k,max}$ and a_k are the maximum speed and acceleration capacity of vehicle, respectively.

3. Step 3: Deceleration. Set velocity restriction when the vehicle in front is too close, thus locates within the effective distance (d_n^{eff}) defined by Knospe (2000).

$$v_n(t+1) = \min(d_n^{eff}, v_n(t+1)) \qquad (5\text{-}3)$$

4. Step 4: Randomization. In real situations, not all drivers or vehicles of the same type are identical. Therefore, in stochastic CA simulations, we assume with probability p that determined in step 1, the velocity of a vehicle will not accelerate or with smaller acceleration at the next time-step.

$$\text{if } (rand() < p) \text{ then } v_n(t+1) = \max(v_n(t+1) - 1, 0) \qquad (5\text{-}4)$$

5. Step 5: Determination of vehicle status identifier $S_n(t)$ in next time-step.

$$S_n(t+1) = \begin{cases} 0 & \text{if } v_n(t+1) > v_n(t) \\ S_n & \text{if } v_n(t+1) = v_n(t) \\ 1 & \text{if } v_n(t+1) < v_n(t) \end{cases} \qquad (5\text{-}5)$$

6. Step 6: Determination of time (t_{st}) stuck inside the jam.

$$t_{st} = \begin{cases} t_{st} = t_{st} + 1 & \text{if } v_n(t+1) = 0 \\ t_{st} = 0 & \text{if } v_n(t+1) > 0 \end{cases} \tag{5-6}$$

7. Step 7: Update position. Move vehicle in accordance with the calculated velocity.

$$x_n(t+1) = x_n(t) + v_n(t+1) \tag{5-7}$$

5.1.3 Lane-change rules

According to the lane-change rules of the basic model present in Chapter 4, the following criteria are considered to make a lane-change more realistic.

1. Step 1: Vehicle orientation. For example, if a vehicle is on the left lane of a two-lane road, the possible lane-changing scenarios are 1→2→3, 2→3, and vice versa, depending on its original locations, as demonstrated in Figure 5-1. Vehicles locate randomly on either inner or outer side within each lane before lane change. However, for simplicity it is assumed that each lane change will be accomplished within 1 time step (1 second), regardless of the initial locations of vehicles.

2. Step 2: Check incentive criterion. If there is long time headway *(t_h)* in front, say, larger than 10 second, there is no incentive for taking lane change. If t_h is not larger than 10 seconds, determine whether the vehicle in front on the other lane moves with higher speed than that of the vehicle in right front. If yes, the vehicle has incentive to change lane.

3. Step 3: Check effective distance ahead. When there is no peer vehicle locates aside on the other lane, estimate the front effective distance at the next time-step. If it is too small, then check the effective distance between the vehicle and its downstream vehicle on the other lane to determine if it allows for a not-decreasing movement when performing a lane-change in the next time-step.

4. Step 4: Check safety criterion. Estimate the gap between the vehicle and its upstream vehicle on the other lane. If the gap on the other lane is larger than its upstream vehicle's velocity in next time-step, it means that a safe lane-change can be performed without cutting in someone else's way at the next time-step.

5. Step 5: Randomization. In real situations, not all drivers will make the lane changes even if the above lane-change rules are satisfied. Thus, in stochastic CA simulations, this paper assumes that with probability *R=0.4* the drivers will remain in-lane provided all lane-change rules are met.

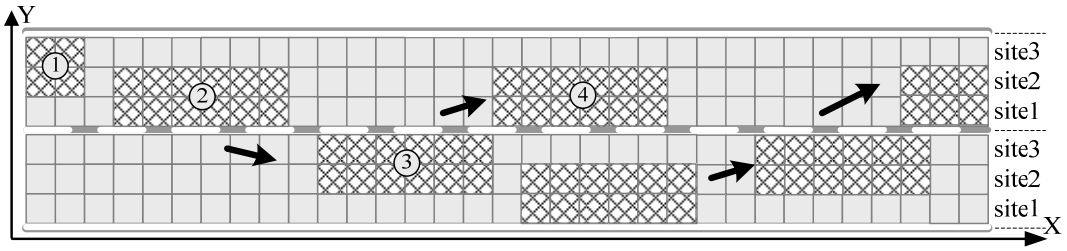

FIGURE 5-1 New lane-change ways for a light vehicle on a two-lane roadway.

The lane change rules can be recapped as:

$$
\begin{aligned}
LC^{l\to r}:\ \text{If}\ & v_{l,n}^{r}(t) > v_{l,n}(t) \\
\text{and}\ & v_n(t) > v_{l,n}(t) \\
\text{and}\ & d_{l,n}^{eff,r}(t) > \min(d_n^{eff}, v_n(t+1)) \\
\text{and}\ & g_{b,n}^{r}(t) > v_{b,n}^{r}(t+1)
\end{aligned}
\tag{5-8}
$$

$$
\begin{aligned}
LC^{r\to l}:\ \text{If}\ & v_{l,n}^{l}(t) > v_{l,n}(t) \\
\text{and}\ & v_n(t) > v_{l,n}(t) \\
\text{and}\ & d_{l,n}^{eff,l}(t) > \min(d_n^{eff}, v_n(t+1)) \\
\text{and}\ & g_{b,n}^{l}(t) > v_{b,n}^{l}(t+1)
\end{aligned}
\tag{5-9}
$$

where, superscript *r, l* represent the right lane and the left lane, suffix *(b, n)* means the vehicle nearby upstream and *(l, n)* represents the leading vehicle (vehicle in front) of vehicle *n*, *g* means the gap.

5.2 Validation

5.2.1 Fundamental traffic features

All the vehicles are set in the front end of the circular track with velocity 0 as the initial condition (at time-step 0). First, for validating our models, both the deterministic (i.e. all the probability parameters in equation (5-1) are set as zero, suggesting that all the drivers have identical driving behaviors) and stochastic CA simulations with different occupancy scenarios are implemented. The maximum speed has been defined in accordance with the regulatory speed limits of Taiwan Freeways, that is, 31cells/sec (111.6 kph).

Figure 5-2 presents the flow-occupancy relations (fundamental diagrams) for the deterministic and stochastic models where the maximum acceleration is set as 3 sites/(time-step)^2 , or equivalently, 3 m/sec^2. For clearer description, the flow rate q(S) is converted from cells into number of vehicles and occupancy ρ(S) is converted into vehicle

per kilometer, as the flow-density relations shown in Figure 5-3. It is noted that, for deterministic model, the max flow rate can reach approximately 5,670 veh/hr, or 2,836 veh/hr/lane, which is higher than 2,400 veh/hr/lane in HCM2000. A reasonable interpretation for this is that the randomization effect, representing the heterogeneity among drivers, has been completely ignored throughout the deterministic simulations, thus significantly diminishing the perturbations between vehicles and leading to such a theoretical maximum flow rate. In other words, this derived maximum flow rate may be deemed as the envelope for the following stochastic simulations. As for stochastic simulations, due to the randomization effect, maximum achievable flow rate is reduced to about 4,480 veh/hr, or 2,240 veh/hr/ln. This is consistent with the empirical data (for example, Chapter 13, HCM2000).

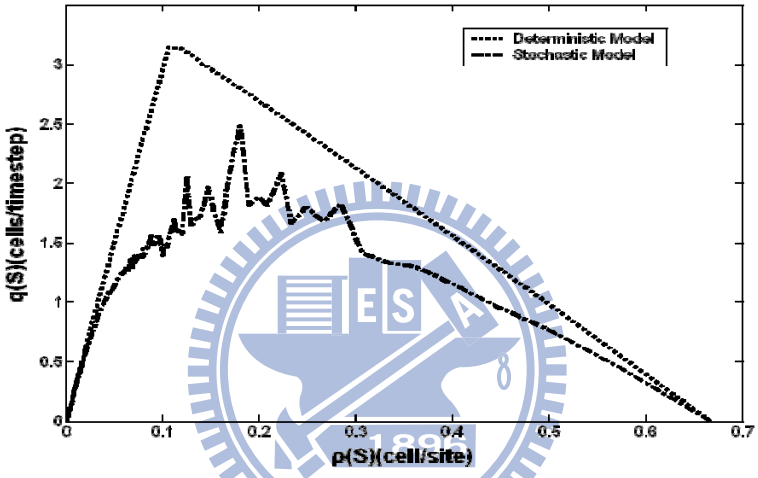

FIGURE 5-2 Flow fundamental diagrams in deterministic and stochastic vehicular traffic (counted in cells/time-step).

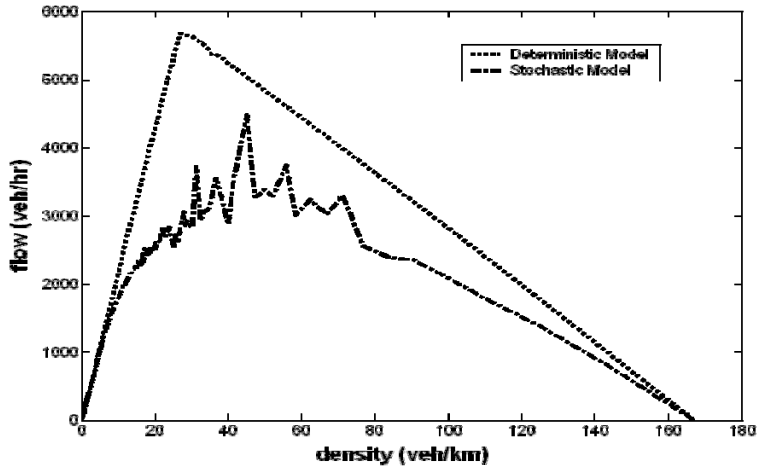

FIGURE 5-3 Flow fundamental diagrams in deterministic and stochastic vehicular traffic (counted in vehicles/hour).

Secondly, from global point of view, the shape of this simulated flow-density result is neither a linear line nor a curve but in a form of coarsely dispersion within a certain area. Repeated simulations are conducted and it reveals that deterministic CA simulations always outcome with identical results. However, due to randomization effect, slight difference always exists for each separate CA stochastic simulations, even with completely identical parameters settings.

Thirdly, we also check the average vehicle speeds throughout the entire simulations and find it reasonably acceptable. For example, in free stream regime where occupancy is low, vehicles are sparely dispersed and thus can move with maximum speeds. The calculated slopes of Figure 5-2 and 5-3 in this regime imply the maximum speeds, i.e., 109.07kph, which locates in the ballpark of the preset one, as mentioned above.

5.2.2 Spatiotemporal traffic patterns

Figures 5-4(a-1), (b-1), (c-1), (d-1) and (e-2) demonstrate the space-time trajectories of vehicles of our stochastic modeling, in which Y-axis represents the vehicles moving from bottom to top and X-axis represents the time advancing from left to right. Figures 5-4(a-2), (b-2), (c-2), (d-2) and (e-2) are the associated spatiotemporal speed patterns. As shown in Figures 5-4(a-1) and (a-2), when with low occupancy, vehicles are sparely distributed, only few interactions among vehicles are expected. Accordingly, free-flow traffic pattern prevails. However, aware that due to stochastic effect, vehicles will occasionally decrease speeds; henceforth, a small region of perturbation can be found. This is so-called “synchronized flow phase” where vehicles may travel at various speeds from high speed (stable state) to low-speed (metastable state). This synchronized traffic region will gradually enlarge and reoccur intermittently downstream and become much clearer as long as occupancy increases, as shown in Figures 5-4(b-1) and (b-2).

As the occupancy (density) increases, furthermore, the platoon preset at t=0 will become more difficult to disperse because vehicles in the upstream will arrive more frequent the rear of platoon to maintain a jammed queue. Quite complex behaviors with noticeable propagation of backward shock waves, or the so-called “wide moving jams,” can be observed. Figures 5-4(c-1) and (c-2) has clearly depicted this phenomenon. Note that the upstream and downstream front of wide moving jam are in the form of parallel lines, moving upstream with the same speed v_g =15.6 kph, again very close to a well-known empirical speed-15 kph evidenced by Kener (2004). Also note that upstream speed of the

downstream front of wide moving jam keep almost identical even when the occupancy continuously increases, as can be seen in Figure 5-4(d-1) and Figure 5-4(e-1). The major traffic pattern change coupled with increasing occupancy is that the considerable extension of both synchronized flow and moving jam region.

(a-1)

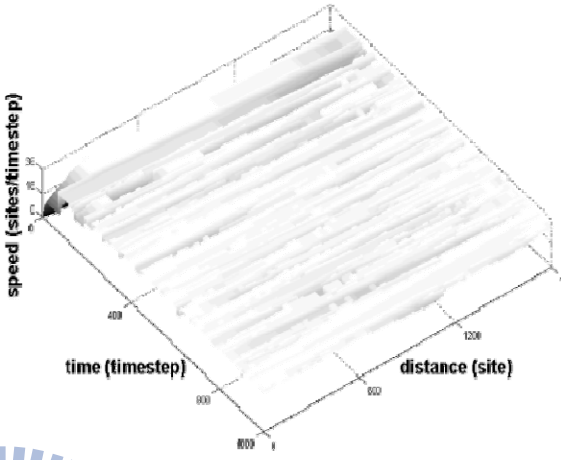

(a-2)

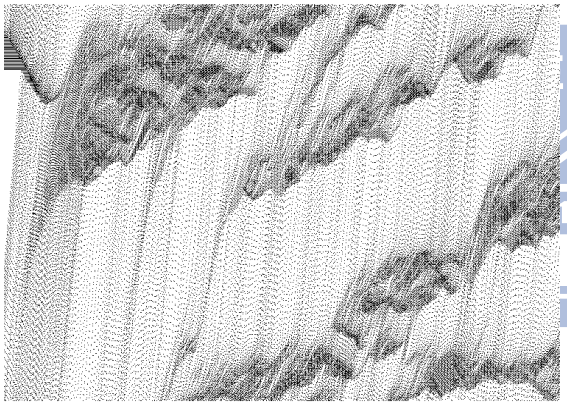

(b-1)

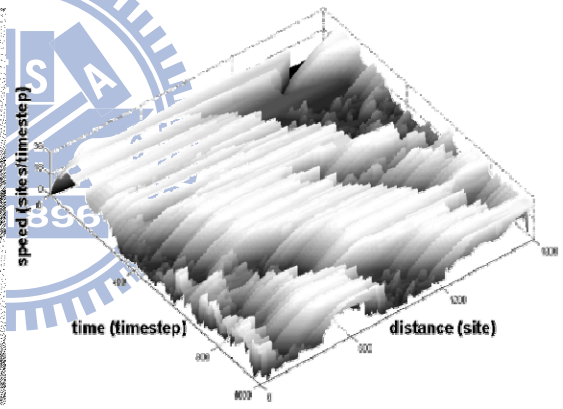

(b-2)

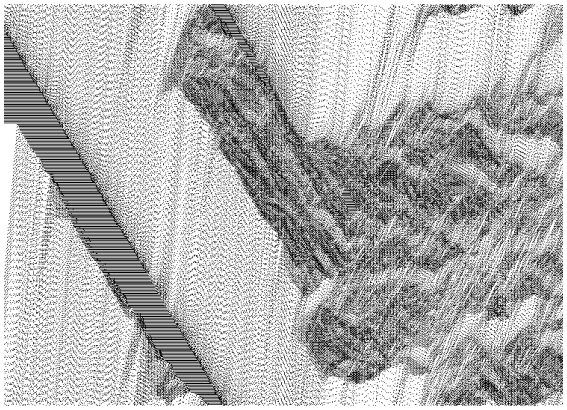

(c-1)

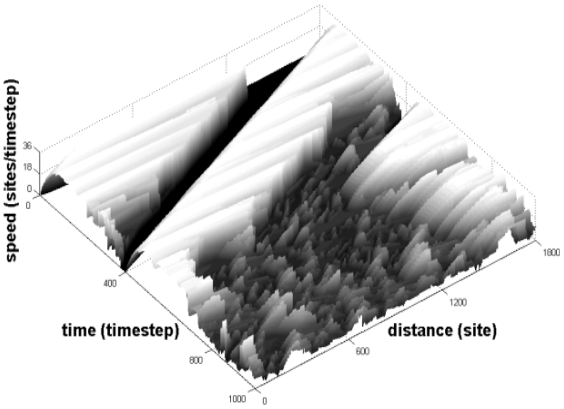

(c-2)

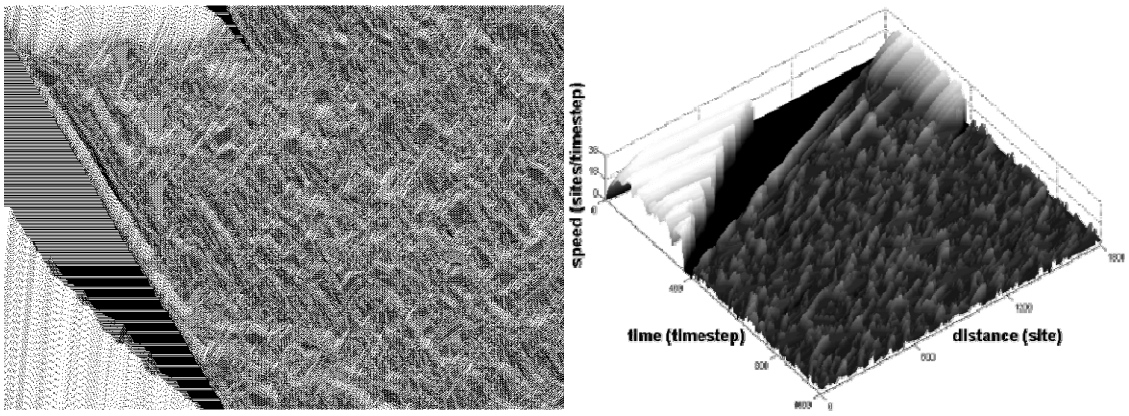

(d-1) (d-2)

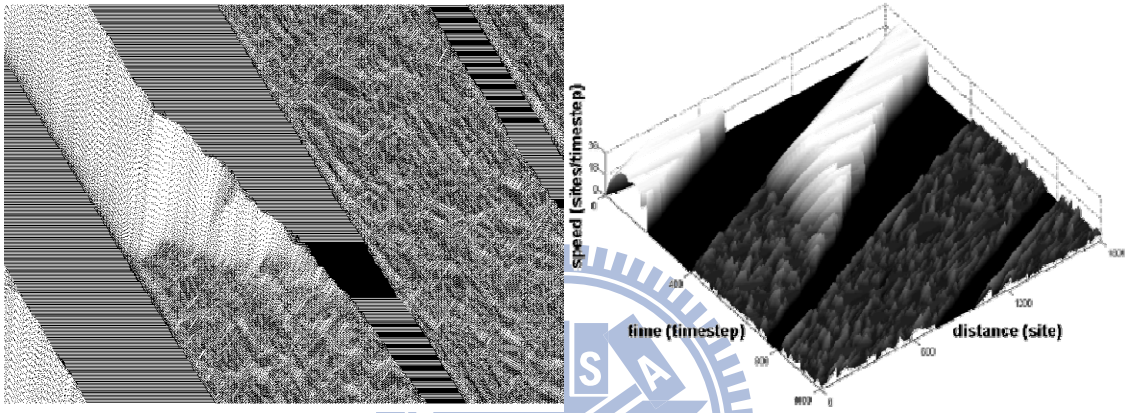

(e-1) (e-2)

FIGURE 5-4 Vehicular trajectories and traffic patterns for different occupancies. (a) $\rho(S)$= 0.020, (b) $\rho(S)$= 0.113, (c) $\rho(S)$= 0.200, (d) $\rho(S)$= 0333, (e) $\rho(S)$= 0.400.

5.3 Effects of Stationary and Moving Bottlenecks

This section further explores more interesting and diversified traffic patterns by introducing a slowly moving vehicle into simulation. We deliberately add one twin-truck into different occupancies. To initiate the simulation, this twin-truck is placed near the middle of the right lane and it will keep remaining on the right lane throughout the simulation (i.e., no lane-change for this twin-truck). In the following, the maximum speeds of this twin-truck will be set equal to zero to represent a stationary bottleneck and equal to 10 and 20 sites/time-step (36 kilometer/hour and 72 kilometer/hour), respectively, to serve as moving bottlenecks. The simulated fundamental diagrams are enclosed as in Figure 5-5 (counted in cell/time-step) and Figure 5-6 (counted in vehicles/hour), to show the impact arouse since. As anticipated, this slow moving vehicle impairs the whole traffic capacity and as a consequence noticeably decreases the maximum flow rate. It is due to the fact that a bottleneck would inevitably restrain the road capacity. Besides, one may tell that along

with lower twin-truck speed, the achievable maximum flow rate also declines. When a fix bottleneck is set on the middle of the road, the traffic capacity would reduce to only about 1,000 vehicles/hours/lane, namely, about 55% of the capacity would be lost.

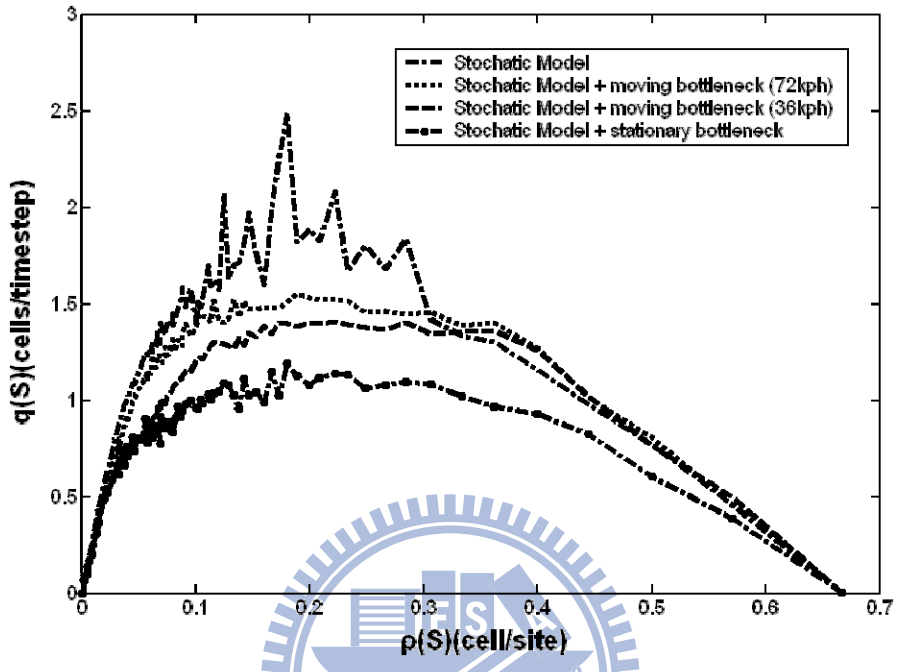

FIGURE 5-5 Impacts of stationary and moving bottlenecks (counted in cells/time-step).

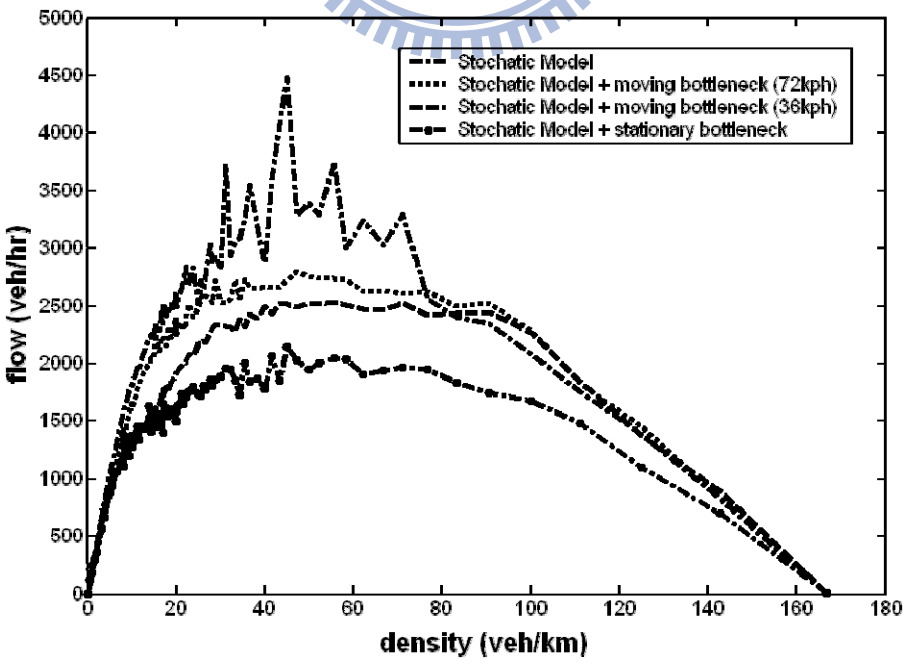

FIGURE 5-6 Impacts of stationary and moving bottlenecks (counted in vehicles/hour).

Another point worthy mentioning is that when introducing a bottleneck, stationary or moving, there is a plateau existent in the fundamental diagrams in the neighborhood of the optimum flow point, with densities ranging from 20 to 90 vehicles/km. A more detailed check of our simulation data reveals that the lane-change rate will be increased, as shown in Figure 5-7. It is obvious that when noticing a bottleneck in front, the drivers will tend to overtake that bottleneck if possible.

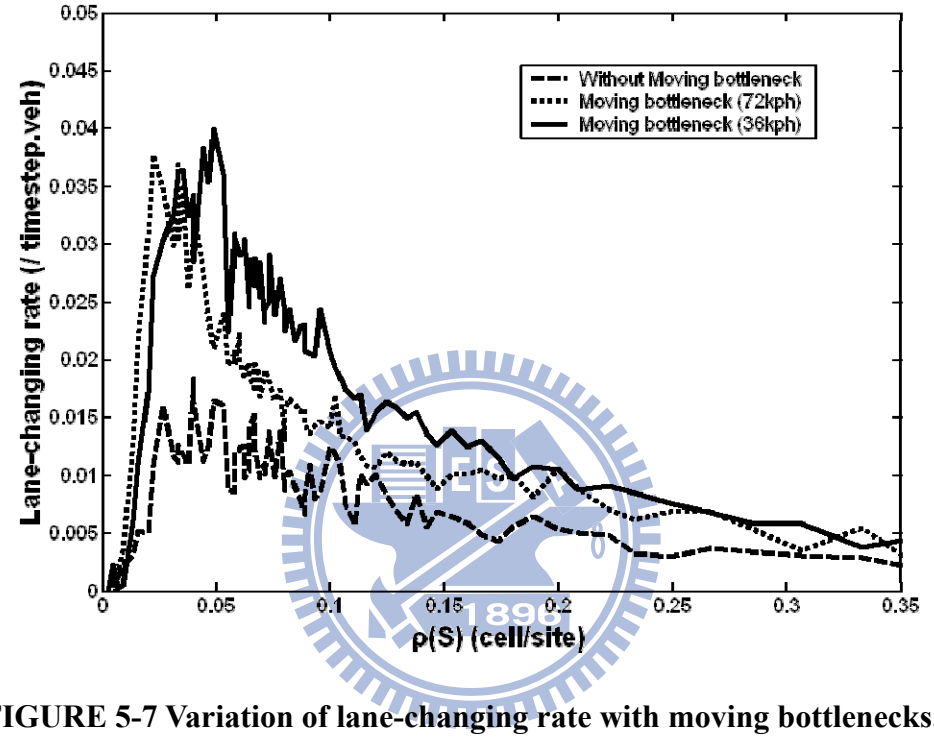

FIGURE 5-7 Variation of lane-changing rate with moving bottlenecks.

The impacts of moving bottlenecks to the originally formed synchronized flow and moving jam can be described through the vehicular space-time trajectories. Figure 5-8 depicts the flow pattern changes aroused since under different occupancies. The left panel of Figure 5-8 represents the original flow pattern, while the right panel indicates the variation when moving bottleneck is brought in. First, even at low occupancy, a moving bottleneck can incur small platoon in behind, as shown in Figure 5-8(a-2). This is consistent with the previous surveys. As occupancy increases, the slow moving vehicle would raise the possibility of the emergence of synchronized region, as shown in Figure 5-8(b-2). However, its impact to the originally existing wide moving jam is quite different. Our simulation shows that a slowly moving vehicle tends to reduce the lifetime of existing moving jam. Since the direct influence of it is to restrain the traffic capacity and reflect in lower flow, vehicles will arrive at the rear of platoon with less frequency, thus accelerate the dissipation pace of moving jam, as shown in Figures 5-8(c-2), (d-2) and (e-2).

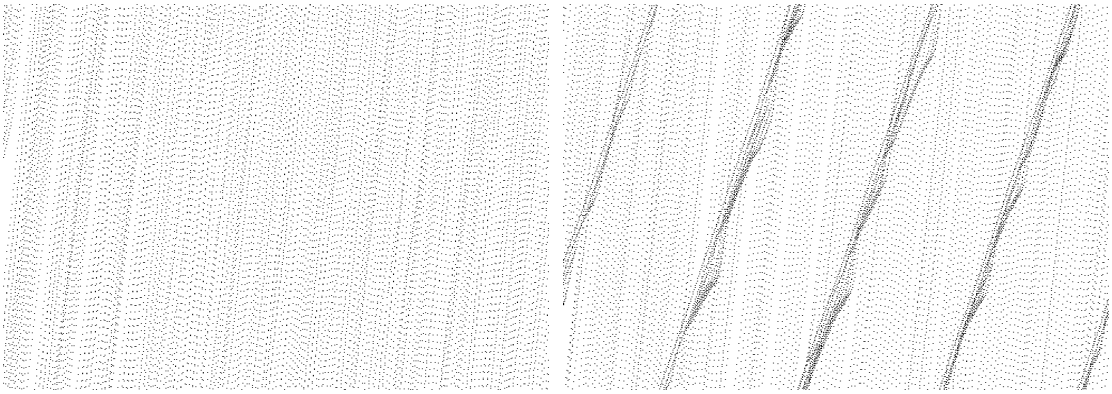

(a-1) (a-2)

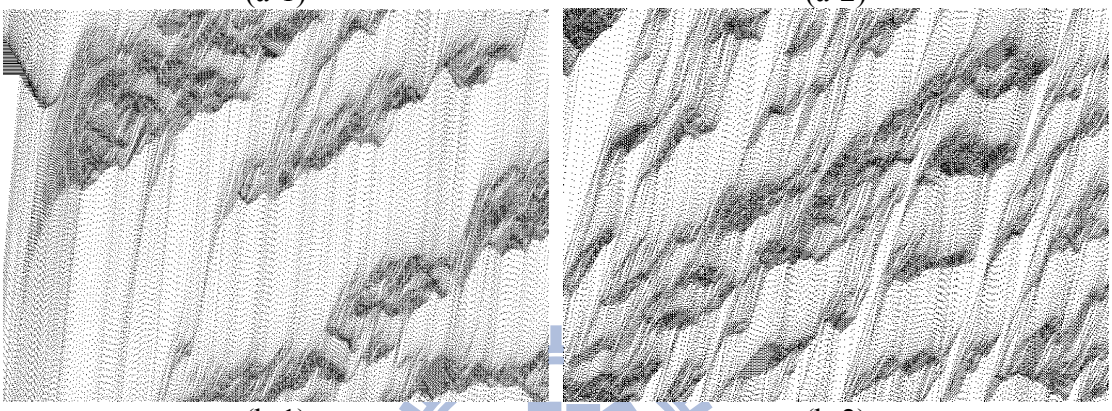

(b-1) (b-2)

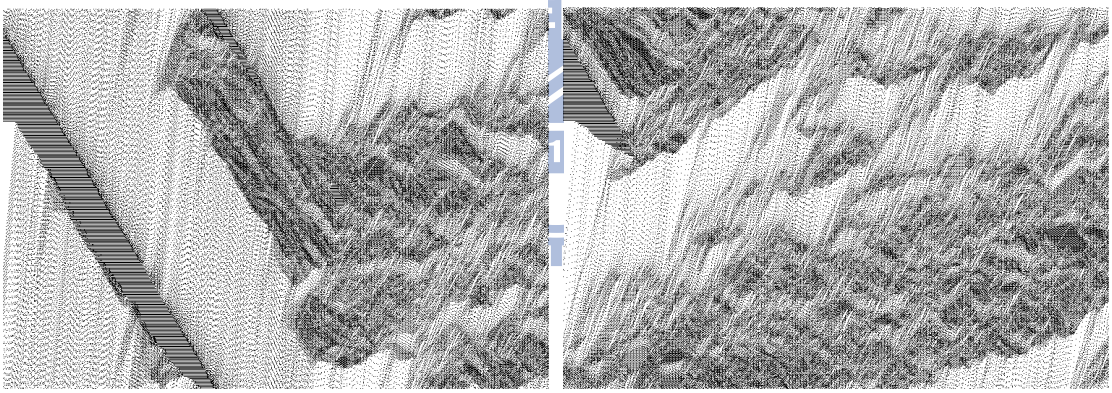

(c-1) (c-2)

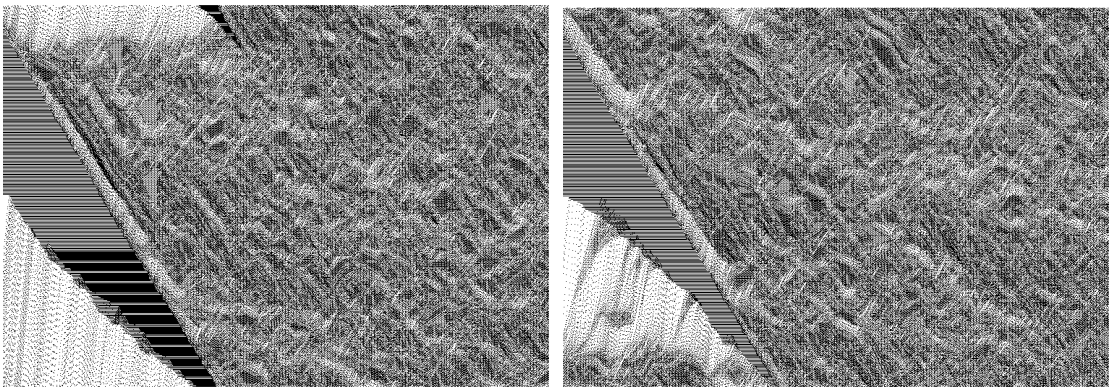

(d-1) (d-2)

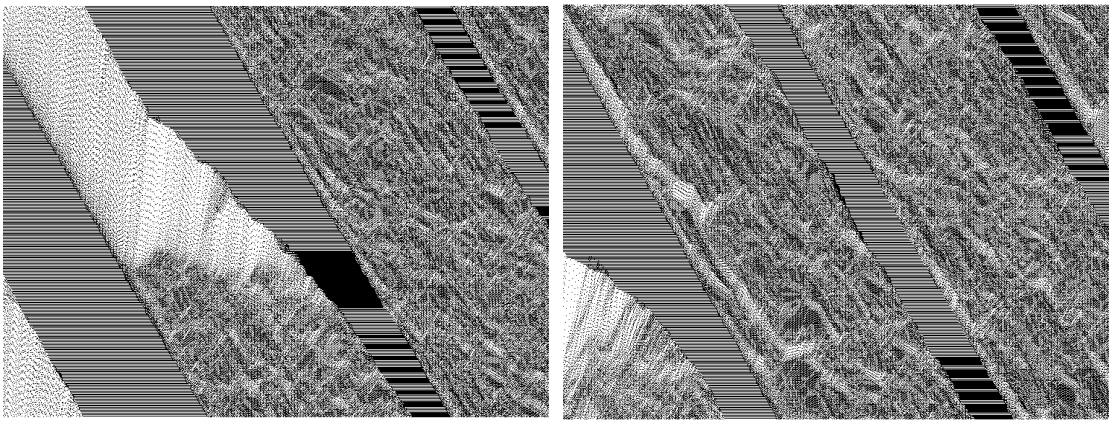

(e-1) (e-2)

FIGURE 5-8 Vehicular trajectories and traffic patterns with a moving bottleneck of speed 36 kph (a) *ρ(S)*= 0.020, (b) *ρ(S)*= 0.113, (c) *ρ(S)*= 0.200, (d) *ρ(S)*= 0333, (e) *ρ(S)*= 0.400.

The effect of stationary bottleneck, on the other hand, is shown in Figure 5-9. It expresses quite different phenomena as compared with the moving bottlenecks. First, one may identify that the front of the synchronized flow is fixed at the stationary bottleneck. Besides, as occupancy increases, a synchronized flow region grows gradually behind the bottleneck and eventually leads to the emergence of narrow moving jam (Figures 5-9(b) and 5-9(c)). These narrow moving jams further extend and merge with each other to transform into wide moving jams. Our simulation result at this point is consistent with that proposed by Kerner (2004).

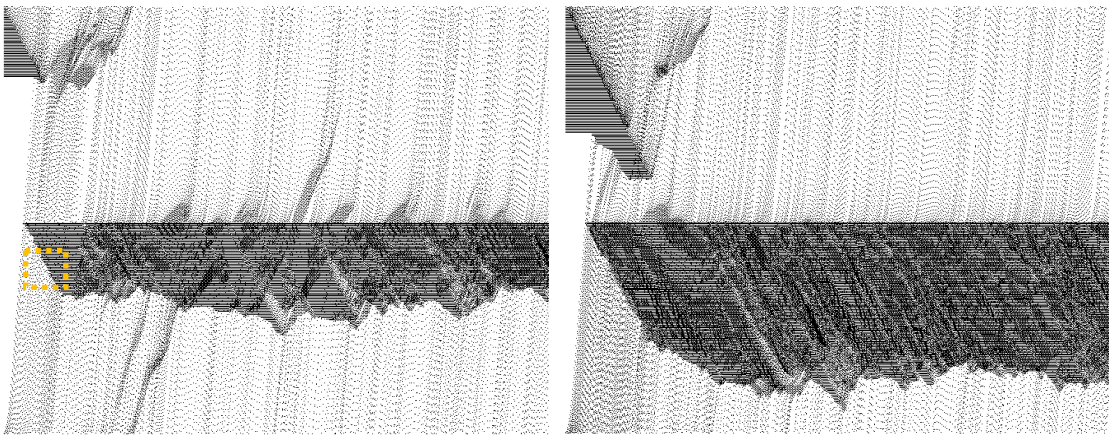

(a) *ρ(S)*= 0.113 (b) *ρ(S)*= 0.200

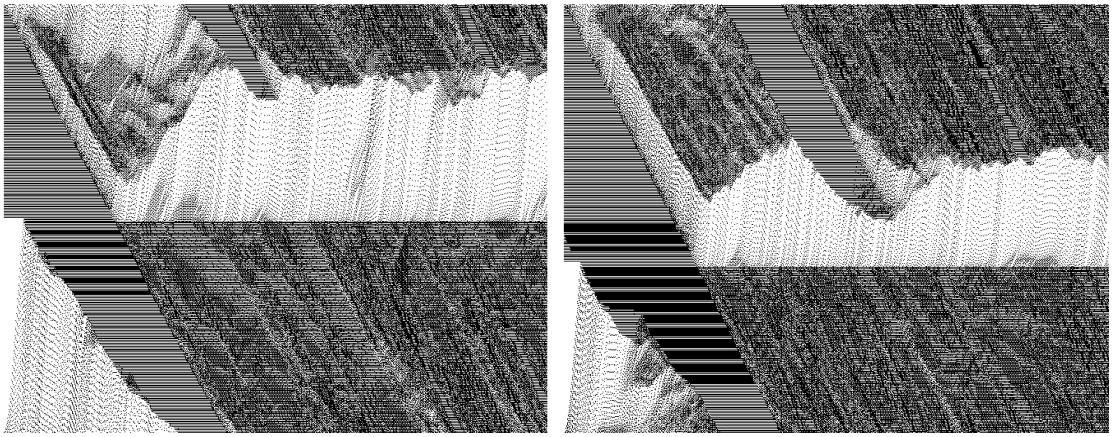

(c) $\rho(S)$= 0.333 (d) $\rho(S)$= 0.400

FIGURE 5-9 Vehicular trajectories and traffic patterns with a stationary bottleneck (a) $\rho(S)$= 0.113, (b) $\rho(S)$= 0.200, (c) $\rho(S)$= 0333, (d) $\rho(S)$= 0.400.

5.4 Summary

The revised CA model has introduced the generalized spatiotemporal definitions for occupancy, flow and speed to precisely capture the collective behaviours of traffic features. They also introduced a refined common unit (CU) system to represent a "fine cell" and a "fine site," which can respectively gauge the non-identical vehicular widths and lengths (to more accurately explicate the spatiotemporal traffic features in mixed flow contexts) and the non-identical lane widths (to more accurately reflect distinct lane widths in different roadway systems such as freeway and urban narrow street). One important advantage of the refined CU system is that the "resolution" of the simulation results has been largely raised. Hence, the variation of vehicular speed as well as the coupled position update can be revealed more precisely. Also the effects of both vehicle width and lane width on traffic characteristics, besides the effects of vehicle length, can be accounted for.

The simulation results have demonstrated that this revised CA models are capable of capturing the essential features of traffic flows which were also found in previous works (for instance, Nagel et al, 1992; Barlović, et al. 1998; Knospe et al, 2000; Jiang et al, 2003; Kerner, 2004). However, the deficit of abrupt change in speed at the upstream front of traffic jam still existed, as shown in Figure 5-10 dotted line circles (enlarged from Figure 5-9(a) dotted line square). It therefore needs further modification to reasonably elucidate the limited deceleration capabilities.

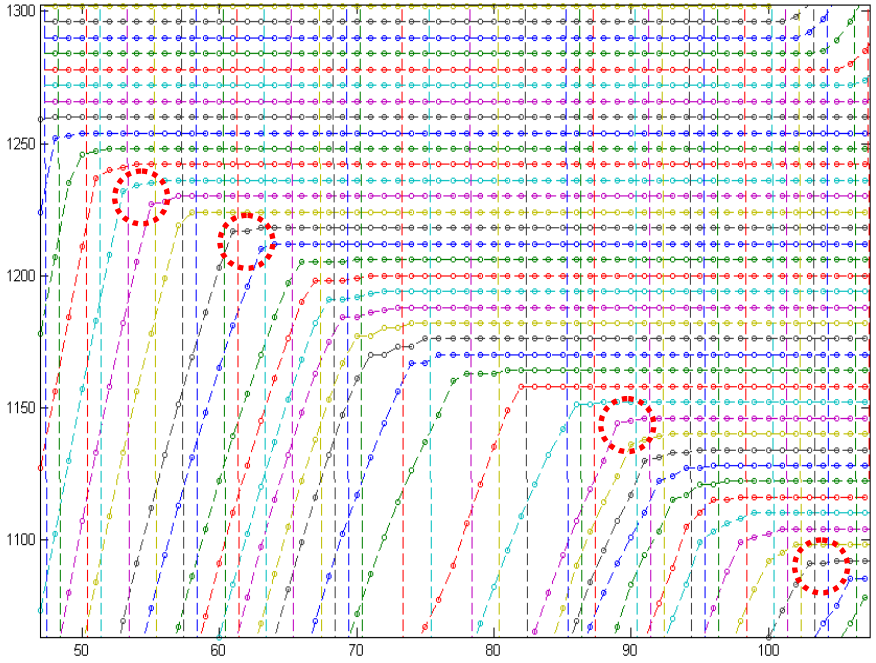

FIGURE 5-10 Abrupt change in speed at the upstream front of traffic jam.

Chapter 6 REFINED CELLULAR AUTOMATON MODEL

Since the revised CA model in chapter 5 basically followed the acceleration rule proposed by Knospe *et al*. (2000) and Jiang and Wu (2003), the deficit of abrupt change in speed at the upstream front of traffic jam still existed. This chapter attempts to further proposes a refined CA model. First, we revise the particle-hopping velocity variation as piecewise-linear to more realistically reflect the genuine vehicle movement. Upon this, the limited deceleration of vehicle is introduced. Section 6.1 discusses the limited deceleration algorithm, which is in essence an extension of the early car-following models proposed by Pipes (1953) and/or Forbes et al. (1958). Some validation and comparison with the conventional CA model are addressed in Section 6.2. To demonstrate the applicability, the refined CA model is further implemented into the traffic simulation at a highway work zone. Variable speed control schemes applied to the upstream subsegments of the work zone are investigated in Section 6.3. This chapter ends with a discussion in Section 6.4.

6.1 Refined Rules

Simulation through the above mentioned CA updated rules has shown its success in capturing essential features of traffic flows that were also found in previous works. However, it is found that although the idea of limited acceleration is implemented (refer to Chapter 5 equation (5-2) hereinabove); deceleration limitation has seldom been considered. In fact, most CA models have considered a collision-free criterion explicitly by imposing arbitrarily large deceleration rates (refer to Chapter 5 equation (5-3) hereinabove), which can be far beyond the practical braking capability under prevailing pavement and tire conditions. Consequently, most previous CA simulations have revealed that, for sake of collision prevention, a vehicle can take as short as 1 second to come to a complete stop, even from a full speed (e.g., 100 kph), apparently exceeding the vehicular deceleration capabilities. Such unrealistic abrupt deceleration can be easily identified via checking the vehicular speed profiles in the front of traffic jams or stationary obstacles.

The revised CA model in Chapter 5 has led to reasonable outcomes if only long-term average traffic features are concerned or only macroscopic traffic phenomena or global traffic parameters are examined because the effects of locally realistic deceleration have been smoothed out. However, if we scrutinize in detail the microscopic traffic parameters or the neighborhood of some unexceptional scenarios, such as an accident vehicle or a work zone blocking the partial lanes, it is evident that the deceleration rule in the revised CA model in Chapter 5 requires further improvement.

As mentioned by Lee *et al.* (2004), however, when setting limited deceleration into simulations, the bounded braking capability would change the collision-free mechanism entirely. In addition, discrete variations of traffic parameters that are essentially the nature of CA model would exaggerate the consequence further. If one characterizes vehicles with finite deceleration capability, the simulations by prevailing CA models would reveal that with high probability vehicles will collide with the front vehicle that is stationary or rapidly decelerated.

Krauss and Wagner (1997) was perhaps the first effort introducing the limited deceleration capability into CA modelling. The so-called "safe speed" was defined through the following concept.

$$v^{(safe)}\tau^{(safe)} + X_d(v^{(safe)}) \le g_n + X_d(v_{l,n}) \tag{6-1}$$

where,

g_n is the space gap.

$X_d(u) = (u - b\tau) + (u - 2b\tau) + \ldots + \beta b\tau = b\tau^2(\alpha\beta + \frac{\alpha(\alpha-1)}{2})$

represents the expected distance traveled with original speed u and deceleration rate b.

$\tau^{(safe)} = v^{(safe)}/b = \alpha_{safe} + \beta_{safe}$ stands for the safe time gap for drivers.

$$\alpha_{safe} = \sqrt{2\frac{X_d(v_{l,n}) + g_n}{b} + \frac{1}{4}} - \frac{1}{2}$$

$$\beta_{safe} = \frac{X_d(v_{l,n}) + g_n}{(\alpha_{safe} + 1)b\tau^2} - \frac{\alpha_{safe}}{2}$$

$v_{l,n}$ is the speed of preceding vehicle.

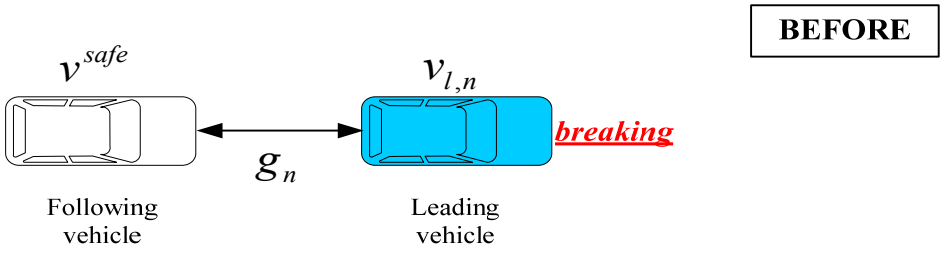

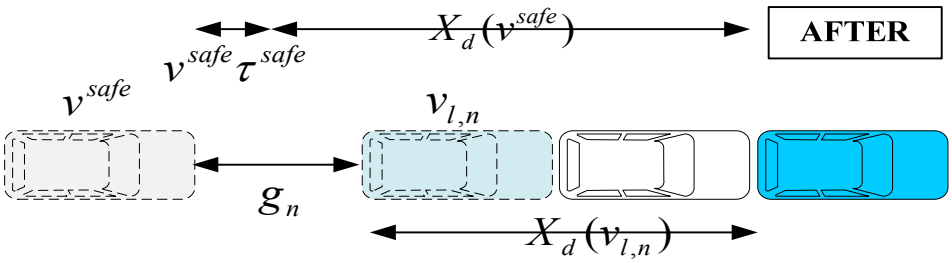

FIGURE 6-1 A sketch diagram of the safety condition for vehicles motion.

Lee *et al.* (2004) further introduced the limited capabilities of acceleration *(a)* and deceleration *(D)* in their model and proposed the following safety criteria for vehicle movement; which is in effect similar to that proposed by Krauss *et al.* as cited above.

$$x_n^t + \Delta + \sum_{i=0}^{\tau_f(c_n^{t+1})} (c_n^{t+1} - Di) \le x_{n+1}^t + \sum_{i=1}^{\tau_l(v_{n+1}^t)} (v_{n+1}^t - Di) \qquad (6\text{-}2)$$

where,

$n(n+1)$: denotations of follower (leader).

c_n^{t+1}: safe speed at time $t+1$.

$x_{n+1}^t(v_{n+1}^t)$: location (speed) of leader at time t.

$x_n^t(v_n^t)$: location (speed) of follower at time t.

$\tau_f(\tau_l)$ *:* time steps required for follower (leader) decelerate to complete stop.

$i = 0, 1, \ldots, \ \tau_f$ for follower and

$i = 1, 2, \ldots, \ \tau_l$ for leader.

D : maximum braking capacity.

Δ : minimum clearance of the follower.

Both of the aforementioned modifications are established under the assumption that the following driver will always be aware of the speed of lead vehicle and hence will continuously maintain adequate distance to prevent collision in case that the preceding vehicle in next time step decelerates to a complete stop. However, it is argued that the following vehicle always taking caution to maintain adequate distance to the lead vehicle is

over-conservative. Drivers can easily sense the relative speeds to, rather than the absolute speeds of, the front vehicles. In other words, drivers would be able to tell they are approaching vehicles in front, primarily due to the changes in apparent size of the vehicles, by perceiving relative speed changes. Only with positive relative speeds to the front vehicles would the following drivers take caution for collision prevention. Based upon this, we propose the following modifications:

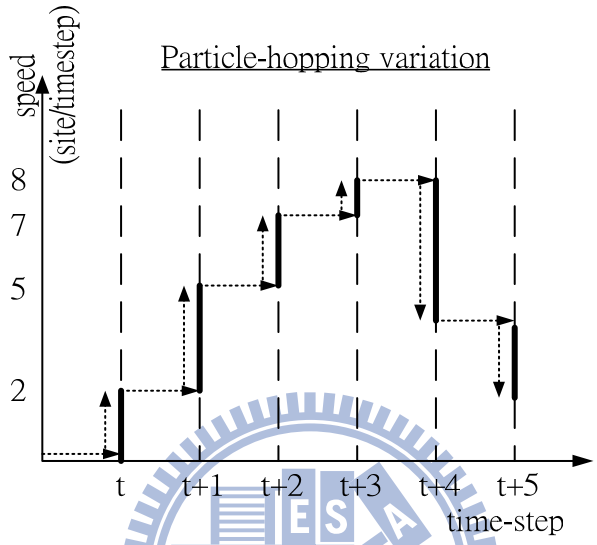

FIGURE 6-2 Different definitions of vehicular speed update: particle-hopping variation.

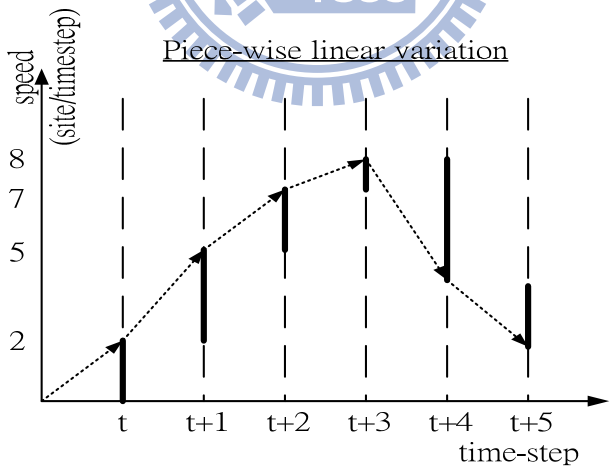

FIGURE 6-3 Different definitions of vehicular speed update: piecewise-linear variation.

Firstly, revise the discrete speed variations to become piecewise-linear in each time-step. The particle-hopping manner, as shown in Figure 6-2, adopted by most existing CA models, is over-simplified. Therefore, we alternatively suggest that vehicles will smoothly vary their speeds from the original ones at the beginning to the desired speed by the end of each time-step, as shown in Figure 6-3. Thus more realistic

accelerating/decelerating behaviors of vehicles can be generated. Secondly, only upon this revision and coupled with the refiner cell/site system can the Newton's kinematics to determine the appropriate deceleration being introduced.

$$\ddot{x}_n(t) = \frac{1}{\tau}[\dot{x}_{n+1}(t) - \dot{x}_n(t)] \tag{6-3}$$

Thirdly, as regard to the location update, since vehicular speed varies piecewise-linearly within each time-step, through basic integral calculation one may find the movement of vehicle is simply the average of the existing speed and the desired speed by the end of each time-step. However, the derived average requires rounding off to the nearest integer since, by nature of CA modeling, vehicles still move on cell/sites basis. This approximation is deemed acceptable when the refined cell/site system is implemented. In this chapter we deliberately choose the truncated integers to ensure that no collision with the front vehicles would be incurred.

Upon the above illustrations, "Chapter 5 equation (5-3) Step 3: Deceleration" and "Chapter 5 equation (5-7) Step 7: Update position" of the former CA updated rules are respectively revised as follows:

1. Revised Step 3: Deceleration. If $v_{n+1}^{t+1} < v_n^{t+1}$, check the following safety criteria to determine speed at the next time step.

$$x_n^{t+1} + \Delta + \sum_{i=1}^{\tau_f(c_n^{t+1})} (c_n^{t+1} - Di) \le x_{n+1}^{t+1} + \sum_{i=1}^{\tau_f(c_n^{t+1})} v_{n+1}^{t+1} \tag{6-4}$$

where,

n(n+1): denotation of the follower (leader).

c_n^{t+1} : safe speed of the follower at time *t+1*.

$x_{n+1}^{t+1}(v_{n+1}^{t+1})$: anticipated location (anticipated speed) of the leader at time *t+1*.

$x_n^t(v_n^t)$: location (speed) of the follower at time *t*.

x_n^{t+1} : location of the follower by end of time *t+1*.

τ_f : time steps required for the follower at time *t+1* with c_n^{t+1} decelerating to v_{n+1}^{t+1}.

D: maximum braking capability; based on our field observation, it is set as *6 m/s*^{2} for light vehicles.

2. Revised Step 7: Update position.

$$x_n^{t+1} = x_n^t + roundoff\left(\frac{v_n^t + v_n^{t+1}}{2}\right) \tag{6-5}$$

6.2 Validation

The validation simulations are performed for pure traffic context. Initially, all the vehicles are set equally spaced or line up from end of road section on the circular track, with speed 0 at time-step 0. We simulate for 600 time-steps. The maximum speeds are defined in accordance with the prevailing speed limits (110 *kph*) on Taiwan's freeways, that is, 31 *cells/time-step* (111.6 *kph*). Maximum acceleration is set as 3m/s^2 whereas maximum deceleration as -6 *m/s*^{2}.

Three criteria are selected for validating the refined CA model:

1. According to the field observation, the backward speed of downstream front of traffic jam should be around 15 *kph*.

Figure 6-4 and 6-5 depict the simulated x-t diagrams of scenarios with different preset densities, in which vehicles line up from the end of road section when the simulation initiates. According to the simulations, the backward speed of downstream front of traffic jam is 14.7 *kph*, very close to the field observation, 15 *kph*.

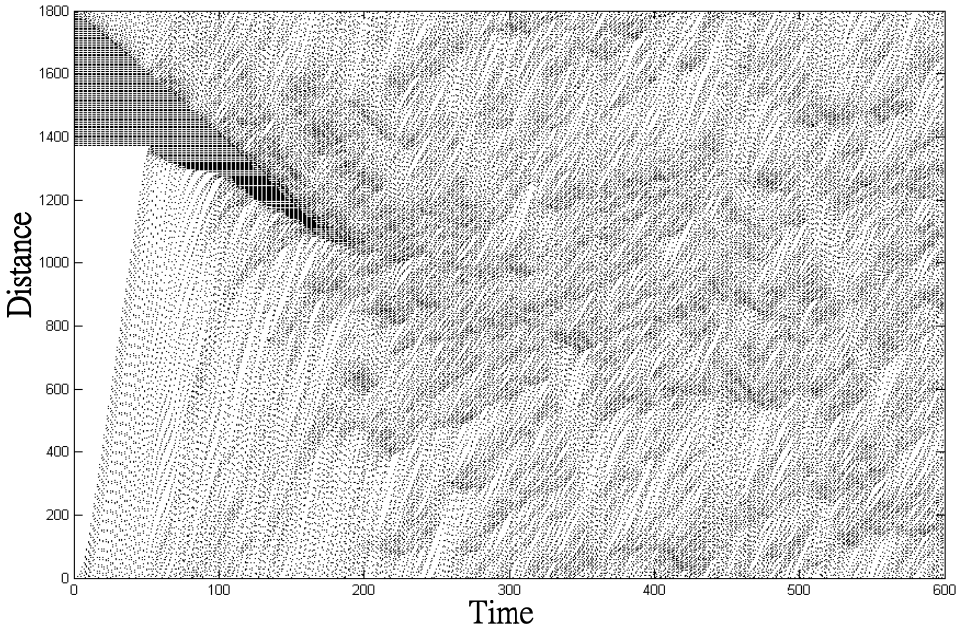

FIGURE 6-4 Simulated x-t diagram, the horizontal axis represents the time passed whereas the vertical axis represents the locations of vehicles (ρ=40 veh/km/lane).

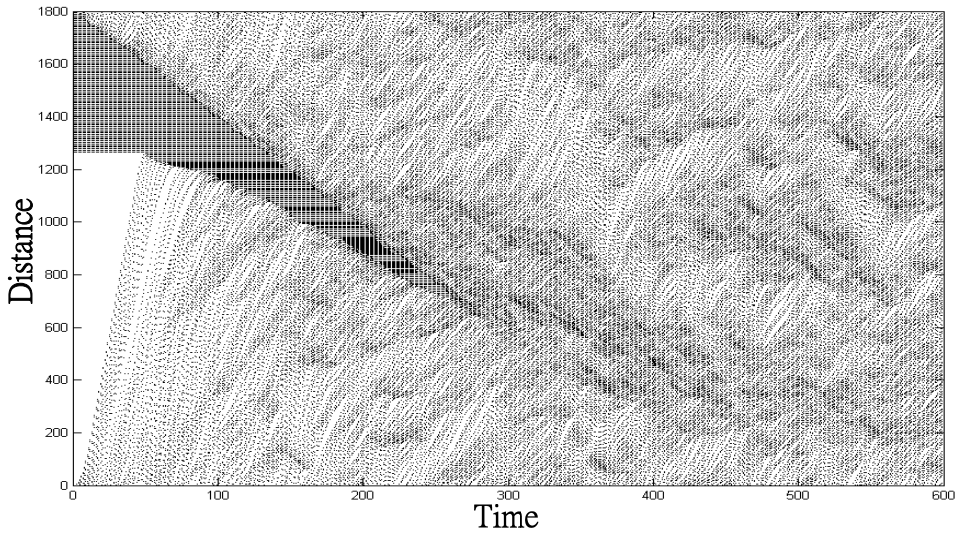

FIGURE 6-5 Simulated x-t diagram, the horizontal axis represents the time passed whereas the vertical axis represents the locations of vehicles (ρ=50 veh/km/lane).

2. The speed drop near upstream front of stationary bottleneck should cope with limited deceleration capability.

Figure 6-6 displays the zoom-out plots of vehicle trajectories when they approach upstream front of traffic jam under different update CA rules. It reveals that the unrealistic abrupt speed drop has been rectified when revised update rules are implemented. Figure 6-7 provides clearer picture of speed variations when vehicles reaching the traffic jam. Here the speed variations of few consecutive running vehicles are selected for elucidation. One could easily tell that the revised CA model has successfully fixed the above mentioned unrealistic deceleration behaviors. Vehicles decelerating in timely manner thus can reflect the genuine driver behaviors in real world.

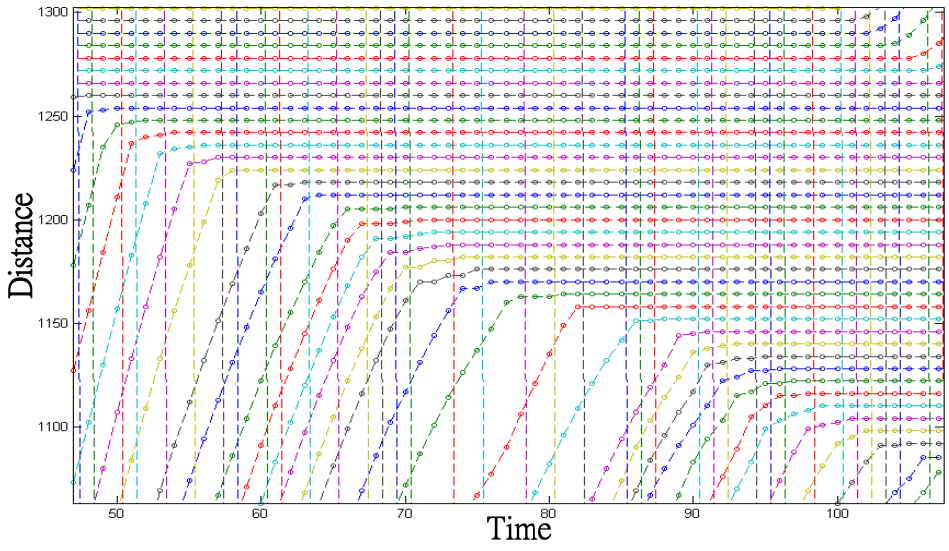

(a) Revised CA Model

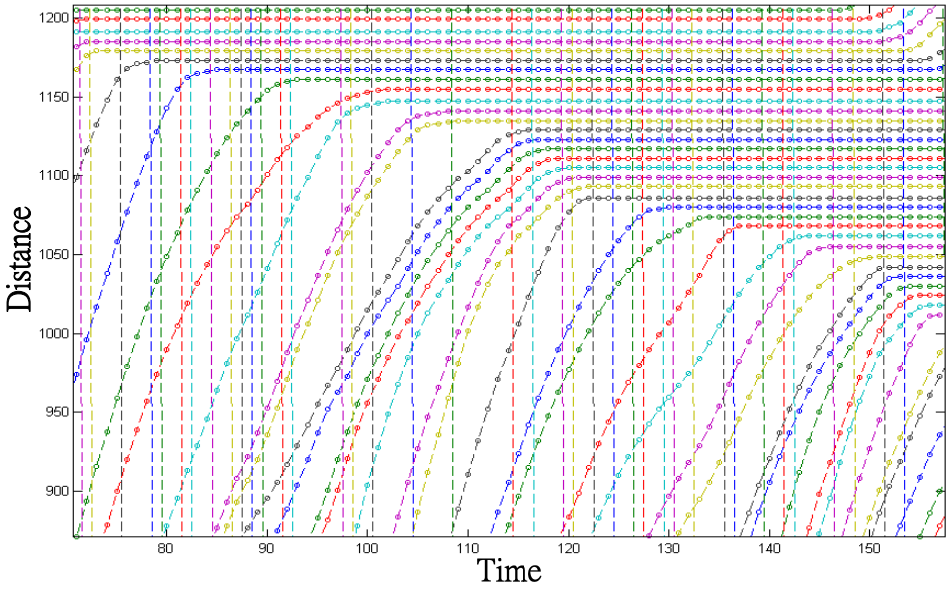

FIGURE 6-6 Comparison of vehicular trajectories when approaching upstream front of traffic jam.

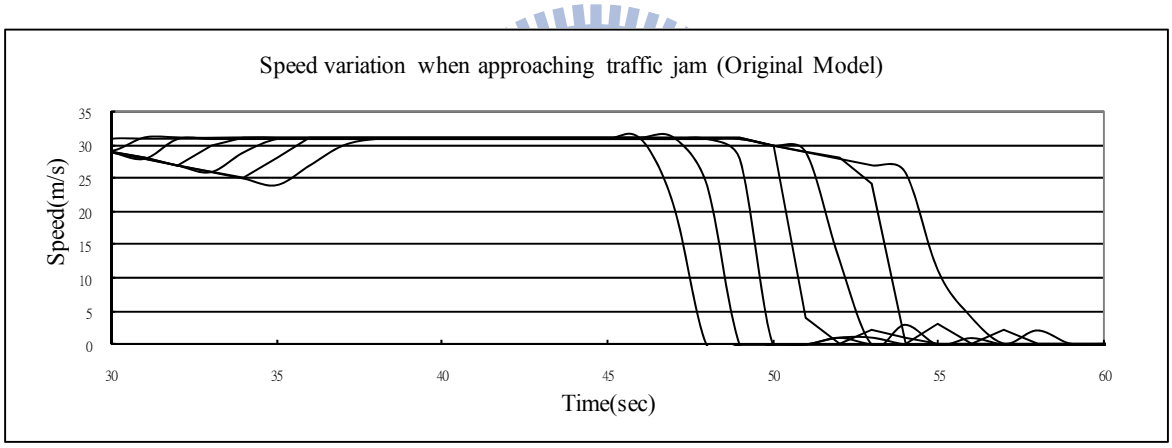

(a) Revised CA model

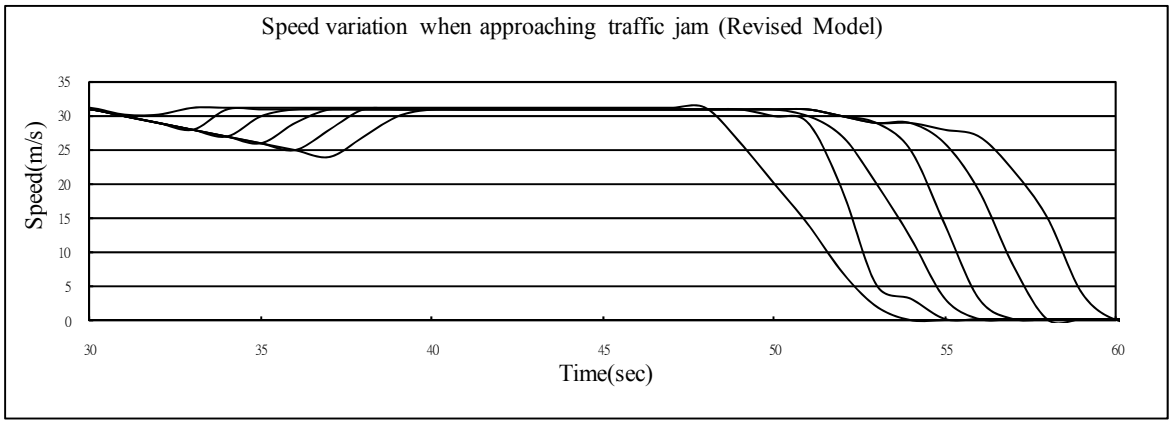

(b) Refined CA Model

FIGURE 6-7 Comparison of speed variations when approaching upstream front of traffic jam.

3. The transition among global traffic patterns, as shown in distance-time (*x-t*) diagram, should be reasonable.

Figure 6-8 further demonstrates the influence of limited deceleration to the x-t diagram. In the beginning of simulations, vehicles are equally spaced in accordance with different preset traffic density values. One may find that, as compared with the original model, the revised model can more precisely reproduce the synchronized flow region, as prevailed in real world. One may also find that some clustered traffic patterns frequently emerge in the original model, even with the refiner cell/site system and low traffic density settings. This is mainly incurred by the unlimited deceleration equipped with vehicles. In contrast, due to the limited deceleration, in the revised model, vehicles operate with moderate speed variation and consequently, the clustered traffic patterns disappear; instead, some wide-dispersed synchronized flow regions can be identified, which are more in line with the field observation.

In addition, through the revised model, the self-induced traffic moving jams can be located as the traffic density increases and exceeds 70 *veh/km/lane*. It is, however, very difficult to appear such moving jams when implementing original CA model, no matter whatsoever the traffic density is. The retro-transitions between traffic patterns, even the parallel moving of traffic jams can also be effectively simulated through the revised CA model.

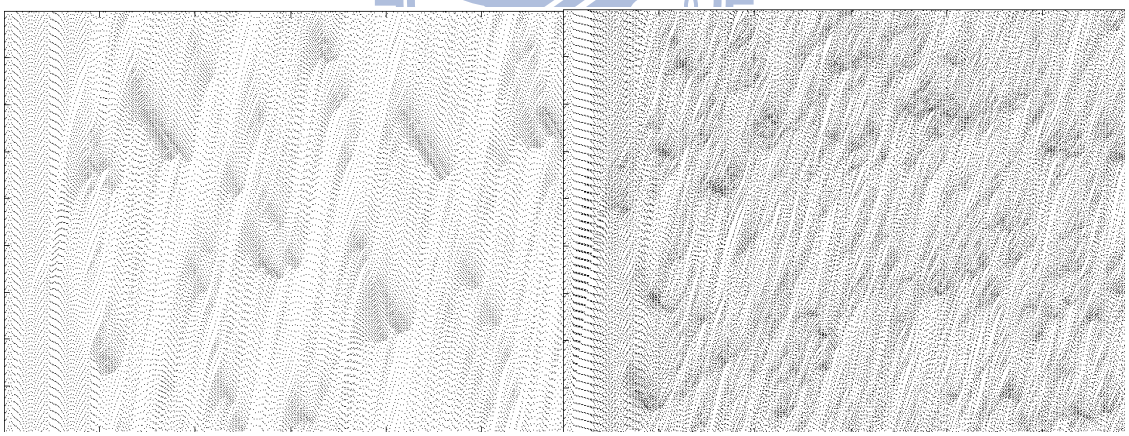

(a) *ρ=30 veh/km/lane*

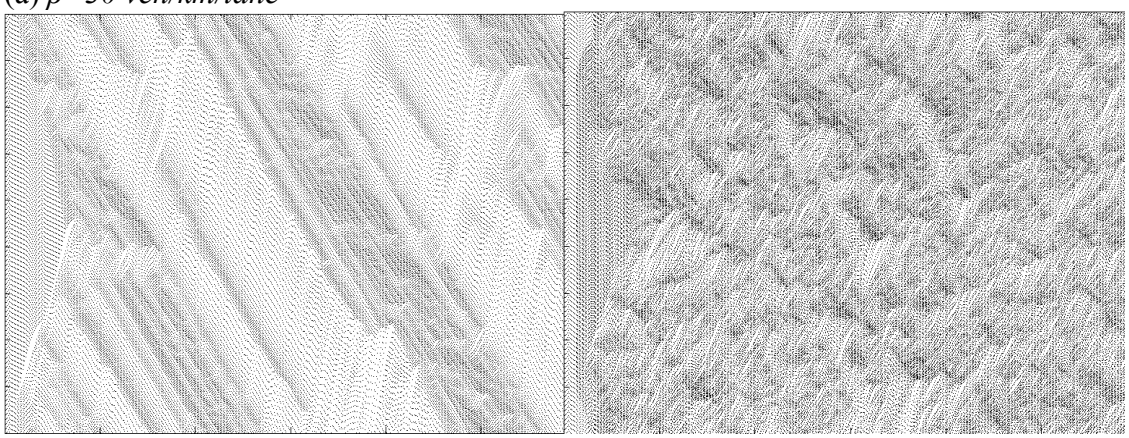

(b) *ρ=50 veh/km/lane*

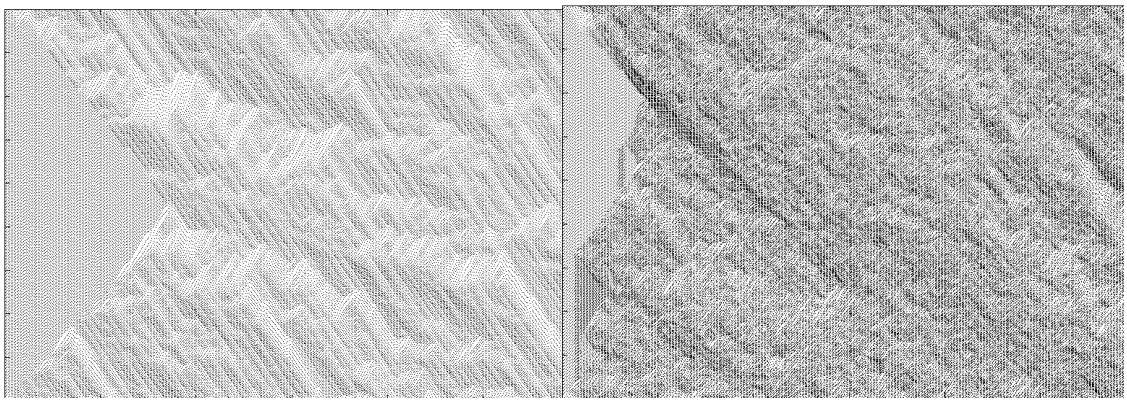

(c) *ρ=71 veh/km/lane*

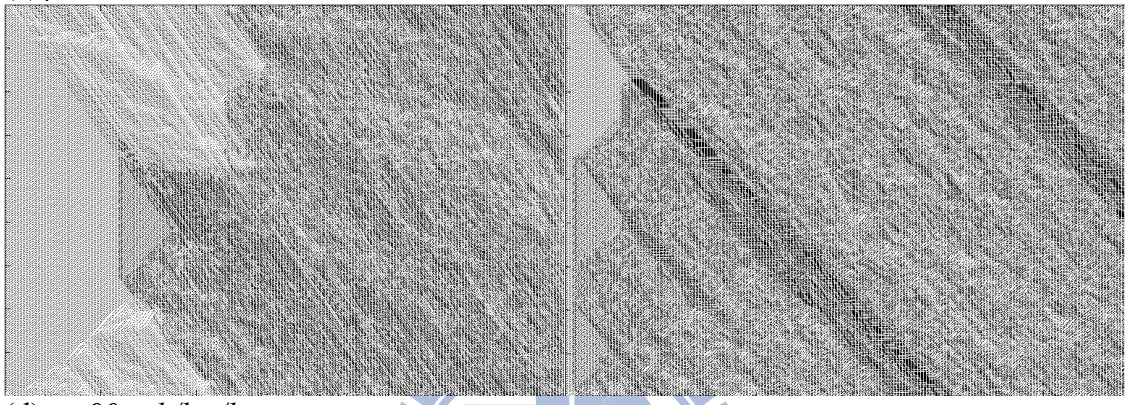

(d) *ρ=90 veh/km/lane*

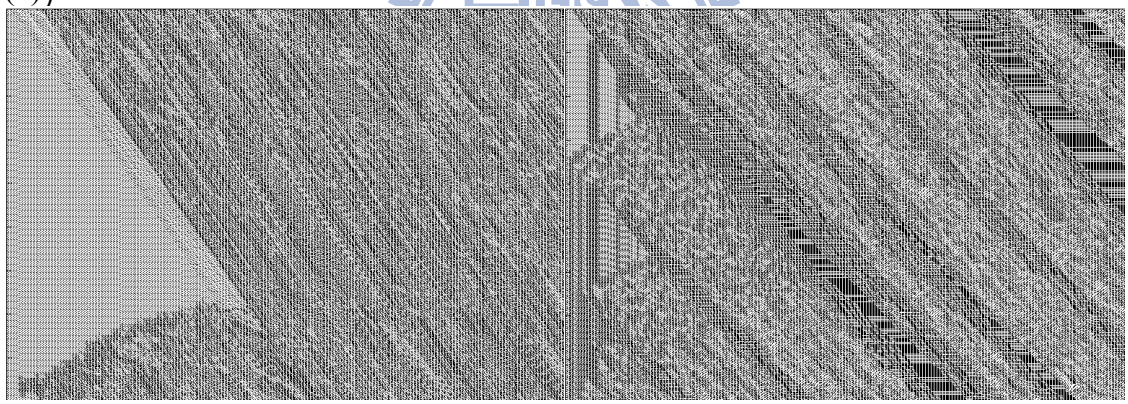

(e) *ρ=110 veh/km/lane*

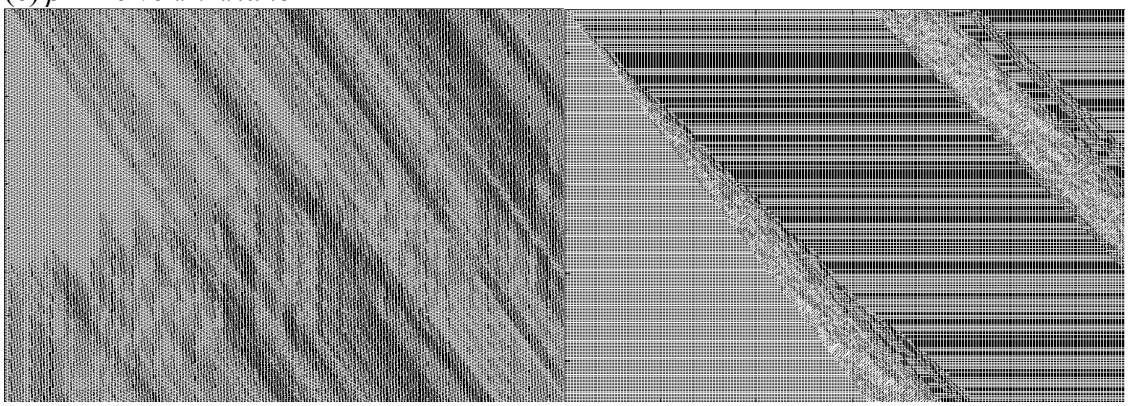

(f) *ρ=143 veh/km/lane*

FIGURE 6-8 Traffic patterns and their transitions-left panels show the simulated results of original CA model, whereas right panels show those from the revised CA model.

We compare the simulated results between the revised model and the refined model. Figure 6-9 presents the global flow-occupancy relations (fundamental diagrams) where maximum acceleration for vehicles is set as 3 *sites/(time-step)*^{2}, or equivalently, 3 *m/sec*^{2}. Besides, according to the field observation, maximum deceleration is set as -6 *sites/(time-step)*^{2}. For clearer description, the flow rate *q(S)* is converted from cells into number of vehicles and occupancy *ρ(S)* is converted into vehicle per kilometer, as the flow-density relations shown in Figure 6-10. It is noticed that due to randomization effect, slight difference always exists but would disperse within a certain area for each separate CA simulation run, even with completely identical parameters settings. Therefore, Figure 6-9 and 6-10 can be deemed as just the typical representative of simulated results.

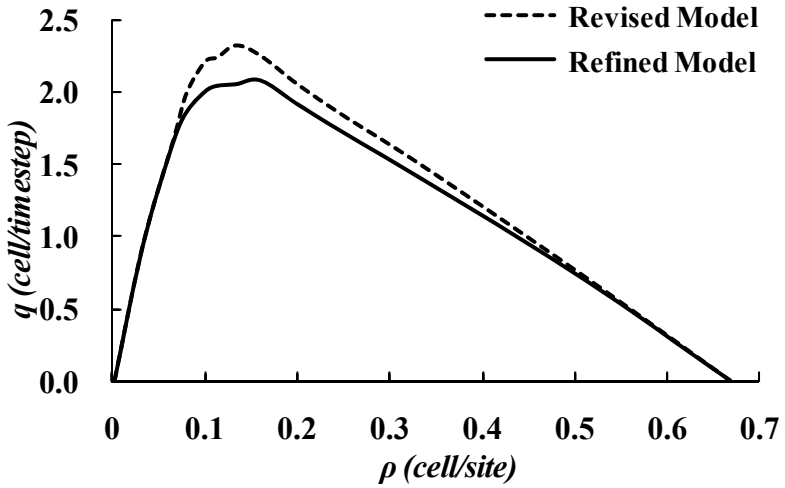

FIGURE 6-9 Comparison of simulated global flow fundamental diagrams of revised model and refined model (Counted in cells/time-step).

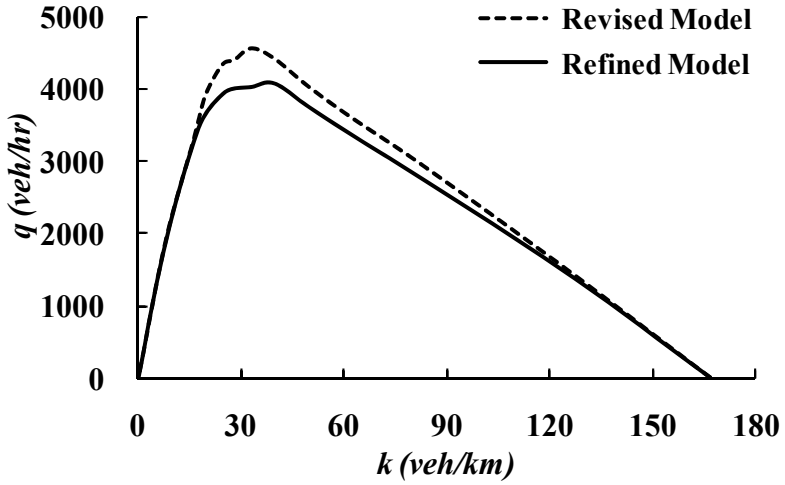

FIGURE 6-10 Comparison of simulated global flow fundamental diagrams of revised model and refined model (Counted in vehicles/hour).

From global point of view, the shapes of simulated flow-density results are principally similar, though the revised model demonstrates lower maximum traffic flow rate-around 2000 *vehicles/hour/lane*. As mentioned above, due to randomization effect, slight difference always exists for each separate CA simulation. It is interesting, nevertheless, to find that occasionally a higher traffic flow rate can still be sustained at the traffic density around 32 *vehicles/kilometer*. This can be interpreted through the derived x-t diagram, as shown in Figure 6-11. Figure 6-11(a) is the ideal, but seldom derived, case in which vehicles move smoothly and basically no complicated interference among them. In this special case, the simulated traffic flow will approach the ideal value—2350 *vehicles/hour/lane*. In contrast, Figure 6-11(b) represents the typical, and the frequently derived, case. In this typical case vehicles also move with no fluctuation first but later start to alter speeds in accordance with the preset deceleration rule when a small perturbation is introduced. This also triggers dramatic traffic pattern change and thus outcomes with less traffic flow rate. This phenomenon is consistent with field observations, for example, those provided by Kerner (2004), that the maximum traffic flow (2400 *vehicles/hour/lane*, as proposed by 2000HCM) is rarely found since it is based upon an ideal condition that there are minimum interactions among vehicles. Accordingly, in most cases maximum traffic rates around 2000~2200 *vehicles/hour/lane* are usually identified.

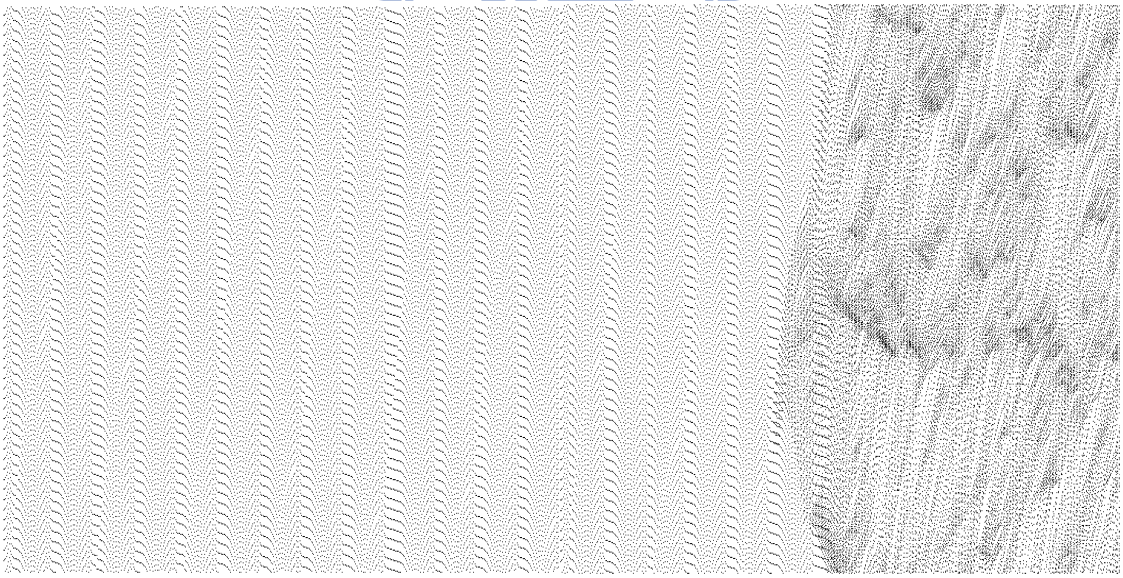

(a) The ideal case (b) The typical case

FIGURE 6-11 The simulated x-t diagrams of same parameters setting (traffic density 32 veh/km) but with different outcomes: (a) The ideal case, interference among vehicles can hardly be observed. (b) The typical case, small perturbation incurs dramatic traffic pattern change.

6.3 Application

This section further explores more interesting and diversified applications by introducing a twenty-meter long work zone, serving as a stationary bottleneck into the refined CA simulation. This work zone is located in the outer lane, middle of the simulated track. Next, various traffic control schemes (e.g., variable speed limits) within the restriction area (upstream of work zone) are implemented. We will impose various speed limits at different upstream locations—129, 258 and 516 meters from the work zone (hereinafter refer to as "reduced speed" RS region), as demonstrated in Figure 6-12. The local flow rate nearby downstream of bottleneck is measured under different densities to determine the optimum control strategy that has smallest impact on the nearby traffic capacity.

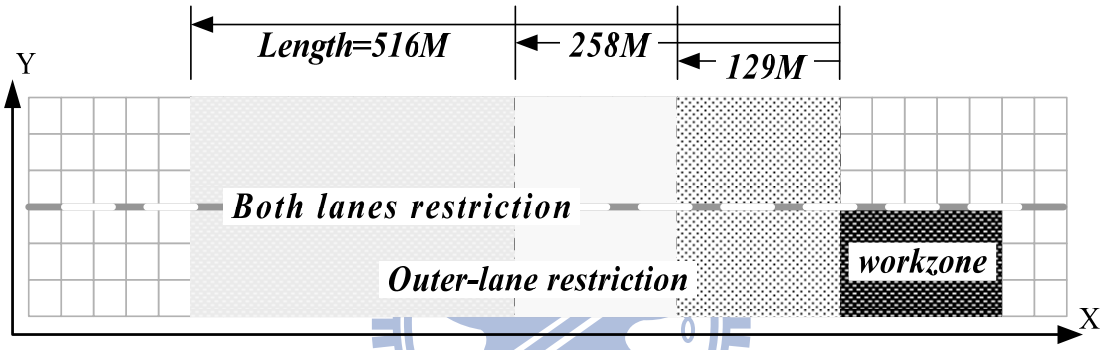

FIGURE 6-12 A simulated scenario for work zone.

First, the effect of RS length is investigated. Figure 6-13, 6-14, 6-15, and 6-15 present the simulated fundamental diagrams (FD) by setting different RS lengths on both lanes and solely on outer lane, respectively, with a speed limit 17 cell/sec (61.2 kph). It should be noted that we slightly modify the lane-change rules, i.e., when vehicles enter the RS region, if situation allows, vehicles in the outer lane will eventually shift to the inner lane with possibility equal to unity. This reflects the fact that when approaching the bottleneck, people will do all their best to overtaking the bottleneck. For clearer description, the global flow rate q(S) is converted into number of vehicles and occupancy ρ(S) into vehicle per kilometer, as shown in Figure 6-14 and Figure 6-16. The RS length is determined through the algorithm defined by Taiwan Roadway Traffic Signal, Sign, and Marking Design Standards. It stipulates that for a highway, the sign notifying the drivers with road width reduction in front of work zones should be located through the formula 0.625V*W, where V is the speed limit, measured in kph and W is the reduced road width, measured in meter. According to this formula, coupled with the normal speed limit 110 kph and the lane width 3.75 meter, we select the simulated RS lengths as 129, 258 and 516 meters, respectively.

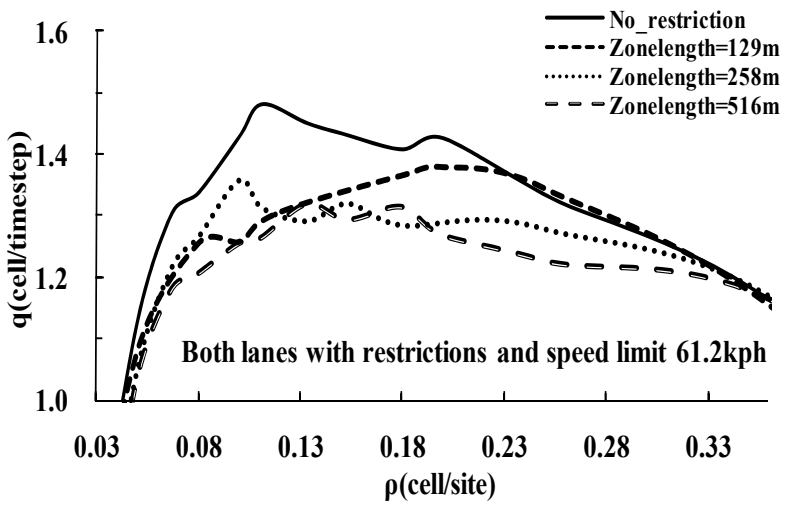

FIGURE 6-13 Fundamental diagrams (FD) with different RS lengths on both lanes. (Counted in cells/time-step).

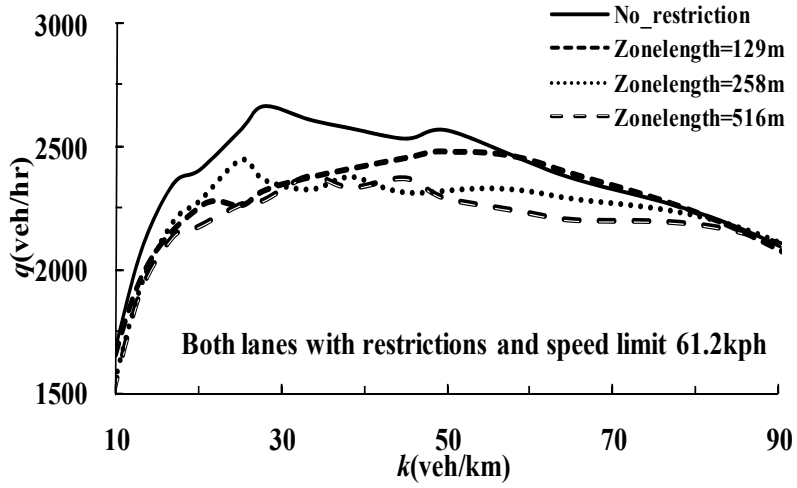

FIGURE 6-14 Fundamental diagrams (FD) with different RS lengths on both lanes. (Counted in vehicles/hour).

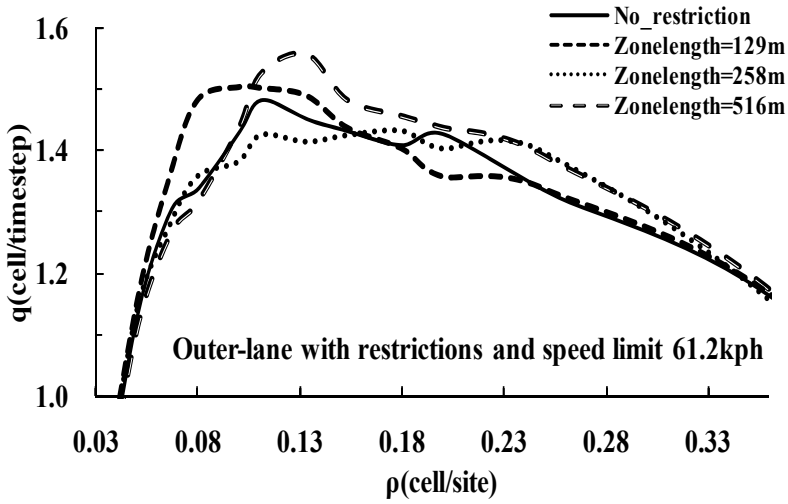

FIGURE 6-15 Fundamental diagrams (FD) with different RS lengths on outer lane only. (Counted in cells/time-step).

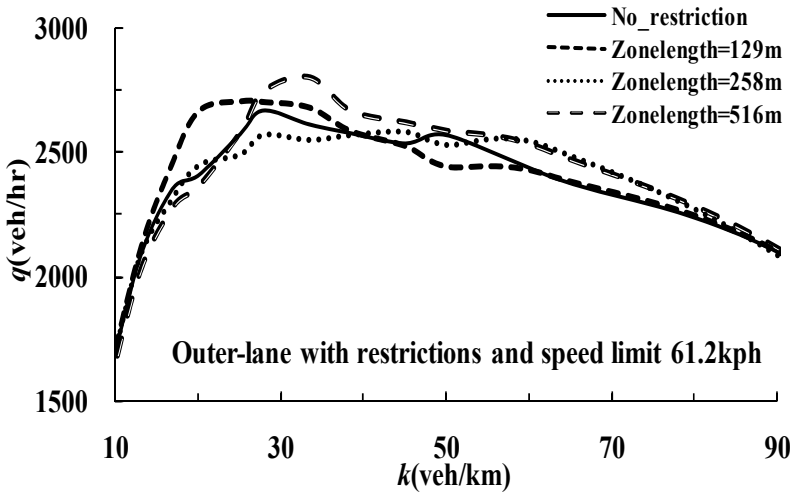

FIGURE 6-16 Fundamental diagrams (FD) with different RS lengths on outer lane only. (Counted in vehicles/hour).

Next, we evaluate the effect of different speed limit settings. Here we fix the RS zone length as 516-meter, the optimum value from the above analysis. Different speed limits within the RS zone such as 14 cell/sec (50.6 kph), 17 cell/sec (61.2 kph), and 23 cell/sec (82.8 kph) are attempted. Figure 6-17 and Figure 6-18 show the simulated results of setting such various speed limits on both lanes. According to Figure 6-17 and Figure 6-18, it can be found that reduced speed limit has negative effect on the maximum flow rate. As speed limit decreases further, the traffic flow rate also declines.

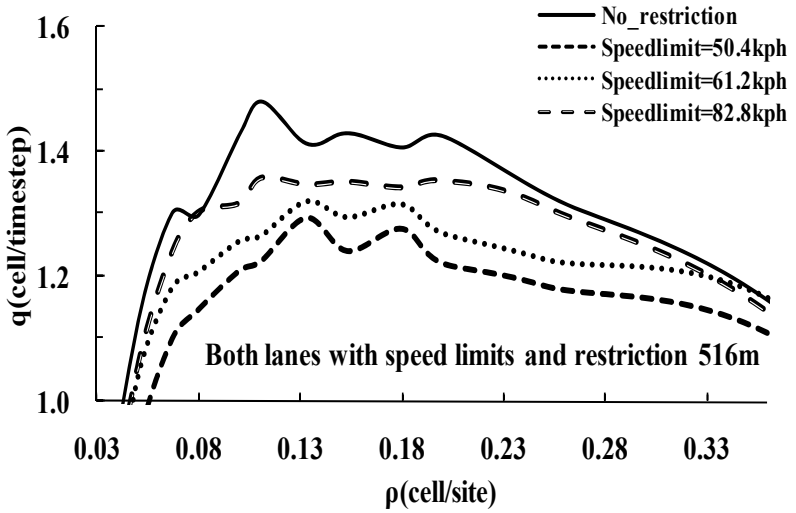

FIGURE 6-17 Fundamental diagrams (FD) with different speed limits on both lanes. (Counted in cells/time-step).

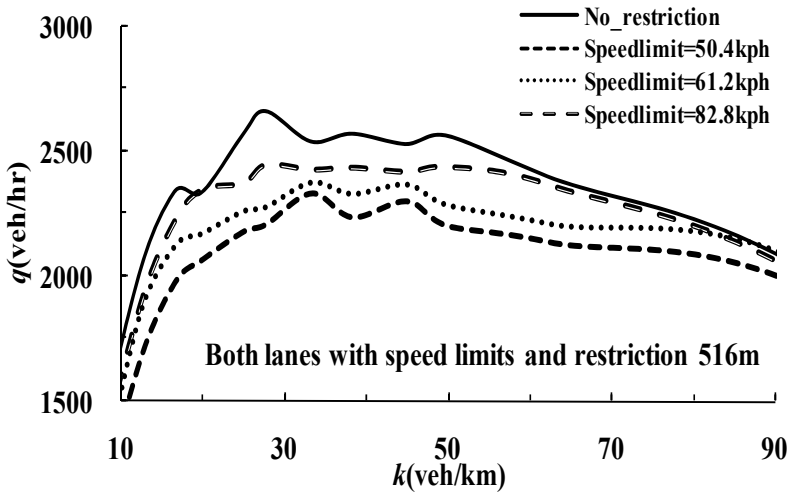

FIGURE 6-18 Fundamental diagrams (FD) with different speed limits on both lanes. (Counted in vehicles/hour).

Figure 6-19 and Figure 6-20 present the simulated results for the scenarios of RS zone being restricted to outer lane only. It is found that only little influence can be identified. However, setting the speed limit 61.2 kph within the RS zone can somehow have slight gain in traffic flow, especially in the neighborhood of maximum flow rate where the density is 32 veh/km/lane, as compared with the no-restriction scenario. It implies that raising the speed limit does not guarantee a higher flow rate. However, for heavy or light traffic (density larger than 50 veh/km/lane or lower than 30 veh/km/lane), no significant effect on the flow rates can be identified.

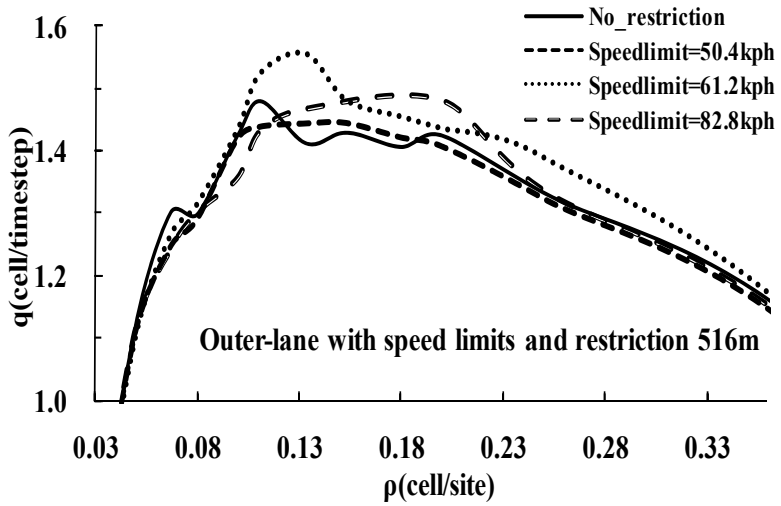

FIGURE 6-19 Fundamental diagrams (FD) with different speed limits on outer lane only. (Counted in cells/time-step).

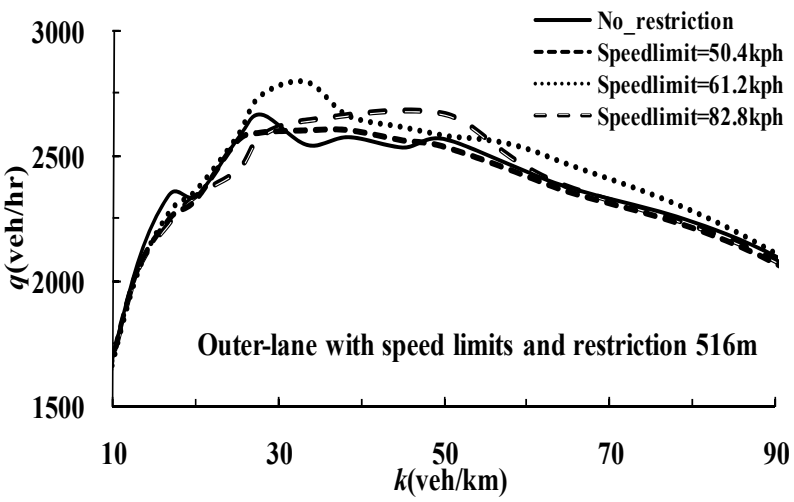

FIGURE 6-20 Fundamental diagrams (FD) with different speed limits on outer lane only. (Counted in vehicles/hour).

This research further inspect the standard deviation of speed variations (an index of safety) among different control schemes—no restriction, RS zone on both lanes, and RS zone on outer lane only—under the optimum simulated condition, that is, RS length equal to 516-meter and speed limit equal to 61.2 kph. The results are displayed in Figure 6-21. It can be found that setting restriction zones on both lanes will impair the flow efficiency, but the speed variations will dramatically drop to about a half, compared with the no restriction case. This should be regarded as a gain of safety at the work zone since vehicles move with more homogeneous speed, thus in turn end up with fewer conflicts (lower collision possibility).

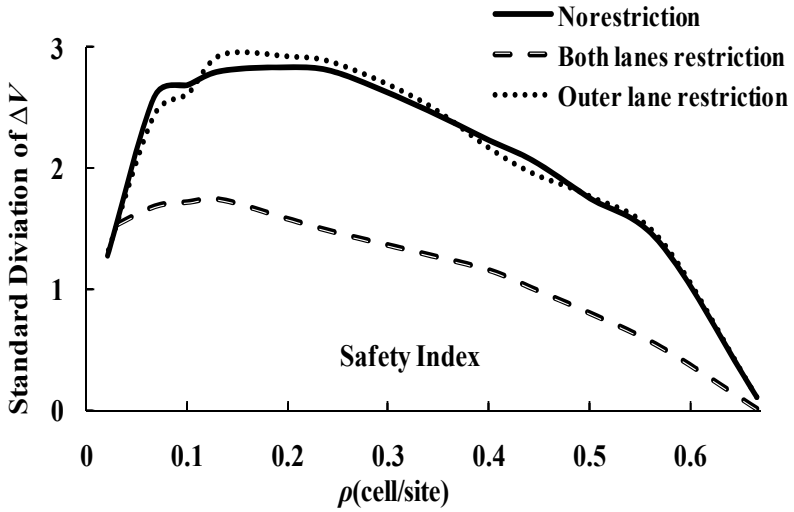

FIGURE 6-21 Comparison of standard deviation of speed variations with different control schemes.

Moreover, we evaluate the capacity loss due to work zone introduced. Figure 6-22 and Figure 6-23 show the comparison between the scenarios with and without work zone. The selected control schemes are: RS lengths equal to 258 and 516-meter whereas speed limit equal to 61.2 kph. According to Figure 6-22 and Figure 6-23, we find that about 43 percent of the capacity has lost to the work zone introduced. Besides that, a plateau regime can easily be identified at density ranging from 30 to 90 veh/km. Our simulation results are consistent with the newly published effort by Zhu *et al.* (2009), who found that when an accident car is introduced, a plateau will emerge in the simulated fundamental diagrams. The coupled induced capacity loss for pure traffic (vehicle of single type) is approximately 45 percent, very close to our simulation results (43 percent loss). This also confirms the validity of our revised CA model.

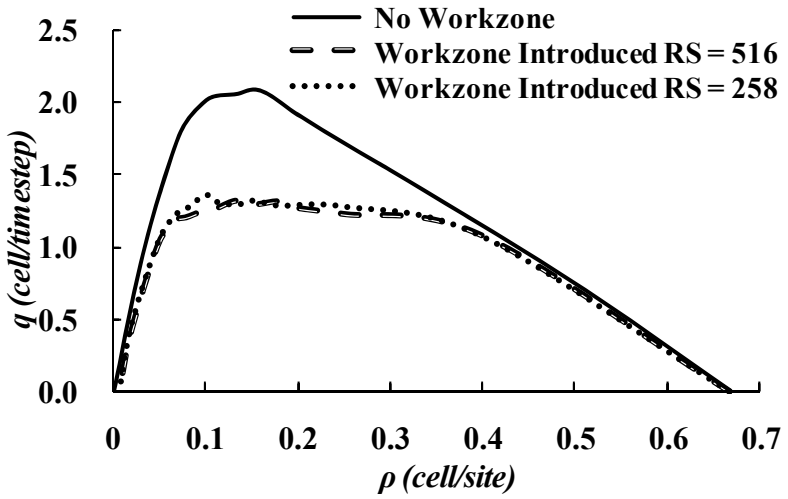

FIGURE 6-22 Traffic capacity loss induced by work zone. (Counted in cells/time-step).

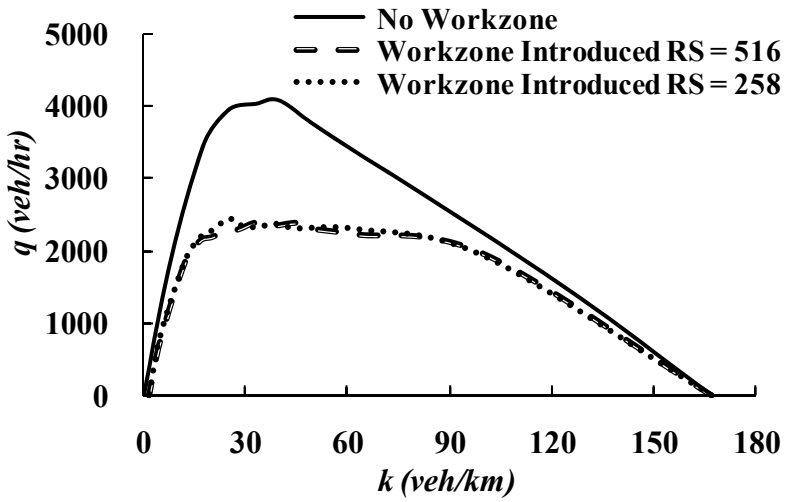

FIGURE 6-23 Traffic capacity loss induced by work zone. (Counted in vehicles/hour).

6.4 Traffic Feature Explorations

In this section we will discuss the discrepancy among the different fundamental diagrams that derived from various traffic scenarios, especially those profiles in the congested traffic flow phases. First the pure traffic (comprised by only one vehicle type) is discussed and followed by discussion of mixed traffic (comprised by two vehicle types) scenarios.

1. Pure-Homogeneous traffic patterns in Free Flow

We first check the simplest case- free flow phase of homogeneous traffic (no perturbation is considered), for both pure and mixed traffic scenarios. Figure 6-24 is the simulated outcome wherein Figure 6-24(a) is the simulated FD diagrams whereas Figure (b), (c) and (d) display the vehicular trajectories of various traffic conditions for Pure-Homogeneous Light Vehicles (PH-LV), Pure-Homogeneous Heavy Vehicles (PH-HV) and Mixed-Homogeneous Light Vehicles and Heavy Vehicles (MH-LHV, mixed traffic under L:H=5:1 ratio) respectively. Likewise the PH-LV case, when no traffic perturbation is considered all light vehicles move with constant velocity (i.e., all vehicular trajectories remain parallel, as shown in Figure 6-24 (b)). When introducing into the FD diagram, it transforms into the orange line segment with positive slope, as shown in Figures 6-24(a). Similarly, the PH-HV free-flow phase (Figure 6-24 (c)) can be represented by the blue line segment of Figures 6-24(a). Besides, Figure 6-24 (d) represents the MH-LHV traffic flow pattern. Since in free flow only low traffic density is considered, all the light vehicles and heavy vehicles move with constant velocity.

2. Pure-Homogeneous traffic patterns in Congested Flow

Next, we analyze the congested flow phase of homogeneous traffic, as shown in Figure 6-25. Again, Figure 6-25 (a) depicts the FD diagram, Figure 6-25 (b) and (c) display the vehicular trajectories of two different occupancies ($\rho_A=0.34$, $\rho_B=0.15$) for PH-LV. The revealed traffic flow patterns for PH-LV can be interpreted as free flow and wide moving jams phase, respectively. In contrast, Figure 6-25 (d) displays the vehicular trajectories for PH-HV and similar traffic patterns. Since all vehicles are setting homogenization (without random term effect), one may easily find that all vehicles travel at nearly maximum speed in free flow phase however their velocities drop significantly to nearly zero when arriving the upstream front of traffic jams. According to Figure 6-25(b), (c) and (d), it is can be identified that traffic jams propagate upward to bottom and thus lead to the so called “wide moving jam” phenomena. Using Figure 6-25 (b) for further explanation, it is found that

vehicles embarked from the initial platoon will first travel in free flow phase till they reach the upstream front of traffic jam to form a backward shockwave, $v_{s(21)}$. Vehicles will remain stationary when stuck in the traffic jam. When reaching the downstream front of traffic jam, vehicles will accelerate again and thus aggregate another backward shockwave, $v_{s(13)}$. It is worthy mentioned here that the shockwave $v_{s(21)}$ and $v_{s(31)}$ are parallel since they have almost identical slope. This means the inflow rate inside traffic jam equals to the outflow rate leaving thereof. This feature remain valid for all densities simulated, regardless with the preset occupancies (ρ_A or ρ_B) or scenarios simulated (refer to Figure 6-25(b), (c) and (d) for detail). However, since no randomization is introduced, some important traffic features, such as traffic hysteresis and capacity drop in the neighborhood of maximum flow rate, can be reproduced as shown in Figure 6-25 (a).

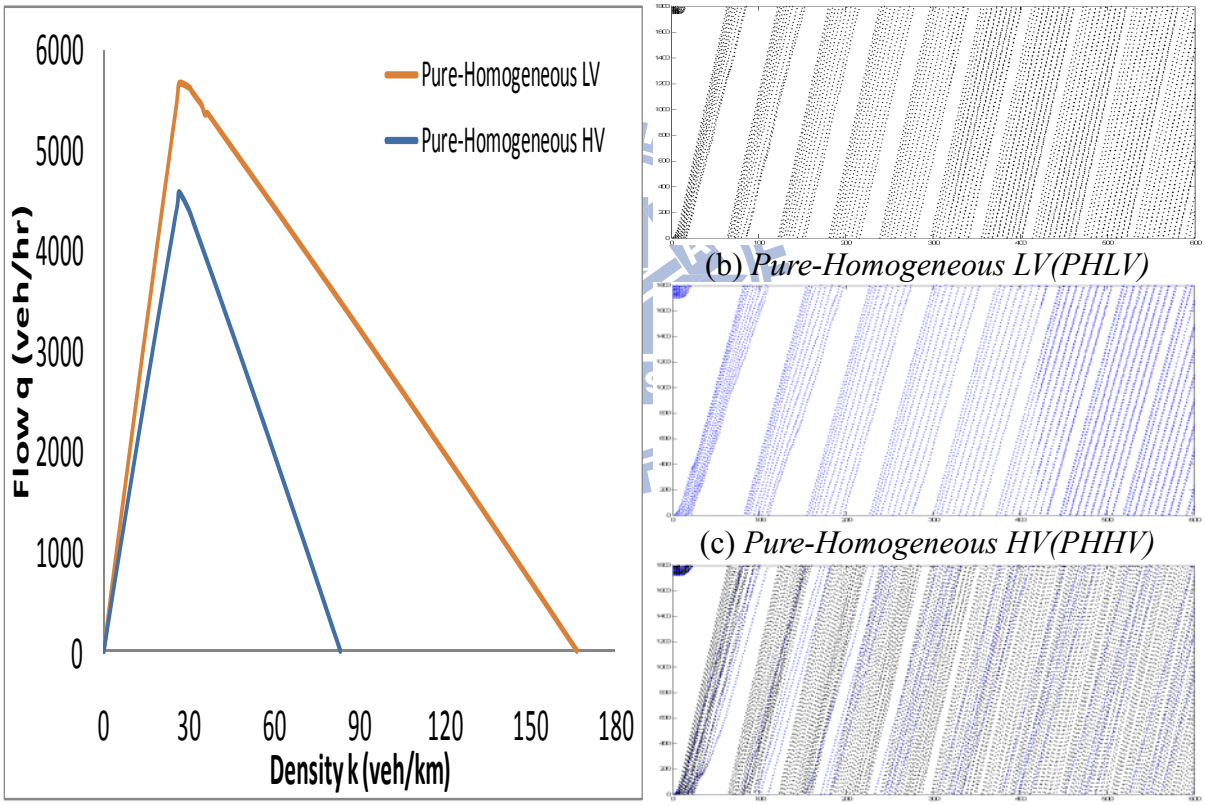

(a) *Pure-Homogeneous traffic- Free Flow*

(b) *Pure-Homogeneous LV(PHLV)*

(c) *Pure-Homogeneous HV(PHHV)*

(d) *Mixed-Homogeneous LHV(L:H=5:1)*

FIGURE 6-24 Pure-Homogeneous traffic patterns in Free Flow and their corresponding lines in FD diagram.

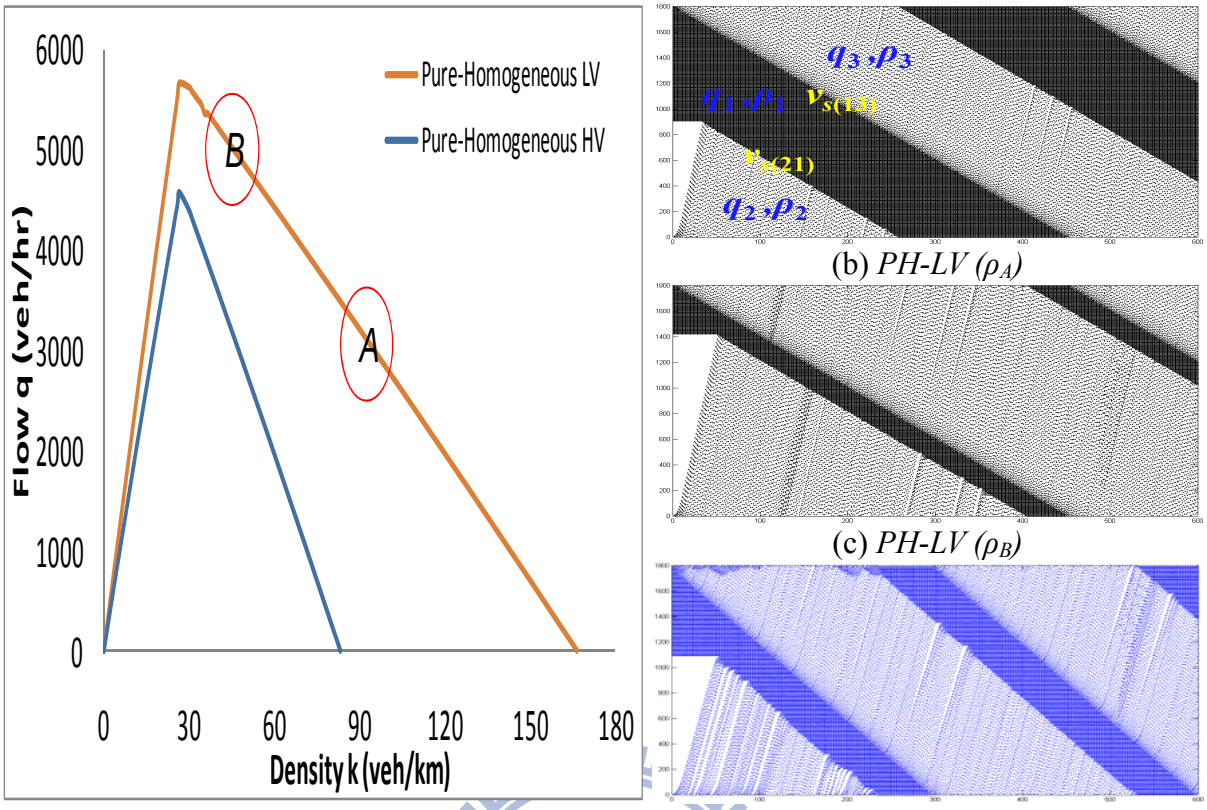

(a) *Pure-Homogeneous traffic- Jam Flow*

(b) *PH-LV* (ρ_A)

(c) *PH-LV* (ρ_B)

(d) *PH-HV*

FIGURE 6-25 Pure-Homogeneous traffic patterns in Jam Flow and their corresponding lines in FD diagram.

3. Pure-Heterogeneous traffic patterns

As mentioned above, the hysteresis effect can not be exhibited if no randomization is considered. Therefore, as the following survey we further introduce the perturbation term into our simulation, as shown in Figure 6-26. Similarly, Figure 6-26(a) serves as the FD diagram and the left panels represent the derived X-t plot for some preset densities. For comparison, we also present one simulated result of one existing study (Benjamin et al., 1996, as Figure 6-26(b)). In our simulations, all the vehicles are set equally spaced on the circular track when simulations start. According to Figure 6-26(c), one can found that a triangle area emerges somewhere in the middle region of x-t plot where traffic jam is triggered owing to the introduction of randomization.. The zoom-out plot of this triangle area, Figure 6-26(d), reveals that there are high inflow rate and lower outflow regarding the emerged traffic jam. This phenomenon agrees with the existing study (Benjamin *et al.*, (1996), Figure 6-26(b)). Figure 6-26 (a) presents the flow-occupancy relations (fundamental diagrams) for both PLV and PHV scenarios, either from deterministic or stochastic viewpoints. According to Figure 6-26(a), one may find that introduction of heterogeneous effect will significantly deteriorate traffic capacity since the congested traffic lines shift downwards. Both PLV (from orange dotted line to coffee line) and PHV (green line)

simulations reveal similar result. Besides, the empirical traffic flow features, the traffic hysteresis and capacity drop are successfully reproduced.

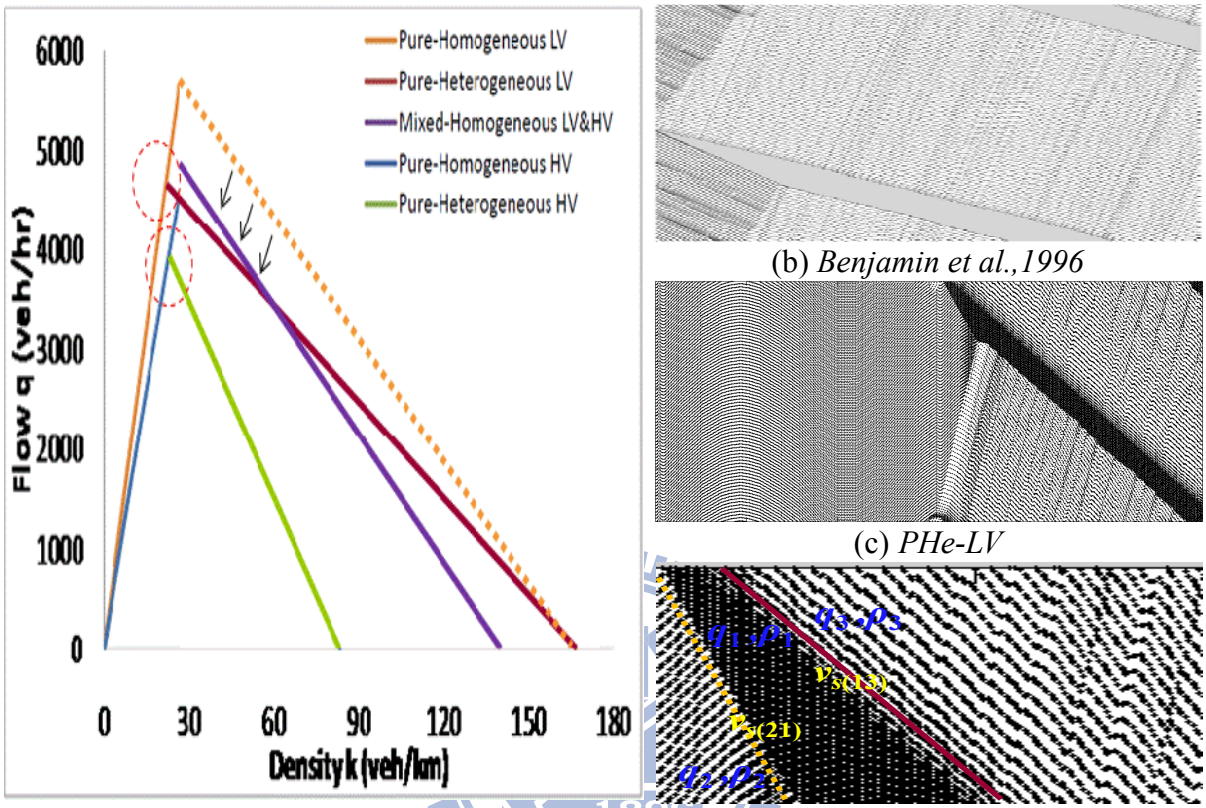

(a) *Pure-Heterogeneous traffic*

(b) *Benjamin et al.,1996*

(c) *PHe-LV*

(d) *PHe-LV*

FIGURE 6-26 Pure-Heterogeneous traffic patterns and their corresponding lines in FD diagram.

4. Mixed-Homogeneous traffic patterns

As mentioned, hysteresis effect can be reproduced if randomization is introduced. However, we found that the hysteresis effect can also be gauged via mixed traffic simulation, even no randomization is considered. According to Figure 6-27(c) and (d), it is found that as adding vehicles of different characteristics (larger size, lower maximum speed), another flow-occupancy curve that reflect the hysteresis effect can be derived, as shown in Figure 6-27(a). Besides, according to Mixed-Homogeneous Light & Heavy Vehicles (MH-LHV) simulations (Figure 6-27 (c) MH-LHV (L:H=5:1) and Figure 6-27 (d) MH-LHV (L:H=3:1)), the mixed traffic effect contributes the increment of variance to vehicular speeds and thus leads to lower traffic flow. This can be supported by the downwards shift of q-k line in Figure 6-27 (a), from orange dotted line to purple line. Accordingly, the empirical traffic flow features, the traffic hysteresis and capacity drop can also be reproduced, even no randomization is considered.

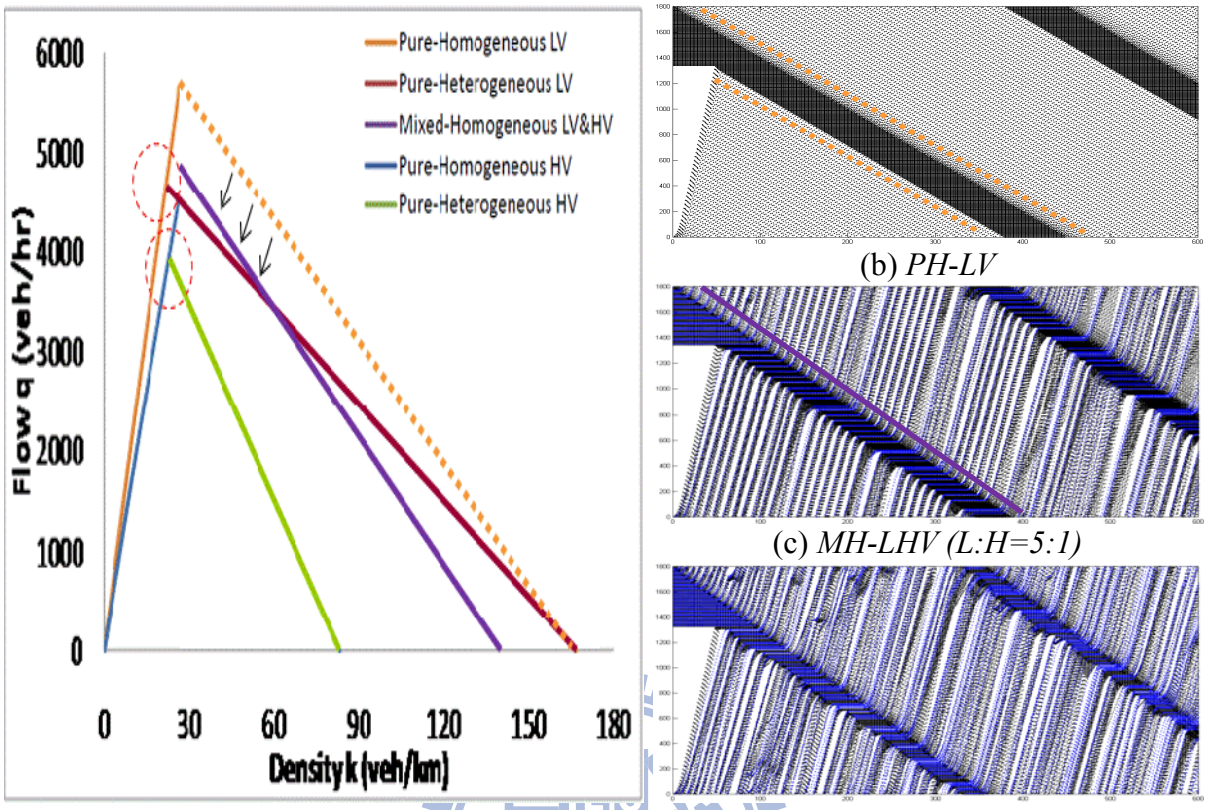

(a) *Mixed-Homogeneous traffic*

(b) *PH-LV*

(c) *MH-LHV (L:H=5:1)*

(d) *MH-LHV (L:H=3:1)*

FIGURE 6-27 Mixed-Homogeneous traffic patterns and their corresponding lines in FD diagram.

5. Mixed-Heterogeneous traffic patterns

As the final survey, we check the most complicated case-mixed traffic with perturbation introduced. Figure 6-28 shows the simulated result for different preset densities. As shown in Figures 6-28 (a), when with low occupancy, since vehicles are sparely distributed, only few interactions among vehicles are expected. Accordingly, free-flow traffic pattern prevails. However, due to heterogeneous effect, occasionally vehicles will decrease speeds; henceforth, a small region of perturbation can be found. This is so-called "synchronized flow phase". This synchronized traffic region will gradually enlarge and reoccur intermittently downstream and become much clearer as long as occupancy increases, as shown in Figure 6-28 (b). As the occupancy (density) increases further, the platoon preset at t=0 will become more difficult to disperse because vehicles in the upstream will arrive more frequent the rear of platoon to maintain a jammed queue. Quite complex behaviors with noticeable propagation of backward shock waves, or wide moving jams can be observed. Figures 6-28 (c) has clearly depicted this phenomenon. Our simulation shows

the flow of MHe-LHV traffic is larger than PHe-HV but smaller than PHe-LV. This phenomenon is consistent with Wang *et al*., (2007) (Figure 6-29).

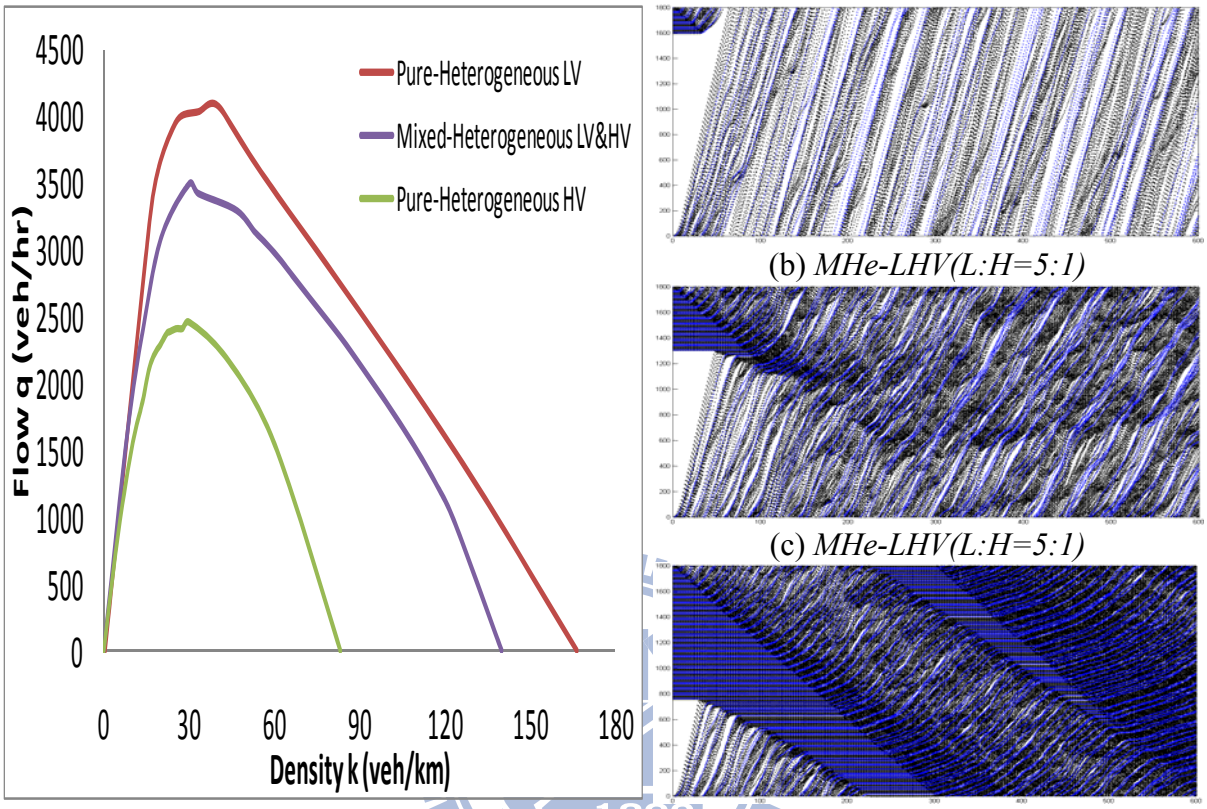

(a) *Mixed-Heterogeneous traffic*

(b) *MHe-LHV(L:H=5:1)*

(c) *MHe-LHV(L:H=5:1)*

(d) *MHe-LHV(L:H=5:1)*

FIGURE 6-28 Mixed-Heterogeneous traffic patterns and their corresponding lines in FD diagram.

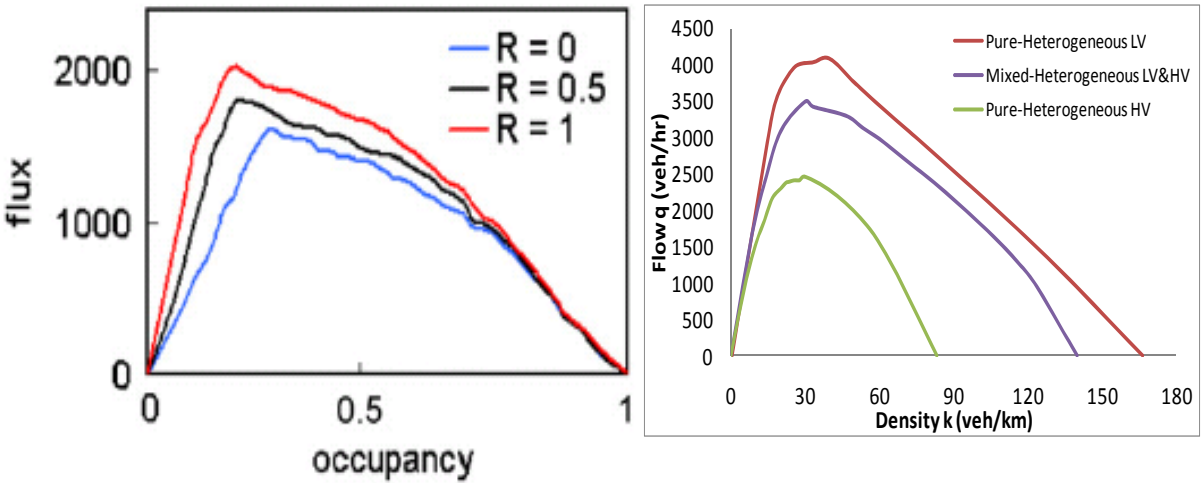

(a) Wang *et al., 2007*

(b) *MHe-LV&HV(L:H=5:1)*

FIGURE 6-29 Comparison of fundamental diagrams for Mixed-Heterogeneous traffic with existing study.

6.5 Summary

This research proposes a new refined CA model with piecewise-linear speed variation as well as limited deceleration capability. The experimental simulations show that it successfully fixes the unrealistic abrupt deceleration behavior found in most previous CA models, thus can reflect the genuine driver behaviors in real world. It is also capable of capturing some important traffic patterns such as the self-induced traffic jams, the transition among traffic patterns, etc.

However, since in this study pure-homogeneous, mixed-homogeneous, and mixed-heterogeneous traffic scenarios are simulated, for simplicity it is assumed that each lane change will be accomplished within 1 time step (1 second), regardless of the initial locations of vehicles. It is still acceptable in accordance with the study by Nagel *et al.* (1998) that in spite of the differences among various lane change rules, similar and realistic results are generated. The proposed refined CA model is further implemented to traffic simulation at a highway work zone. Various reduced speed limits in conjunction with different reduced speed zone lengths are simulated to identify the optimum traffic control scheme. It is found that setting reduced speed limit on both lanes of the work zone will impair the traffic capacity but can significantly gain the traffic safety by smoothing out the speed deviations. However, the effect of both speed limit and length of reduced speed zone can yet be clearly concluded so far since no solid evidences have been materialized from this study.

Chapter 7 CONCLUSIONS AND RECOMMENDATIONS

This research proposes CA modeling for heterogeneous mixed traffic simulations to explore traffic patterns in freeway context. The contributions and findings are concluded in Section 7.1. Recommendations for further research were addressed in Section 7.2.

7.1 Conclusions

The contributions and findings in this study are summarized in the following points:

1. The previous CA Model, no matter basing on the single-lane or multiple-lane simulation environment, takes only one-dimension forward movement on the lane into consideration. This study introduced "common unit (CU)" to represent a "fine cell" and a "fine site" to facilitate the CA simulations in describing the different vehicle sizes moving on non-identical lane widths existent in different roadways. The vehicles are represented by a group of cells depending on their dimensions required for movements and roadway spaces are denoted by sites. Each cell or site is exactly the same size as one CU, which is a much finer squared grid (1.25×1 meters) than most of the previous CA models (7.5×7.5 meters). With our finer-cell definition, study of small-sized vehicles moving alone with other large-sized vehicles would become much easier and more realistic. In view that different vehicle types will occupy different space areas, for instance, a bus may take three times of the space area that a car will occupy. Therefore this research proposes the generalized definition of the traffic stream variables in spatiotemporal sense to precisely capture the collective traffic behavior and to reveal the traffic features.

2. The basic CA model utilizing the generalized spatiotemporal definitions of traffic variables can better elucidate the traffic flow features in the contexts of mixed traffic traveling in multi-lane roadways.

3. The revised CA model considering anticipation effect, velocity-dependent randomization, slow-to-start, lane change, and interaction among vehicles has successfully explored the fundamental traffic features. The effects of both stationary and slow-moving bottlenecks on global traffic are examined. Vehicular trajectories, flow-occupancy, and spatiotemporal traffic patterns under deterministic and stochastic conditions are displayed. The results reveal noticeable traffic patterns with free flow, wide moving jam and synchronized flow phases, suggesting that the revised CA model is capable of capturing the essential features of traffic flows.

4. The refined CA model using Forbes' car-following concept associated with a piecewise-linear movement can satisfactorily rectify the abrupt deceleration found in most existent CA literature. The refined CA model is capable of revealing Kerner's

three-phase traffic patterns and phase transitions among them. The refined CA model is also applied to simulate a highway work zone wherein traffic efficiency (maximum flow rates) and safety (speed deviations) impacted by various control schemes are examined.

7.2 Recommendations

Although this study has taken a step forward in developing more advanced CA models, some avenues for future studies are identified as follows.

1. In the future study, simulations on three- or more-lane freeway with more vehicle types can be performed. Besides, the traffic features under various mixed ratios deserve to explore. The effects of diverse lengths of stationary bottlenecks at construction work zones and the effects of slow vehicles management tactics can be examined using our proposed CA models. Moreover, in surface street environments, bicycles and motorcycles can be added to the mixed traffic simulations. The formation of traffic patterns due to pedestrian or vehicle crossing, bus stop or curb parking, and signal control are also interesting and challenging for further explorations.

2. To define the optimum traffic control scheme at the highway work zone, it is recommended that more sophisticated human factors be introduced into the future CA simulations, including the in-homogeneity among drivers and among vehicles. In addition, real-time intelligent traffic controls, based on local traffic conditions at the work zones, can also be introduced into the CA simulation. Trade-off between traffic safety (speed deviations) and traffic efficiency (capacity) at the highway work zones is a challenging topic worthy for further exploration.

3. In this study, each car away from the lane markings needs to take 2 time-steps to make a lane-change. This is perhaps an over-conservative restriction. Besides, each vehicle only evaluating the surrounding traffic conditions for the next one or two time-steps is perhaps also beyond reality. One future avenue is the introduction of anticipation of surrounding conditions with more extended time-steps. The effect of various maximum speeds for slow vehicles can be considered in the further study.

REFERENCES

Bando, M., Hasebe, K., Nakayama, A., Shibata, A., and Sugiyama. Y., (1994). Structure stability of congestion in traffic dynamics. *Jpn. J. Ind. Appl. Math.* 11, pp. 203–223.

Bando, M., Hasebe, K., Nakayama, A., Shibata, A., and Sugiyama. Y., (1995). Dynamic model of traffic congestion and numerical simulation. *Physical Review E*, volume 51(2), pp. 1035–1042.

Barlović, R., Santen, L., Schadschneider, A., and Schreckenberg, M. (1998). Metastable states in cellular automata for traffic flow. *European Physical Journal B* 5, pp. 793–800.

Barlović, R., (2003). Traffic Jams – Cluster formation in low-dimensional cellular automata models for highway and city traffic. *Ph.D. thesis*, University at Duisburg-Essen, Standort Duisburg.

Benjamin, S. C., Johnson, N. F. and Hui, P., (1996). Cellular automata models of traffic flow along a highway containing a junction. *Journal of Physics A: Mathematical and General*, Vol. 29, pp. 3119–3127.

Bham, G.H. and Benekohal, R.F., (2004). A high fidelity traffic simulation model based on cellular automata and car-following concepts. *Transportation Research C* 12, pp. 1-32.

Brackstone, M. and M. McDonald., (1999). Car-following: a historical review. *Transportation Research F*, Vol. 2, pp. 181-196.

Brilon, W. and Wu, N., (1999). Evaluation of cellular automata for traffic flow simulation on freeway and urban streets, *Traffic and Mobility: Simulation-Economics-Environment, Institut für Kraftfahrwesen*, RWTH Aachen, Duisburg, pp.163-180.

Chakroborty, P. and S. Kikuchi., (1999). Evaluation of the general motors based car-following models and a proposed fuzzy inference model. *Transportation Research C*, Vol. 7, pp. 209-235.

Chandler, R.E., Herman, R., Montroll, E., (1958). Traffic dynamics: Studies in car following. *Operations Research* 6, pp. 165–184.

Chowdhury, D., Wolf, D.E. and Schreckenberg, M., (1997). Particle-hopping models for two-lane traffic with two kinds of vehicles: effects of lane-changing rules. *Physica A* 235, pp. 417-439.

Chowdhury, D., Santen, L., and Schadschneider, (2000). A. Statistical physics of vehicular traffic and some related systems. *Physics Reports,* Vol. 329, pp. 199-329.

Daganzo, C. F., (1997). *Fundamentals of Transportation and Traffic Operations*. Elsevier Science Ltd. Pergamon.

Daganzo, C. F., (1994). The cell transmission model: a dynamic representation of highway traffic consistent with the hydrodynamic theory. *Transportation Research B*, Vol. 28, pp. 269-287.

Daganzo, C.F., (1995). A finite difference approximation of the kinematic wave model of traffic flow. *Transportation Research Part B,* Vol. 29B, pp. 261-276.

Daganzo, C.F., (1999). The lagged cell-transmission model. *International Symposium on Transportation and Traffic Theory*, Ceder, A. (Ed.), New York, Pergamon.

Daganzo, C. F., (2002). A behavioral theory of multi-lane traffic flow. Part I: Long homogeneous freeway sections. *Transportation Research B*, Vol. 36, pp. 131-158.

Daganzo, C. F., (2002). A behavioral theory of multi-lane traffic flow. Part II: Merges and the onset of congestion. *Transportation Research B*, Vol. 36, pp. 159-169.

Ebersbach, A., Schneider, J., Morgenstern, I. and Hammwohner, R., (2000). The influence of trucks on traffic flow an investigation on the Nagel-Schreckenberg model, *International Journal of Modern Physics C* 11 (4), pp. 837-842.

Emmerich, H. and Rank, E., (1997). An improved cellular automaton model for traffic flow simulation, *Physica A*, Vol.234, pp. 676-686.

Ez-Zahraouya, H., Jetto, K. and Benyoussef, A., (2004). The effect of mixture lengths of vehicles on the traffic flow behaviour in one-dimensional cellular automaton, *European Physical Journal B* 40, pp. 111-117.

Forbes, T.W., Zagorski, H.J., Holshouser, E.L. and Deterline, W.A., (1958). Measurement of driver reactions to tunnel conditions. *Highway Research Board, Proceedings* 37, pp. 345-357.

Forbes, T.W., (1963). Human factor considerations in traffic flow theory. *Highway Research Record* 15, pp.60-66.

Gazis, D.C., Herman, R., Potts, R.B., (1959). Car-following theory of steady-state traffic flow. *Operations Research* 7, pp. 499–505.

Gazis, D.C., Herman, R., Rothery, R.W., (1961). Nonlinear follow-the-leader models of traffic flow. *Operations Research* 9, pp. 545–567.

Hamed, M.M., Easa, S.M., and Batayneh, R.R., (1997). Disaggregate Gap-Acceptance Model for Unsignalized T-Intersections. *J. Transportation. Engineering*, Vol. 123, pp. 36-42.

Helbing, D. and Schreckenberg M., (1999). Cellular automata simulating experimental properties of traffic flow, *Physical Review E*, Vol.59, pp. 2505-2508.

Helbing, D., (2001). Traffic and related self-driven many particle systems. *Reviews of Modern Physics*, 73, pp. 1067-1141.

Hsu, C.C., Lin, Z.S., Chiou, Y.C. and Lan, L.W., (2007). Exploring traffic features with stationary and moving bottlenecks using refined cellular automata. *Journal of the Eastern Asia Society for Transportation Studies* 7, pp. 2246-2260.

Jiang, R. and Wu, Q.S., (2003). Cellular automata models for synchronized traffic flow, *J. Phys. A: Math. Gen.* 36, pp. 381–390.

Jiang, R. and Wu, Q.S., (2004). Spatial–temporal patterns at an isolated on-ramp in a new cellular automata model based on three-phase traffic theory. *Journal of Physics A: Mathematical & General* 37, pp. 8197–8213.

Jiang, R., Mao-Bin H., Bin, J., Ruili, W. and Wu, Q.S., (2008). Enhancing highway capacity by homogenizing traffic flow. *Transportmetrica*, Vol. 4, No. 1, pp. 51-61

Kerner, B.S., Rehborn, H., (1996). Experimental features and characteristics of traffic jams. *Physical Review E* 53, pp. R1297-R1300.

Kerner, B. S., (1998). Experimental features of self-organization of traffic flow. *Physical Review Letter*, Vol. 81, 1998, pp. 3797-3800.

Kerner, B.S., Klenov, S.L., (2002). A microscopic model for phase transitions in traffic flow. *Journal of Physics A* 35, pp. L31-L43.

Kerner, B.S., Klenov, S.L., Wolf, D.E., (2002). Cellular automata approach to three-phase traffic theory. *Journal of Physics A* 35, 9971-10013.

Kerner, B.S. and Klenov, S.L., (2003). Microscopic theory of spatial-temporal congested traffic patterns at highway bottlenecks, *Physical Review E*, Vol.68, pp. 036130.

Kerner, B.S., Klenov, S.L., (2004). Spatio-temporal patterns in heterogeneous traffic flow with variety of driver behavioural characteristics and vehicle parameters. *Journal of Physics A* 37, pp. 8753-8788.

Kerner, B.S., Rehborn, H., Aleksic, M. and Haug, A., (2004). Recognition and tracking of spatial–temporal congested traffic patterns on freeways, *Transportation Research Part C*, Vol.12, pp. 369-400.

Kerner, B.S., (2004). *The physics of traffic*, Springer-Verlag Berlin Heidelberg.

Kerner, B. S., (2005). Control of spatiotemporal congested traffic patterns at highway bottlenecks. *Physica A*, Vol. 355, pp. 565-601.

Kerner, B.S., Klenov, S.L., Hiller, A., and Rehborn, H., (2006). Microscopic features of moving traffic jams, *Physical Review E*, Vol.73, pp. 046107.

Knospe, W., Santen, L., Schadschneider, A. and Schhreckenberg, M., (2000). Towards a realistic microscopic description of highway traffic. *Journal of Physics A* 33, pp. 477-485.

Knospe, W., Santen, L., Schadschneider, A. and Schreckenberg, M., (1999). Disorder effects in cellular automata for two-lane traffic, *Physica A* 265, pp. 614-633.

Koshi, M., Iwasaki, M., Ohkura, I., (1983). Some findings and an overview on vehicular flow characteristics. In: Hurdle, V., Hauer, E., Stuart, G. (Eds.), *Proceedings, 8th International Symposium on Transportation and Traffic Flow Theory*, pp. 403-426.

Krauss S. and Wagner, P., (1997). Metastable states in a microscopic model of traffic flow. *Physical Review E* 55(5), pp. 5597-5602.

Kühne, R. in: Gartner, N. Messner, C.J. and Rathi, A.J. (eds.), (1998). *Traffic Flow Theory*, 2nd ed. Transportation Research Board, Special Report 165.

Lan, L. W. and H. H. Yeh., (2001). Car following behavior for drivers with non-identical risk aversion: ANFIS approach. *Journal of the Chinese Institute of Civil and Hydraulic Engineering*, Vol. 13, No. 2, 2001, pp. 427-434.

Lan, L.W. and Chang, C.W., (2003). Moving behaviors of motorbikes in mixed traffic: particle hopping model, *Journal of the Eastern Asia Society for Transportation Studies*, Vol. 5, pp. 23-37.

Lan, L.W. and Chang, C. W., (2005). Inhomogeneous cellular automata modeling for mixed traffic with cars and motorcycles, *Journal of Advanced Transportation* 39 (3), pp. 323-349.

Lan, L. W. and Hsu, C. C., (2005). Using cellular automata to explore spatiotemporal traffic patterns, *Proceedings, 10th International Conference of Hong Kong Society for Transportation Studies*, pp. 210-219.

Lan, L. W. and Hsu, C. C., (2006). Formation of spatiotemporal traffic patterns with cellular automaton simulation, *Transportation Research Board, 85th Annual Meeting*, Washington, DC, in CD-ROM.

Lan, L.W., Chiou, Y.C., Hsu, C.C. and Lin, Z.S., (2007). Spatiotemporal mixed traffic patterns with revised cellular automaton simulation. *Proceedings, 12th International Conference of Hong Kong Society for Transportation Studies,* pp. 133-142.

Lan, L.W., Chiou, Y.C., Lin, Z.S. and Hsu, C.C., (2008). A new cellular automaton model in traffic simulation at a highway work zone. *Proceedings, 10th International Conference on Applications of Advanced Technologies in Transportation.* Athens, Greece.

Lárraga, M.E., del Río, J.A., Alvarez-lcaza, L., (2005). Cellular automata for one-lane traffic flow modeling. *Transportation Research C* 13, pp. 63-74.

Lee, H.K., Barlovic, R., Schreckenberg, M. and Kim, D., (2004). Mechanical restriction versus human overreaction triggering congested traffic states. *Physical Review Letter*, 92(23), pp. 238702-1~238702-4.

Lighthill, M. H. and G. B. Whitham., (1955), On kinematic waves: a theory of traffic flow on long crowed roads, *Proceedings of the Royal Society*, Series A, No. 229, pp. 317-345.

Liu, G., A. S. Lyrintzis, and P. G. Michalopoulus., (1998). Improved high-order model for freeway traffic flow. *Transportation Research Record*, No. 1644, pp. 37-46.

Mahmassani, H., and Sheffi, Y., (1981). Using gap sequences to estimate gap acceptance functions. *Transportation Research Part B*, Vol. 15, pp. 143-148.

May, A. D., (1990). *Traffic Flow Fundamentals*. Prentice-Hall Inc., New Jersey.

Meng, J. P., Dai, H. Q., Dong, L. Y. and Zhang, J. F., (2007). Cellular automaton model for mixed traffic flow with motorcycles. *Physica A 380, Mathematical & General*, pp. 470-480.

Nagel, K. and Schreckenberg, M., (1992). A cellular automaton model for freeway traffic. *Physics I* 2, pp. 2221-2229.

Nagel, K., (1996). Particle-hopping models and traffic flow theory. *Physical Review E* 53, pp. 4655-4672.

Nagel, K., (1998). From particle-hopping models to traffic flow theory, *Transportation Research Record* 1644, pp. 1-9.

Nagel, K., Wolf, D. E., Wagner, P. and Simon, P., (1998). Two-lane traffic rules for cellular automata: A systematic approach. *Physical Review E* 58, pp. 1425-1437.

Nakanishi, K., Itoh, K., Igarashi, Y., Bando, M., (1997). Solvable optimal velocity models and asymptotic trajectory. *Physical Review E*, volume 55, pp. 6519–6532.

Newell, G.F., (1965). Instability in dense highway traffic, a review. In: Almond, J. (Ed.), *Proceedings of 2nd International Symposium on the Theory of Road Traffic Flow*, pp. 73–83.

Payne, H. J., (1971). Model of freeway traffic and control. *Mathematics of Public Systems*, Vol. 1, pp. 51-61.

Pipes, L.A., (1953). An operational analysis of traffic dynamics. *Journal of Applied Physics,* Vol. 24 (3), pp. 74–281.

Polus, A., Shmueli-Lazar, S., and Livneh, M., (2003). Critical gap as a function of waiting time in determining roundabout capacity. *Journal of Transportation Engineering*, 129(4), pp.504-509.

Pottmeier, A., Barlovic, R., Knospe, W. and Schadschneider, A., (2002). Localized defects in a cellular automaton model for traffic flow with phase separation, *Physica A*, 308, pp. 471-482.

Richards, P. I., (1956). Shock waves on highway. *Operations Research*, Vol. 4, No. 1, pp. 42-51.

Rickert, M., Nagel, K., Schreckenberg, M. and Latour, A., (1996). Two lane traffic simulations using cellular automata, *Physica A*, 231, pp. 534-550.

Rothery, R.W. in: Gartner, N. Messner, C.J. and Rathi, A.J. (eds.), (1998). *Traffic Flow Theory*, 2nd ed. Transportation Research Board, Special Report 165.

Sheu, J.B., (2008). A quantum mechanics-based approach to model incident-induced dynamic driver behavior, *Physica D*, Vol. 237, pp. 1800-1814.

Sugiyama, Y., Yamada, H., (1997). Simple and exactly solvable model for queue dynamics, *Physical Review E* 55, pp. 7749-7752.

Transportation Research Board, (2000). *Highway Capacity Manual*, National Research Council, Washington D.C.

Treiterer, J., Myers, J.A., (1974). The hysteresis phenomenon in traffic flow. In: Buckhy, D.J. (Ed.), *Proceedings of 6th International Symposium on Transportation and Traffic theory*, pp. 13–38.

Wang, R., Jiang, R., Wu, Q.S. and Liu, M., (2007). Synchronized flow and phase separations in single-lane mixed traffic flow, *Physica A*, 378, pp. 475-484.

Wang, B.H., Wang, L., Hui, P.M. and Hu, B., (2000). The asymptotic steady states of deterministic one-dimensioned traffic flow models, *Physica B*, 27, pp. 237-239.

Wolfram, S., (1986). Theory and Applications of Cellular Automata. *Word Scientific*, Singapore.

Wolf, D.E., (1999). Cellular automata for traffic simulations, *Physica A*, 263, pp. 438-451.

Wong, G. C. K. and S. C. Wong., (2002). A multi-class traffic flow model – an extension of LWR model with heterogeneous drivers. *Transportation Research A*, Vol. 36, pp. 827-841.

Zhang, H. M., (1998). A theory of nonequilibrium traffic flow. *Transportation Research B*, Vol. 32, pp. 485-498.

Zhang, H. M. and T. Kim., (2005). A car-following theory for multiphase vehicular traffic flow. *Transportation Research B*, Vol. 39, pp. 385-399.

Zhu H.B., L. Lei, and S.Q. Dai., (2009). Two-lane traffic simulations with a blockage induced by an accident car, *Physica A*, Vol. 388, pp. 2903-2910.

APPENDIX

Publications related to dissertation research

A. Refereed Papers

1. Lan, L.W., Chiou, Y.C., Lin, Z.S. and **Hsu, C.C.** (2010) Cellular automaton simulations for mixed traffic with erratic motorcycles behaviors. *Physica A*, Vol. 389, pp. 2077-2089. (**SCI**, 2009 Impact Factor: 1.562)
2. 邱裕鈞、藍武王、鐘仁傑、**許志誠**、林日新 (2010) 兩階段模糊邏輯控制之匝道儀控細胞自動機模擬 *運輸學刊* 第二十二卷第二期，pp. 159-184. (**TSSCI**).
3. Lan, L.W., Chiou, Y.C., Lin, Z.S. and **Hsu, C.C.** (2009) A refined cellular automaton model to rectify impractical vehicular movement behavior. *Physica A*, Vol. 388, pp. 3917-3930.(**SCI**, 2009 Impact Factor: 1.562)
4. **Hsu, C.C.**, Lin, Z.S., Chiou, Y.C. and Lan, L.W. (2007) Exploring traffic features with stationary and moving bottlenecks using refined cellular automata. *Journal of the Eastern Asia Society for Transportation Studies,* Vol. 7, pp. 2246-2260. (**Yasoshima Prize**: Best paper award out of 507 accepted papers)

B. Conference Papers

1. Lan, L.W., Chiou, Y.C., Lin, Z.S., and **Hsu, C.C.,** (2008). A new cellular automaton model in traffic simulation at a highway work zone. *Proceedings, 10th International Conference on Applications of Advanced Technologies in Transportation, Athens.*
2. Lan, L.W., Chiou, Y.C., **Hsu, C.C.,** and Lin, Z.S., (2007). Spatiotemporal mixed traffic patterns with revised cellular automaton simulation. *Proceedings, 12th International Conference of Hong Kong Society for Transportation Studies*, pp. 133-142.
3. Lan, L. W., and **Hsu, C.C.,** (2006). Formation of Spatiotemporal Traffic Patterns with Cellular Automaton Simulation. *Transportation Research Board, 85th Annual Meeting*, CD-ROM, Washington, DC, January 22-26.
4. Lan, L. W. and **Hsu, C.C.,** (2005). Using Cellular Automata to Explore Spatiotemporal Traffic Patterns. *Proceedings of the 10th International Conference of Hong Kong Society for Transportation Studies*, PP. 210-219, Hong Kong, December 10.

C. Research Reports

1. 藍武王、邱裕鈞、**許志誠**、林日新 (2009)，異質混合車流細胞自動機模式之研究 (III)：市區道路環境測試與驗證，國科會研究報告，計畫編號：NSC 95-2211-E-451-015-MY3。
2. 藍武王、邱裕鈞、**許志誠**、林日新 (2008)，異質混合車流細胞自動機模式之研究 (II)：高速公路環境測試與驗證，國科會研究報告，計畫編號：NSC 95-2211-E-451-015-MY3。
3. 藍武王、邱裕鈞、**許志誠**、林日新 (2007)，異質混合車流細胞自動機模式之研究(I)：細胞自動機基本規則與車輛時空特性之關係，國科會研究報告，計畫編號：NSC 95-2211-E-451-015-MY3。

VITA

CHIH-CHENG HSU

教育

高雄市立高雄高級中學	(1990)
中央警察大學交通學系 學士	(1995)
中央警察大學交通管理研究所 碩士	(2000)
國立交通大學交通運輸研究所 博士	(2010)

獲獎

東亞運輸協會(EASTS)年會 最佳論文獎(Yasoshima Prize)(2007)

經歷

臺北縣政府警察局新莊分局 巡官	(1995)
臺北縣政府警察局交通隊 分隊長	(2000)
臺北縣政府警察局交通隊 警務員	(2005)
臺北縣政府交通局 專員	(2008)
臺北縣政府交通局 科長	(2009)